NASA/TM—2008-215418

Assessment of the Partially Resolved Numerical Simulation (PRNS) Approach in the National Combustion Code (NCC) for Turbulent Nonreacting and Reacting Flows

Tsan-Hsing Shih
Ohio Aerospace Institute, Brook Park, Ohio

Nan-Suey Liu
Glenn Research Center, Cleveland, Ohio

October 2008

NASA STI Program . . . in Profile

Since its founding, NASA has been dedicated to the advancement of aeronautics and space science. The NASA Scientific and Technical Information (STI) program plays a key part in helping NASA maintain this important role.

The NASA STI Program operates under the auspices of the Agency Chief Information Officer. It collects, organizes, provides for archiving, and disseminates NASA's STI. The NASA STI program provides access to the NASA Aeronautics and Space Database and its public interface, the NASA Technical Reports Server, thus providing one of the largest collections of aeronautical and space science STI in the world. Results are published in both non-NASA channels and by NASA in the NASA STI Report Series, which includes the following report types:

- TECHNICAL PUBLICATION. Reports of completed research or a major significant phase of research that present the results of NASA programs and include extensive data or theoretical analysis. Includes compilations of significant scientific and technical data and information deemed to be of continuing reference value. NASA counterpart of peer-reviewed formal professional papers but has less stringent limitations on manuscript length and extent of graphic presentations.

- TECHNICAL MEMORANDUM. Scientific and technical findings that are preliminary or of specialized interest, e.g., quick release reports, working papers, and bibliographies that contain minimal annotation. Does not contain extensive analysis.

- CONTRACTOR REPORT. Scientific and technical findings by NASA-sponsored contractors and grantees.

- CONFERENCE PUBLICATION. Collected papers from scientific and technical conferences, symposia, seminars, or other meetings sponsored or cosponsored by NASA.

- SPECIAL PUBLICATION. Scientific, technical, or historical information from NASA programs, projects, and missions, often concerned with subjects having substantial public interest.

- TECHNICAL TRANSLATION. English-language translations of foreign scientific and technical material pertinent to NASA's mission.

Specialized services also include creating custom thesauri, building customized databases, organizing and publishing research results.

For more information about the NASA STI program, see the following:

- Access the NASA STI program home page at *http://www.sti.nasa.gov*

- E-mail your question via the Internet to *help@sti.nasa.gov*

- Fax your question to the NASA STI Help Desk at 301–621–0134

- Telephone the NASA STI Help Desk at 301–621–0390

- Write to:
  NASA Center for AeroSpace Information (CASI)
  7115 Standard Drive
  Hanover, MD 21076–1320

NASA/TM—2008-215418

Assessment of the Partially Resolved Numerical Simulation (PRNS) Approach in the National Combustion Code (NCC) for Turbulent Nonreacting and Reacting Flows

Tsan-Hsing Shih
Ohio Aerospace Institute, Brook Park, Ohio

Nan-Suey Liu
Glenn Research Center, Cleveland, Ohio

National Aeronautics and
Space Administration

Glenn Research Center
Cleveland, Ohio 44135

October 2008

Acknowledgments

This work was supported by the NASA Fundamental Aeronautics Program. The authors would like to thank Dr. Jeffrey P. Moder for his useful comments and suggesstions on the development and application of the Partially Resolved Numerical Simulation (PRNS). The authors would also like to thank Mr. Lancert Foster and Mr. Anthony C. Iannetti for the grid generation of the C4 configuration.

This report contains preliminary findings, subject to revision as analysis proceeds.

This work was sponsored by the Fundamental Aeronautics Program at the NASA Glenn Research Center.

Level of Review: This material has been technically reviewed by technical management.

Available from

NASA Center for Aerospace Information
7115 Standard Drive
Hanover, MD 21076–1320

National Technical Information Service
5285 Port Royal Road
Springfield, VA 22161

Available electronically at http://gltrs.grc.nasa.gov

Contents

Assessment of the Partially Resolved Numerical Simulation (PRNS) Approach in the National Combustion Code (NCC) for Turbulent Nonreacting and Reacting Flows

Tsan-Hsing Shih
Ohio Aerospace Institute
Brook Park, Ohio 44142

Nan-Suey Liu
National Aeronautics and Space Administration
Glenn Research Center
Cleveland, Ohio 44135

Summary

This paper describes an approach which aims at bridging the gap between the traditional Reynolds-averaged Navier-Stokes (RANS) approach and the traditional large eddy simulation (LES) approach. This approach affords an intermediate resolution of turbulent scales relative to those of RANS and LES, and has the characteristics of the very large eddy simulation (VLES). In the present work, the very large scales of turbulence are directly calculated, and the effects of the unresolved scales are accounted for by an eddy viscosity model plus the nonlinear source terms representing the effects of anisotropy and rotation. The dependent variables and governing equations are based on a temporal filtering with a constant filter width. The contents of both resolved and unresolved scales are regulated by the width of the temporal filter. In the present approach, the dependent variables and governing equations will naturally evolve from RANS to VLES and further towards LES, when the width of the temporal filter decreases from the turbulent integral time scale to its fraction and all the way towards the Taylor micro time scale. We call this approach the partially-resolved numerical simulation (PRNS). The main features of the PRNS are: the filtered governing equations are mathematically grid invariant; the subscale model is the one evolved from state-of-the-art models used in the RANS approach; and its nonlinear formulation explicitly accounts for the important features occurring in the regime of the very large eddy simulation.

The concept of PRNS approach, the basic equations and the subscale model are described in detail. Systematic simulations using the National Combustion Code (NCC) have been carried out for fully developed turbulent pipe flows at different Reynolds numbers to evaluate the PRNS approach. The calculated results and the influences of the numerical settings used in the NCC are assessed.

Also presented are the sample results of two demonstration cases: non-reacting flow in a single injector flame tube and reacting flow in a Lean Direct Injection (LDI) hydrogen combustor. These results indicate that the PRNS approach is able to capture important large scale turbulent structures and thereby improve the fidelity of numerical simulations while keeping the computational costs much lower than that required by the LES.

I. Introduction

1. Background of PRNS

Flows in combustors are three dimensional and intrinsically unsteady due to massive separation and strong swirling. These flows contain large scale, coherent structures which play a very important role in determining the turbulent mixing of the fuel, air and other reactants. This, in turn, will heavily influence the flame structure and flame stability via turbulence-chemistry interaction, consequently, also the efficiency, robustness and emissions of the combustion. Apparently, the capability of explicitly capturing these coherent flow structures in the computation is critical for improving the fidelity of simulations of turbulent combustion.

Since, by its definition, the state-of-the-art Reynolds averaged Navier-Stokes (RANS) approach has been aimed at establishing the long-time averaged statistics of flow variables, it can not provide any information on those instantaneous coherent flow structures; hence it is very difficult to accurately account for the turbulent mixing and the turbulence-chemistry interaction in the RANS calculations. On the other hand, the state-of-the art traditional large eddy simulation (LES), which can capture the unsteady coherent flow structures in the computation but typically requires grid sizes down to the inertial sub-range of the local turbulence, is often too costly for practical engineering applications. There is a need for approaches which are capable of capturing the dynamically dominant large-scale flow structures in the computation but at a reasonable computational cost.

One type of these approaches is illustrated by the recent development of various hybrid RANS/LES methodology (References [1, 2, 3, 4, 5, 6, 7]). The basic strategy is to reduce the turbulent eddy viscosity in the fine grid regions to promote LES type of simulation and revert to RANS type of simulation in the coarse grid regions. The switch between RANS and LES is usually based on a criterion in terms of local grid spacing and local flow quantities. Most of them invoke spatially-filtered equations for the resolved scales of turbulence, and the sub-grid model explicitly has the local computational mesh size as a parameter. In addition, the local grid spacing is typically considered as the local width of the spatial filter. There are several troublesome issues associated with the spatially-filtered equations and the use of computational mesh size as a parameter in the sub-grid model as discussed in Reference [8]. However, if we use a temporal filter with a fixed filter width to define the large scales of turbulence, together with a sub-scale model which does not have a grid spacing parameter in its constitutive equation, then all of these issues can be avoided. This leads to our proposed approach termed as the partially resolved numerical simulation (PRNS).

2. Basic Concept of PRNS

PRNS is aiming at the very large eddy simulation (VLES) of high Reynolds number turbulent flows using a relatively coarse grid which is comparable to the one used in the RANS approach. PRNS is based on the concept of using the temporal filter to define the large or very large scales of turbulence. The basic equations for the resolved scales of turbulence are the temporally filtered Navier-Stokes equations. The large scales of turbulence are directly calculated by solving these temporally filtered equations, just like any other spatially filtered LES approaches. However, the effects of the unresolved scales are modeled by a dynamic equation system which is evolved from the state-of-the-art RANS models. The contents of both resolved and unresolved turbulence are notionally regulated by a “resolution control parameter” (RCP), which is related to the ratio of the temporal filter width to the global time scale of the turbulent flow of interest. In practice, the value of the RCP affects the effectual separation of the resolved scales from the unresolved ones in the computation. The basic equations of PRNS as well as the subscale models are thus, in theory, grid independent or grid invariant. The nature of the

mathematical solution of the PRNS equations will mainly depend on the magnitude of RCP under the imposed boundary and initial conditions. As RCP varies from 0 to 1, the nature of the solution should vary from the direct numerical simulation (DNS), LES, VLES and toward RANS. In the actual computational simulations, however, the appropriate grid resolution must be provided for a given value of RCP to support a meaningful turbulent simulation. Overly fine grid will not change the nature of the simulation, although numerical effects such as less numerical dissipation are expected. This is because the basic equations and subscale models of PRNS do not involve any parameters containing the grid size, unlike the traditional LES approaches that are directly dependent on the mesh size.

The basic equations of PRNS and the subscale models are described in Chapter II, Sections 1.2 and 1.4. Some remarks about planning the VLES, choosing an appropriate value of RCP, and the main features of the dynamic equation system of the subscale model are discussed in Chapter II, Section 1.4.5.

3. The National Combustion Code (NCC)

The approach of PRNS can be easily implemented into an unsteady computational fluid dynamics (CFD) code. In the present effort, we have used the National Combustion Code developed at NASA GRC [9, 10, 11, 12, 13, 14, 15]. The NCC is an integrated system of modules based on unstructured meshes and running on parallel computing platforms. It has five major modules: a gaseous flow module solving the three-dimensional, unsteady, compressible Navier-Stokes equations; a turbulence module including the nonlinear k-ε models; a chemistry module solving the species conservation equations, or using the Intrinsic Low Dimensional Manifold (ILDM) method to determine the species mass fractions; a turbulence-chemistry interaction module employing eddy-breakup model, or assumed pdf approach, or solving the transport equation of the probability density function (pdf) for species and enthalpy; and a spray module solving the liquid droplet transport equations. The interacting multi-phase, physical-chemical processes embodied in these major modules are emulated via a hybrid Eulerian-Lagrangian-Monte Carlo solution algorithm. Over the years, the NCC has served as a test bed for assessing turbulent combustion models and computational technologies in a semi-engineering environment. We have been prudently using the NCC within its current limitations for technology program support while concurrently improving its fidelity and extending its capability.

The implementation and evaluation of the PRNS mainly involve the gaseous flow module and the turbulence module, therefore, a brief description of these two modules is in order. The flow module solves unsteady, three-dimensional, compressible Navier-Stokes equations. The discretization begins by dividing the computational domain into a large number of mesh elements, which can be of mixed type. A central-difference finite-volume scheme is used for spatial discretization while a three-time-level backward differencing is used for temporal discretization. Therefore, the nominal discretization accuracy is second order both in space and in time. These discretized equations are then

advanced temporally to the next physical-time step by a so called "dual-time-step" approach, in which a four-stage Runge-Kutta scheme is used to iteratively drive the solutions of the "pseudo-time" towards convergence with respect to the pseudo time. Upon the convergence of this "inner" iteration, the implicit advancement to the next physical-time step is achieved. In order to accelerate the convergence, particularly when the flow Mach number is small, the pseudo-time term is preconditioned, and the static pressure is decomposed into a constant reference pressure and a gauge (or fluctuating) pressure. Sometimes, residual smoothing is also applied to smooth the computed residuals to enhance the convergence rate. Since central differencing is employed for the spatial discretization, artificial dissipation is added to maintain the numerical stability, we have been using the Jameson dissipation operator, which is a blend of second-difference and fourth-difference terms. Consequently, for a practical computation, the numerical setting will then include the truncation errors of the discretization, the level of the reference pressure, the convergence criterion for the inner iteration, the use of residual smoothing, and the amount of the added artificial dissipation. A sufficiently "clean" numerical setting is the prerequisite for a rigorous evaluation of the turbulence models. By clean, we mean that the spurious effects originated from the inherent numerical artifacts are much smaller than the effects originated from the employed physical models on the solutions. In other words, the behaviors of the calculated solutions are controlled by the physical models, not by the numerical artifacts, although some limited yet small contaminations are always present.

The turbulence module is based on the k-ε models, and has the following options: high Reynolds number wall function or low Reynolds number wall integration, linear or non-linear turbulent stress-strain relationship. Details of an advanced nonlinear k-ε RANS model and a recently developed generalized 3-D turbulent wall function can be found in references [15] and [17], respectively. The module also contains some LES sub-grid models [18, 19].

4. Scope of Assessment Effort

Recently, PRNS is being implemented in the NCC for performing the very large eddy simulation of combustor flows. The focus of the current effort is the fundamental assessment of the implemented subscale model and the establishment of an appropriate numerical setting. Experiences have shown that both the physics based model and the appropriate numerical setting are equally important for yielding an accurate numerical simulation. In the past, the NCC has successfully produced many RANS simulations for various reacting combustor flows. The code is robust and has a set of default numerical parameters to speed up the convergence and to stabilize the numerical simulation. Some of these parameters/options (e.g., the reference pressure, residual smoothing, added numerical dissipations, etc.) are common practice, and the RANS results are often not overly sensitive to a range of their values. However, we have observed that these parameters/options can significantly affect and, in some cases, even dominate the simulation of turbulent fluctuations. Subsequently, we have conducted systematic studies to sort out the effects of each of these parameters/options on the calculation of turbulent

fluctuations, and, as a result, we have established a sufficiently "clean" numerical setting for the PRNS calculation. The simulations presented in this paper are all conducted using this numerical setting as the baseline.

At this stage of the assessment of the PRNS approach, we have selected the fully developed turbulent pipe flows as the focus, as they are well known fundamental flows with available experimental data [20]. Furthermore, these cases are amenable to the use of periodic boundary conditions in the simulations, thereby, free from the complicating issues of inflow and out flow boundary conditions. In this report, we will present the assessment results obtained for a moderately large Reynolds number of 150,000 and a relatively low Reynolds number of 15,000 (based on the centerline axial velocity and the pipe diameter). The basic criteria for a successful simulation of large and very large scales of turbulence are set as follows: it must reveal a broadband scales of turbulent fluctuations, the power spectrum has to show at least two or three orders energy variations from large to small scales, and it must produce reasonable or better mean profiles than those produced by the RANS simulation, when compared with experimental data.

Finally, we also present the sample results of two demonstration cases to indicate the intended applications of the PRNS approach. These two cases are: non-reacting flow in a single injector flame tube and the reacting flow in a Lean Direct Injection (LDI) hydrogen combustor.

II. Partially Resolved Numerical Simulation

In this chapter, we will first describe the basics of PRNS approach for the very large eddy simulation, the advantages of its grid-invariant feature and its subscale dynamic equation system. Then, we will present the critical evaluations of PRNS using the NCC code for fully developed pipe flows at various Reynolds numbers.

Some interesting phenomena were observed, which seem to reveal some deficiencies resided in all of the turbulent simulations that are based solely on the subscale eddy viscosity concept. More advanced subscale models may be needed to more comprehensively mimic the physical interactions between the resolved and unresolved scales, especially when the unresolved scales become larger or the flows are at lower Reynolds numbers.

In addition, sample results of applications to complex non-reacting and reacting flows will also be presented to show the intended applications of this approach.

1. Basics of Partially Resolved Numerical Simulation

In the PRNS approach, the resolved turbulent scales are defined by a temporal filter. This is based on the premise that small scale motions tend to have small time scales. A temporal filter with a fixed small width can then capture the large scale turbulence.

The PRNS equations are the temporally filtered Navier-Stokes equations, which govern the motion of the resolved large scale turbulence. There are unclosed terms in these PRNS equations, which represent the effects from the unresolved small scale turbulence, and they must be modeled in order to solve the PRNS equations to obtain the numerical solution of large scale turbulence.

It is noted here that the above procedure in PRNS is very similar to that in the traditional LES, except that the filter used to define the large scale turbulence is different in these two approaches. PRNS uses a temporal filter while LES uses a spatial filter (with its width often being identical to the numerical grid size). There are substantial advantages in using a temporal filter. For example, PRNS equations are mathematically grid-invariant; they are, in theory, valid for any type of numerical grids (structured or unstructured, homogeneous or inhomogeneous); PRNS equations have a unified feature facilitating the evolution from DNS, LES and towards RANS when the width of the temporal filter varies from zero, a small but finite value and towards a large value (e.g., the integral time scale). In addition, some important turbulent correlation relationships can be unambiguously established allowing an exact comparison between the measurements and numerical simulations.

In order to be consistent with the grid invariance of the PRNS equations, the subscale model of PRNS must also be grid-independent; it can be formed by invoking a more general constitutive relationship in conjunction with a dynamic equation system consisting of the subscale turbulent kinetic energy and dissipation rate. This type of models enables PRNS to perform a very large eddy simulation with a relatively coarse grid, hence, consuming less computing resources.

In a preliminary study, we have noticed that the non-linear constitutive relationship for the subscale model exhibits significant advantages over the eddy viscosity model. This suggests that the interactions between the resolved and the unresolved scales are not just through the eddy viscosity, and that the nonlinear terms are needed as additional sources to mimic other types of physical interactions.

1.1 Definition of Large-Scale Turbulence

Using a homogeneous temporal filter $G(t-t')$, the large-scale turbulent variable $\bar{\phi}$ and its density-weighted variable $\tilde{\phi}$ can be defined as

$$\bar{\phi}(t, x_i) = \int \phi(t', x_i)\, G(t-t')\, dt', \quad \tilde{\phi} = \frac{\overline{\rho\phi}}{\bar{\rho}} \tag{1}$$

where the integral is over the entire time domain and G satisfies the normalization condition: $\int G(t-t')\, dt' = 1$. There are many such temporal filters. One of the simplest

filters is the top hat filter. For example, the following top hat filter with the width Δ_T is used in the current PRNS:

$$G(t-t') = \begin{cases} 1/\Delta_T, & if \left|t-t'\right| \le \Delta_T/2 \\ 0 \quad , & otherwise. \end{cases} \tag{2}$$

Using this filter, the left part of Equation (1) will become

$$\bar{\phi}(t, x_i) = \frac{1}{\Delta_T} \int_{t-\Delta_T/2}^{t+\Delta_T/2} \phi(t', x_i)\, dt'. \tag{3}$$

Equation (3) reveals an unified feature of $\bar{\phi}$ and $\tilde{\phi}$, because they will become the exact Reynolds-averaged quantity and Favre-averaged quantity when $\Delta_T \to \infty$. On the other hand, they will become the instantaneous turbulent quantity as $\Delta_T \to 0$. For a finite Δ_T, they represent the quantities of large scale turbulence.

1.2 Basic Equations for PRNS

Performing operation (1) on the Navier-Stokes equations, we obtain a set of basic equations for the resolved large scale turbulence ($\bar{\phi}$ and $\tilde{\phi}$):

$$\left(\bar{\rho}\tilde{u}_i\right)_{,t} + \left(\bar{\rho}\tilde{u}_i\tilde{u}_j\right)_{,j} = -\bar{p}_{,i} - \tau_{ij,j} + \left(2\bar{\mu}\tilde{s}_{ij} - \frac{2}{3}\delta_{ij}\bar{\mu}\tilde{s}_{kk}\right)_{,j}, \tag{4}$$

$$\left(\bar{\rho}\tilde{e}\right)_{,t} + \left(\bar{\rho}\tilde{u}_i\tilde{e}\right)_{,i} = \left(\bar{\kappa}\tilde{T}_{,i}\right)_{,i} + \overline{ps_{kk}} - q_{i,i} + \left(2\bar{\mu}\widetilde{s_{ij}s_{ij}} - \frac{2}{3}\bar{\mu}\widetilde{s_{kk}s_{ii}}\right) + \bar{Q}, \tag{5}$$

$$\bar{\rho}_{,t} + \left(\bar{\rho}\tilde{u}_i\right)_{,i} = 0, \quad \bar{p} = \bar{\rho}R\tilde{T}, \tag{6}$$

where $s_{ij} = \left(u_{i,j} + u_{j,i}\right)/2$. The symbols $(\ )_{,t}$ and $(\ )_{,i}$ represent the temporal and spatial derivatives, respectively. ρ, u_i, T, p, e, and Q are the density, velocity, temperature, pressure, internal energy per unit mass, and the radiation rate. μ and κ are the viscosity and heat conductivity. R is the universal gas constant. τ_{ij} and q_i are the extra terms that are created during the process of temporally filtering Navier-Stokes equations:

$$\tau_{ij} \equiv \bar{\rho}(\widetilde{u_iu_j} - \tilde{u}_i\tilde{u}_j), \quad q_i \equiv \bar{\rho}(\widetilde{u_ie} - \tilde{u}_i\tilde{e}). \tag{7}$$

They represent the effects from the unresolved subscale turbulence. They are not in a closed form, hence must be modeled. We refer them as the unresolved turbulent stresses and heat fluxes.

Note that there are two types of resolved large-scale turbulent variables, $\overline{\phi}$ and $\tilde{\phi}$, appeared in the above equations. Where $\overline{\phi}$ is defined by a temporal filtering and $\tilde{\phi}$ is defined by a density-weighted temporal filtering.

1.3 Time-Averaging Relationships

Since various filters can be used to define the calculated, resolved turbulence quantities, a practical, yet somewhat overlooked, question is how to conduct an apple-to-apple comparison between the calculated results and the experimental data.

Most of the turbulent experimental data are the "mean" values of turbulent variables (e.g., velocity, temperature, pressure, etc.); they are either the pure time-averaged values (for incompressible flows) or the density-weighted time-averaged values, i.e., the Favre-averaged values (for compressible flows):

$$\langle \phi \rangle = \lim_{T\to\infty} \frac{1}{T} \int_{-T/2}^{T/2} \phi \, dt, \quad [\phi] = \lim_{T\to\infty} \frac{1}{\langle \rho \rangle T} \int_{-T/2}^{T/2} \rho\phi \, dt, \tag{8}$$

where ϕ represents an instantaneous turbulent quantity, it can be u_i, $u_i u_j$, or $u_i u_j u_k$, etc., T is the entire time domain. $\langle \phi \rangle$ is the pure time-averaged (Reynolds-averaging) quantity and $[\phi]$ is the density-weighted time-averaged (Favre-averaging) quantity. Such defined experimental data are actually based on the assumption that the measured turbulent flows are statistically steady, or at least approximately steady. Otherwise, the experimental data of "mean" values must be redefined using the ensemble average of many repeated realizations of the same experiment, i.e.,

$$\{\phi\} = \lim_{M\to\infty} \frac{1}{M} \sum_{i=1}^{M} \phi^{(i)}, \quad \frac{\{\rho\phi\}}{\{\rho\}} = \lim_{M\to\infty} \frac{1}{\{\rho\} M} \sum_{i=1}^{M} (\rho\phi)^{(i)}, \tag{9}$$

where M is the number of realizations and $\phi^{(i)}$ and $(\rho\phi)^{(i)}$ are the individual realization. The symbol $\{\ \}$ represents the ensemble average. For statistically steady turbulent flows, the time average and the ensemble average become identical, i.e.

$$\{\phi\} = \langle \phi \rangle, \quad \frac{\{\rho\phi\}}{\{\rho\}} = [\phi]. \tag{10}$$

In summary, the experimental "mean" values for the compressible flow are either the density-weighted time average $[\phi]$ or the density-weighted ensemble average $\{\rho\phi\}/\{\rho\}$, expressed by Equations (8) and (9), respectively.

Now, in PRNS, the temporally filtered values $\overline{\phi}$, $\tilde{\phi}$ of turbulent variables are directly calculated. As a result, this enables an apple-to-apple comparison between the PRNS data and experimental data. In Reference [8], relations between the PRNS data and the experimental data have been established for the first order, second order and higher order correlations. Furthermore, the relations for the Reynolds stresses and the scalar fluxes (which are second order moments formed by the zero-mean fluctuating velocities and scalars) can also be derived. Here we list these relations under the statistically steady condition:

$$[u_i] = \langle \overline{\rho}\, \tilde{u}_i \rangle / \langle \overline{\rho} \rangle, \quad [e] = \langle \overline{\rho}\, \tilde{e} \rangle / \langle \overline{\rho} \rangle \tag{11}$$

$$[u_i e] = \left\langle \overline{\rho \widetilde{u_i e}} \right\rangle / \langle \overline{\rho} \rangle, \quad [u_i u_j] = \left\langle \overline{\rho \widetilde{u_i u_j}} \right\rangle / \langle \overline{\rho} \rangle, \quad [u_i u_j u_k] = \left\langle \overline{\rho \widetilde{u_i u_j u_k}} \right\rangle / \langle \overline{\rho} \rangle, \cdots. \tag{12}$$

Equation (11) indicates that the experimentally measured mean velocity and mean scalar (terms on the left hand side of the equation) can be compared directly with the post-processed PRNS data (terms on the right hand side). Equation (12) cannot be used for direct comparison, because the unclosed terms are involved; however, they are useful for establishing the following relations for the Reynolds stresses and the scalar fluxes:

$$R_{ij} = T_{ij} + \langle \tau_{ij} \rangle / \langle \overline{\rho} \rangle, \tag{13}$$

$$R_i = T_i + \langle q_i \rangle / \langle \overline{\rho} \rangle, \tag{14}$$

where,

$$R_{ij} \equiv \langle \rho (u_i - [u_i])(u_j - [u_j]) \rangle / \langle \rho \rangle = [u_i u_j] - [u_i][u_j], \tag{15}$$

$$R_i \equiv \langle \rho (u_i - [u_i])(e - [e]) \rangle / \langle \rho \rangle = [u_i e] - [u_i][e], \tag{16}$$

$$T_{ij} = \langle \overline{\rho}\, \tilde{u}_i \tilde{u}_j \rangle / \langle \overline{\rho} \rangle - \langle \overline{\rho}\, \tilde{u}_i \rangle \langle \overline{\rho}\, \tilde{u}_j \rangle / \langle \overline{\rho} \rangle^2, \tag{17}$$

$$T_i = \langle \overline{\rho}\, \tilde{u}_i\, \tilde{e} \rangle / \langle \overline{\rho} \rangle - \langle \overline{\rho}\, \tilde{u}_i \rangle \langle \overline{\rho}\, \tilde{e} \rangle / \langle \overline{\rho} \rangle^2. \tag{18}$$

The experimentally measured Reynolds stresses R_{ij} and the scalar fluxes R_i are determined according to Equations (15) and (16), respectively. Their PRNS counterparts consists of two components: the first component, T_{ij} or T_i, can be determined by using the directly calculated variables according to Equation (17) or (18); the second component, the unresolved turbulence stresses τ_{ij} or the scalar fluxes q_i, will have to be provided by the subscale models discussed in the next section. It is not difficult to recognize that this second component will actually become the total Reynolds stresses and fluxes when the width of the temporal filter becomes sufficiently large, as the contributions from both T_{ij} and T_i will vanish.

1.4 Mathematical Models for Unresolved Turbulent Stresses and Fluxes

In order to obtain the solution for the large scale turbulence using PRNS equations (4) - (6), we must close this set of equations by modeling the unclosed terms defined in Equation (7): $\tau_{ij} \equiv \bar{\rho}(\widetilde{u_i u_j} - \tilde{u}_i \tilde{u}_j)$, $q_i \equiv \bar{\rho}(\widetilde{u_i e} - \tilde{u}_i \tilde{e})$. They represent the effects of unresolved turbulence in the form of stresses and fluxes.

There are many ways to model these unclosed terms. The more sophisticated method is to directly solve the transport equations of the unresolved turbulent stresses and fluxes, which can be derived from the Navier-Stokes equations (see Reference [8]). This method will require modeling of even higher order unclosed terms appearing in the quite complex transport equation system of τ_{ij} and q_i. A less complicated way is to start from a general constitutive relationship between the unresolved turbulent stresses τ_{ij} and the strain rate of resolved large scale turbulence $\tilde{s}_{ij}$, $\tilde{\omega}_{ij}$. This general constitutive relationship is then simplified according to the flow complexity by truncating the higher order nonlinear terms of $\tilde{s}_{ij}$, $\tilde{\omega}_{ij}$. For example, the simplest form is just a linear relationship; and this is the widely used eddy viscosity model. Even at this level, there exists many approaches to provide the eddy viscosity. The simplest one is the Smagorinsky model [21] and its variations, which explicitly uses the grid size Δ as the length scale. A more sophisticated one is the one-equation model, such as the one proposed by Menon [19], which solves the transport equation of the unresolved turbulent kinetic energy k, and using $\sqrt{k}$ as the velocity scale, but still using the grid size as the length scale. In the PRNS approach, a two-equation model is adopted, which solves the transport equations of the turbulent kinetic energy k and its dissipation rate ε, and uses them to form the length and velocity scales for the unresolved turbulence, thereby eliminating the use of grid size as the length scale for the unresolved turbulence.

Here, we will present a constitutive relationship for the unresolved turbulent stresses, which is derived and simplified from the general constitutive relationship [22] by using the realizability and rapid distortion theory limit. This model contains linear, quadratic and cubic terms.

1.4.1 Modeling of Unresolved Turbulent Stresses τ_{ij}

The model proposed for PRNS is the following:

$$\begin{aligned}\tau_{ij} = & -2 f_1 C_\mu \bar{\rho} \frac{k^2}{\varepsilon}\left(\tilde{s}_{ij} - \delta_{ij}\tilde{s}_{kk}/3\right) + \frac{2}{3}\delta_{ij}\bar{\rho}k \\ & - A_3 f_3 \bar{\rho} \frac{k^3}{\varepsilon^2}\left(\tilde{s}_{ik}\tilde{\omega}_{kj} - \tilde{\omega}_{ik}\tilde{s}_{kj}\right) \\ & + 2A_5 f_5 \bar{\rho} \frac{k^4}{\varepsilon^3}\left[\tilde{\omega}_{ik}\tilde{s}_{kj}^2 - \tilde{s}_{ik}^2\tilde{\omega}_{kj} + \tilde{\omega}_{ik}\tilde{s}_{km}\tilde{\omega}_{mj} - \tilde{\omega}_{kl}\tilde{s}_{lm}\tilde{\omega}_{mk}\delta_{ij} + II_s(\tilde{s}_{ij} - \delta_{ij}\tilde{s}_{kk}/3)\right].\end{aligned} \tag{19}$$

Where, $\tilde{s}_{ij} = \left(\tilde{u}_{i,j} + \tilde{u}_{j,i}\right)/2$, $\tilde{\omega}_{ij} = \left(\tilde{u}_{i,j} - \tilde{u}_{j,i}\right)/2$, $II_s = \left(\tilde{s}_{kk}\tilde{s}_{mm} - \tilde{s}_{kl}\tilde{s}_{lk}\right)/2$. The model coefficients C_μ, A_3 and A_5 are constrained by the realizability condition and rapid distortion theory limit. They are not arbitrary but formulated as (see Reference [22]):

$$C_\mu = \frac{1}{4.0 + A_s \dfrac{k}{\varepsilon} U^*}, \quad A_3 = \frac{\sqrt{1.0 - A_s^2 C_\mu^2 \left(\dfrac{k}{\varepsilon} S^*\right)^2}}{0.5 + 1.5 \dfrac{k^2}{\varepsilon^2} \Omega^* S^*}, \quad A_5 = \frac{1.6 C_\mu \bar{\rho} \dfrac{k^2}{\varepsilon}}{\bar{\rho} \dfrac{k^4}{\varepsilon^3} \dfrac{7 S^* S^* + \Omega^* \Omega^*}{4}}, \tag{20}$$

in which,

$$A_s = \sqrt{6}\cos\varphi, \quad \varphi = \frac{1}{3}\arccos\left(\sqrt{6} W^*\right), \quad W^* = \frac{S_{ij}^* S_{jk}^* S_{ki}^*}{(S^*)^3}, \tag{21}$$

$$U^* = \sqrt{(S^*)^2 + (\Omega^*)^2}, \quad S^* = \sqrt{S_{ij}^* S_{ij}^*}, \quad \Omega^* = \sqrt{\omega_{ij}\omega_{ij}}, \quad S_{ij}^* = \tilde{s}_{ij} - \frac{1}{3}\delta_{ij}\tilde{s}_{kk} \tag{22}$$

The coefficients f_1, f_3 and f_5 are functions of Δ_T/T , i.e. the ratio of the temporal filter width to the global time scale of the turbulent flow of interest. These functions must have the following property:

$$f_i\left(\frac{\Delta_T}{T}\right) = \begin{cases} 0 & \text{if } \dfrac{\Delta_T}{T} \to 0 \\ 1 & \text{if } \dfrac{\Delta_T}{T} \to 1 \end{cases} \tag{23}$$

This is because the unresolved turbulent stresses τ_{ij} must vanish when the filter width Δ_T vanishes, and τ_{ij} must approach the Reynolds stresses R_{ij} as Δ_T increases towards T. In PRNS, $\Delta_T/T < 1$, so we may make the following expansion:

$$f_i\left(\frac{\Delta_T}{T}\right) = C_0^i + C_1^i \frac{\Delta_T}{T} + C_2^i \left(\frac{\Delta_T}{T}\right)^2 + \cdots \qquad i = 1,3,5. \tag{24}$$

Where all C_0^i must be zero, because f_i must be zero as Δ_T goes to zero. If we retain only the leading term as a first order approximation, then all f_i will have the same form:

$$f_i\left(\Delta_T/T\right) \approx \Delta_T/T \tag{25}$$

We refer the ratio Δ_T/T as the resolution control parameter (RCP). It controls the content of the resolved turbulent scales in the PRNS simulation. We will further discuss this parameter in Section 1.4.5. It should be pointed out that f_i may not be all that simple as shown in Equation (25), more complex functional forms are possible, such as

$$f_i = \left[1 - \exp\left(-A_1^i \cdot \Delta_T / T\right)\right]^{A_2^i} \tag{26}$$

It satisfies the requirement of Equation (23), where A_1^i, A_2^i are constants and need to be determined.

1.4.2 Physical Effects of Unresolved Turbulence

It is important to identify the various mechanisms occurring in the interactions between the resolved and unresolved turbulent scales, and how they are actually modeled in the numerical simulations. In the momentum Equation (4), these interactions are accounted for by the term $\tau_{ij,j}$, which is unclosed and must be modeled. In traditional LES, this term is modeled via the isotropic eddy viscosity. Therefore, the effect of unresolved, small scales appears to be only a modification to the viscosity of the fluid. However, the real, physical situation may be much more complex than just interaction via the eddy viscosity. In fact, the general constitutive relationship of τ_{ij} contains more than just the contribution from an eddy viscosity. As an example, Equation (19), a model for τ_{ij}, contains two parts: linear term and nonlinear (quadratic and cubic) terms. Each part plays different role in the momentum equation. The linear part acts like additional viscosity (called subscale eddy viscosity); and the nonlinear terms act like additional source terms to promote the resolved large scale turbulence. This can be clearly identified by plugging τ_{ij} model into Equation (4),

$$\left(\bar{\rho}\tilde{u}_i\right)_{,t} + \left(\bar{\rho}\tilde{u}_i\tilde{u}_j\right)_{,j} = -\left(\bar{p} + \frac{2}{3}\bar{\rho}k\right)_{,i} + \left(2\left(\bar{\mu} + \mu_T\right)\tilde{s}_{ij} - \frac{2}{3}\delta_{ij}\left(\bar{\mu} + \mu_T\right)\tilde{s}_{kk}\right)_{,j} + S_i^T, \tag{27}$$

where,

$$\mu_T = f_1 C_\mu \bar{\rho}\frac{k^2}{\varepsilon} \tag{28}$$

$$\begin{aligned} S_i^T = &\left\{A_3 f_3 \bar{\rho}\frac{k^3}{\varepsilon^2}\left(\tilde{s}_{ik}\tilde{\omega}_{kj} - \tilde{\omega}_{ik}\tilde{s}_{kj}\right)\right\}_{,j} \\ &-\left\{2A_5 f_5 \bar{\rho}\frac{k^4}{\varepsilon^3}\left[\tilde{\omega}_{ik}\tilde{s}_{kj}^2 - \tilde{s}_{ik}^2\tilde{\omega}_{kj} + \tilde{\omega}_{ik}\tilde{s}_{km}\tilde{\omega}_{mj} - \tilde{\omega}_{kl}\tilde{s}_{lm}\tilde{\omega}_{mk}\delta_{ij} + II_s(\tilde{s}_{ij} - \delta_{ij}\tilde{s}_{kk}/3)\right]\right\}_{,j} \end{aligned} \tag{29}$$

Apparently, the linear part of the model adds an additional subscale eddy viscosity μ_T (which is isotropic) to the physical viscosity of the fluid $\bar{\mu}$; and the nonlinear part provides a complex source term S_i^T, which accounts for the effects of anisotropy and rotation.

We have noticed that, although different subscale eddy viscosity models have been used in different LES approaches, they all have neglected the source term S_i^T. Our preliminary study shows that the source term could become critically important for some flow simulations, especially at relatively low Reynolds numbers, and this will be briefly presented in Section 2.3.

1.4.3 Subscale $k-\varepsilon$ Transport Equations

To complete the proposed model for τ_{ij}, we need k and ε, the unresolved turbulent kinetic energy and its dissipation rate. Their exact transport equations can be derived from the Navier-Stokes equations, and contain some higher order unclosed terms due to the temporal filtering operation. Here, we briefly describe the procedure of the derivation. The first step is to establish the transport equation for τ_{ij}, followed by tracing to establish the equation for τ_{ii} (which is $2\bar{\rho}k$), and this leads to the transport equation for k.

The exact transport equation for the unresolved turbulent stresses τ_{ij} ($\widetilde{\bar{\rho}u_i u_j} - \bar{\rho}\tilde{u}_i\tilde{u}_j$) is

$$\tau_{ij,t} + \left(\tilde{u}_k\,\tau_{ij}\right)_{,k} = D_{ij} + \Phi_{ij} + P_{ij} - \bar{\rho}\,\varepsilon_{ij}\ , \tag{30}$$

where D_{ij}, Φ_{ij}, P_{ij} and $\bar{\rho}\varepsilon_{ij}$ are the diffusion term, the pressure-strain term, the production term, and the dissipation term, respectively. The following expressions indicate that all terms on the right hand side of the equation, except for the production term P_{ij}, are unclosed and must be modeled.

$$\begin{aligned}
D_{ij} &= -\left(\bar{\rho}\widetilde{u_i u_j u_k} - \bar{\rho}\widetilde{u_i u_j}\,\tilde{u}_k\right) + \left\{2\bar{\mu}\widetilde{u_j s_{ik}} - \frac{2}{3}\delta_{ik}\bar{\mu}\widetilde{u_j s_{mm}} - \left[\widetilde{u}_j\left(2\bar{\mu}\,\tilde{s}_{ik} - \frac{2}{3}\delta_{ik}\bar{\mu}\,\tilde{s}_{mm}\right)\right]\right\}_{,k} \\
&\quad + \left(\tau_{ik}\tilde{u}_j + \tau_{jk}\tilde{u}_i\right)_{,k} - \left(\overline{pu_j}\,\delta_{ik} + \overline{pu_i}\,\delta_{jk} - \bar{p}\,\tilde{u}_j\,\delta_{ik} - \bar{p}\,\tilde{u}_i\,\delta_{jk}\right)_{,k} \\
&\quad + \left\{2\bar{\mu}\widetilde{u_i s_{jk}} - \frac{2}{3}\delta_{jk}\bar{\mu}\widetilde{u_i s_{mm}} - \left[\tilde{u}_i\left(2\bar{\mu}\,\tilde{s}_{jk} - \frac{2}{3}\delta_{jk}\bar{\mu}\,\tilde{s}_{mm}\right)\right]\right\}_{,k} \\
\Phi_{ij} &= 2\overline{ps_{ij}} - 2\bar{p}\,\tilde{s}_{ij} \\
P_{ij} &= -\tau_{ik}\tilde{u}_{j,k} - \tau_{jk}\,\tilde{u}_{i,k} \\
\bar{\rho}\,\varepsilon_{ij} &= \left[2\bar{\mu}\left(\widetilde{s_{ik}u_{j,k}} + \widetilde{s_{jk}u_{i,k}}\right) - \frac{4}{3}\bar{\mu}\,\widetilde{s_{mm}s_{ij}}\right] - \left[2\bar{\mu}\left(\tilde{s}_{ik}\tilde{u}_{j,k} + \tilde{s}_{jk}\tilde{u}_{i,k}\right) - \frac{4}{3}\bar{\mu}\,\tilde{s}_{mm}\tilde{s}_{ij}\right].
\end{aligned}$$

Now, if the diffusion term D_{ij} is modeled by a gradient-type diffusion of the eddy viscosity, then the trace of Equation (30) becomes

$$\frac{\partial}{\partial t}\overline{\rho}\,k+\frac{\partial}{\partial x_i}\overline{\rho}\,\tilde{u}_i\,k=\frac{\partial}{\partial x_i}\left[\left(\overline{\mu}+\mu_T\right)\frac{\partial}{\partial x_i}k\right]-\tau_{ij}\tilde{s}_{ij}-\overline{\rho}\,\varepsilon \tag{31}$$

in which, Φ_{ii} has also been neglected by ignoring the compressibility.

The dissipation rate is defined by $\overline{\rho}\,\varepsilon_{ii}/2$, i.e.,

$$\overline{\rho}\,\varepsilon=\left(2\overline{\mu}\,\widetilde{s_{ij}s_{ij}}-\frac{2}{3}\overline{\mu}\,\widetilde{s_{mm}s_{ii}}\right)-\left(2\overline{\mu}\,\tilde{s}_{ij}\tilde{s}_{ij}-\frac{2}{3}\overline{\mu}\,\widetilde{s_{mm}}\,\widetilde{s_{ii}}\right) \tag{32}$$

A model transport equation for the dissipation rate ε can be constructed by the analogy to Equation (31) as

$$\frac{\partial}{\partial t}\overline{\rho}\,\varepsilon+\frac{\partial}{\partial x_i}\overline{\rho}\,\tilde{u}_i\,\varepsilon=\frac{\partial}{\partial x_i}\left[\left(\overline{\mu}+\mu_T\right)\frac{\partial}{\partial x_i}\varepsilon\right]-C_{\varepsilon 1}\tau_{ij}\tilde{s}_{ij}\frac{\varepsilon}{k}-C_{\varepsilon 2}\frac{\overline{\rho}\,\varepsilon^2}{k} \tag{33}$$

where $C_{\varepsilon 1}$ and $C_{\varepsilon 2}$ are the model coefficients. We have adopted the commonly used values of $C_{\varepsilon 1}=1.45$ and $C_{\varepsilon 2}=1.92$ in the present work; keeping in mind that they can be further constructed as functions of local turbulence quantities [23].

1.4.4 Modeling of Unresolved Turbulent Fluxes q_i

A common practice in modeling the unresolved turbulent fluxes $q_i\equiv\overline{\rho}(\widetilde{u_i e}-\tilde{u}_i\tilde{e})$ is to employ the following isotropic model:

$$q_i=-\kappa_T\,\tilde{e}_{,i} \tag{34}$$

κ_T is the eddy diffusivity for the heat, which is often modeled as $\kappa_T=\mu_T/\mathrm{Pr}_T$, where Pr_T (about 0.9) is the turbulent Prandtl number. However, based on the analysis of constitutive relationship (see References [24, 25]), the simplest form that considers the effects of strain and rotation should be

$$q_i=-\kappa_T\tilde{e}_{,i}-\kappa_T\frac{k}{\varepsilon}\left(c_1\tilde{s}_{ij}+c_2\tilde{\omega}_{ij}\right)\tilde{e}_{,j} \tag{35}$$

Where c_1 and c_2 are some undetermined coefficients. This more general model will add modifications to both the diffusion and source terms in Equation (5):

$$\left(\overline{\rho}\,\tilde{e}\right)_{,t}+\left(\overline{\rho}\,\tilde{u}_i\,\tilde{e}\right)_{,i}=\left(\left(\tilde{\kappa}+\kappa_T\right)\tilde{e}_{,i}\right)_{,i}+\overline{ps_{kk}}+\left(2\overline{\mu}\,\widetilde{s_{ij}s_{ij}}-\frac{2}{3}\overline{\mu}\,\widetilde{s_{kk}s_{ii}}\right)+\overline{Q}+S_T^e \tag{36}$$

where the extra source term from the unresolved turbulent fluxes is

$$S_T^e = \left[\kappa_T \frac{k}{\varepsilon} \left(c_1 \tilde{s}_{ij} + c_2 \tilde{\omega}_{ij} \right) \tilde{e}_{,j} \right]_{,i} \tag{37}$$

So far, this term has not been considered in any of the CFD simulations that we are aware of, including the present work.

1.4.5 Resolution Control Parameter *RCP*

In the PRNS approach, the resolution control parameter *RCP*, i.e., the ratio Δ_T / T, is used to regulate the scale content of the resolved field through its role in the models of the unresolved turbulent stresses and fluxes; it implicitly determines the low-end of the resolved, large scales. When $RCP \to 1.0$, the low-end of the resolved scales becomes the scale of turbulent mean flow field, therefore, the unresolved field covers all scales of the turbulence, and the PRNS simulation essentially becomes an unsteady RANS simulation. As the value of *RCP* decreases, the low-end of the resolved scales is expected to move towards small scales; and the unresolved field will only cover the rest of smaller scales.

In planning a very large eddy simulation, we are often concerned with the following questions: how to choose the value of *RCP* from the outset followed by estimating the corresponding numerical grid size required for this simulation? Alternatively, for a given numerical grid size, how to choose *RCP* to yield a resolved scale level that the numerical grid can support?

The following length scale definitions and relationships discussed in References [8], [26] and [27] may help to answer these questions. Let us denote k_{RANS}, ε_{RANS} and k, ε the total turbulent kinetic energy, the total dissipation rate and the subscale turbulent kinetic energy, the subscale dissipation rate, respectively. A simple dimensional analysis suggests that an estimate for the smallest turbulent length scale that can be practically resolved by PRNS is $\eta_{PRNS} = \left(\nu_T^3 / \varepsilon \right)^{1/4}$, where ν_T is the subscale viscosity and ε the subscale dissipation rate. In other words, η_{PRNS} represents the low-end of the resolved scales in PRNS. Similarly, the turbulent integral length scale is estimated to be of the order of $\ell_{RANS} = (\nu_{RANS}^3 / \varepsilon_{RANS})^{1/4}$ (this is consistent with a common estimation given by $k_{RANS}^{3/2} / \varepsilon_{RANS}$), where ν_{RANS} denotes the total turbulent eddy viscosity. Obviously, the mesh size Δ should be smaller than or equal to η_{PRNS}, and the following relationship can be derived using the definition of *RCP* (see [8, 26, 27]):

$$RCP \geq \left(\frac{\Delta}{\ell_{RANS}} \right)^{4/3} \left(\frac{k}{k_{RANS}} \right)^{-2}, \tag{38}$$

When *RCP* is given from the outset, Equation (38) can be used to estimate the largest possible value of the grid spacing Δ relative to the turbulent integral length scale ℓ_{RANS} for a given ratio of k/k_{RANS} (e.g., 10%). On the other hand, if the mesh size is given from the outset, Equation (38) can be used to estimate the value of *RCP* that the given grid size can support. For example, when a given grid resolution Δ/ℓ_{RANS} is about 1.5% and k/k_{RANS} about 11%, Equation (38) indicates that this grid resolution can support PRNS simulations having *RCP* from 1.0 to a value as small as 0.3. For the same given grid, we would obtain RANS type results if *RCP* were about 1.0, and LES or VLES type results if *RCP* were about 0.3 - 0.4. This has been demonstrated in the simulation of the flow field in a single injector flame tube (see Section 3.1). The vorticity contour plots clearly illustrate that the simulated flow field transits from RANS type toward LES type when *RCP* varies from 1.0 to 0.38.

Furthermore, let L be the length of the computational domain, Δ_{RANS} be the mesh size used in the RANS simulation, then the number of grid points needed for a PRNS simulation, $N_{PRNS} \approx \left(L/\Delta\right)^3$, can be estimated as

$$N_{PRNS} \geq N_{RANS} \cdot \left(\Delta_{RANS}/\ell_{RANS}\right)^3 \cdot Rcp^{-9/4} \left(k/k_{RANS}\right)^{-9/2}, \tag{39}$$

where $N_{RANS} \approx \left(L/\Delta_{RANS}\right)^3$ represents the number of grid points required by RANS. Equation (39) provides an estimation of the number of grid points needed for a PRNS simulation when the ratio $\Delta_{RANS}/\ell_{RANS}$ (e.g., 2%) and k/k_{RANS} (e.g., 10%) are given.

2. Evaluation of PRNS using NCC

Ultimately, we want to use the NCC for performing the very large eddy simulation of combustor flows. At the present stage, the focus is the fundamental assessment of the implemented subscale model and the establishment of a sufficiently "clean" numerical setting for the PRNS calculations.

We have conducted systematic studies to examine the effects of the following numerical artifacts on the calculation of turbulent fluctuations: the truncation errors associated with the temporal-spatial discretization, the convergence errors associated with the "pseudo-time" iteration, the generation of disturbances by forcing the redistribution of the residuals, the round off errors associated with the computation of the pressure gradient in low Mach number compressible flow, and the added artificial dissipation required for maintaining the numerical stability. The results of these studies indicate that the calculated turbulent fluctuations are quite sensitive to the setting of these numerical artifacts, and we have established a sufficiently "clean" numerical setting for the PRNS calculations (see the following section). The simulations presented in this paper are all conducted using this numerical setting as the baseline.

At this stage of the evaluation, we have selected the fully developed turbulent pipe flows as the focus, because they are well known fundamental flows with experimental data [20], and they are amenable to the use of periodic boundary conditions, thereby, allowing us to concentrate on the subscale model itself and free from the complicating issues associated with the inflow and outflow boundary conditions. We will at first examine the PRNS results obtained from using only the eddy viscosity type of model at different Reynolds numbers, followed by exploring the behavior of a more general subscale model that accounts for both the effect of eddy viscosity and the effects of anisotropy and rotation.

In this report, we will present the results obtained using various values of RCP for a moderately large Reynolds number of 150,000 and a relatively low Reynolds number of 15,000 (based on the centerline axial velocity and the pipe diameter). Our criteria for a successful simulation are: the simulation must produce a broadband scales of turbulent fluctuations, in particular, the power spectrum must cover at least two or three orders energy variations from large to small scales; and the simulation must produce reasonable or better mean profiles than those provided by the RANS simulation, when compared with available experimental data.

In the following, Sections 2.1 and 2.2, discuss the PRNS results obtained by using a subscale model accounting for only the effect of eddy viscosity, i.e., the unresolved turbulent stress τ_{ij} is represented only by the linear part of Equation (19). Subsequently, the results of a preliminary study are described in Section 2.3, which demonstrate that the nonlinear part of τ_{ij} can have a significant effect on the numerical solution, especially for flows at lower Reynolds numbers.

2.1 Turbulent Pipe Flow at Reynolds Number 150,000

A fully developed turbulent pipe flow at Reynolds number 150,000 has been selected to represent turbulent pipe flows at moderate or large Reynolds numbers, in which the turbulent fluctuations are quite energetic and will not be easily damped by the inherent numerical dissipation of a CFD code. Figure 1 shows the computational domain of the pipe with a diameter of 0.12936 m, which has an aspect ratio (length to diameter) of five and 900,705 hexahedra elements. Such a grid resolution is typical for a fine grid RANS simulation. We will use this same grid for all PRNS simulations.

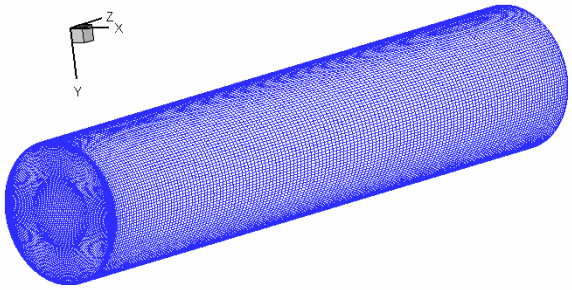

Figure1: Computational domain for the pipe flow simulations.

Periodic boundary conditions are imposed at the inlet and the outlet of the computational domain. A generalized wall function [17] is applied for the solid wall. The initial conditions are created by a specified axial velocity profile randomly disturbed in all three directions. All simulations are performed using the NCC code, which uses the dual time stepping method. The baseline numerical setting is the following:

- Initial gauge (fluctuating) pressure = 0.0.
- No residual smoothing is applied.
- Coefficients of the second- and fourth-difference dissipation terms (2^{nd} and 4^{th}) are 0.0 and 0.001, respectively.
- For the convergence of the pseudo-time (inner) iteration, three orders of magnitude reduction in the residuals is typically required, i.e., the convergence order = 3. Otherwise, it is stipulated that the iteration must reach the maximum number of 120. The CFL number for the pseudo time is 1.0.
- The physical time step dt = 2.5E-05 second.

Following the analysis described in Section 1.4.5, in order for the present grid resolution to be able to capture those turbulent fluctuations that are responsible for more than 90% of the total turbulent kinetic energy, the value of RCP should be between 0.3-0.4. If RCP increases, the content of the unresolved scales will expand into larger eddies, and the unsteadiness of the calculated, resolved part will diminish. Keep increasing RCP, the PRNS solution will eventually become the RANS solution. This trend can be observed from the numerical results with RCP = 0.2, 0.3, 0.34, 0.4, 0.5, 0.8 and 1.0, which are presented in sections A.1-A.7 of the Appendix A. Furthermore, the results obtained by the traditional RANS approach are also shown in section A.8. Note that the numerical setting for RANS is somewhat different from the numerical setting of PRNS, but the same grid is used.

Here, we present the numerical simulation with RCP = 0.3 as a representative of PRNS simulation of very large scale turbulence. We consider simulations with RCP ≥ 0.4 as the very, very large eddy simulations.

Figure 2 shows the time histories of velocity components recorded at the probe 1, which is located at the centerline of the pipe. Here, u and v are the tangential and the radial velocity components, respectively; and w is the axial velocity component. Time histories at other locations, such as the probe 6 (the point between the centerline and the wall) and the probe 14 (near the wall), can be found in Section A.2. These time histories indicate that the turbulent fluctuations are fully developed after 10,000 time steps. The fully developed, various turbulent scales can also be seen from the snap shots of various turbulent quantities, such as u, v, w, pg, k, and $\mu + \mu_T$. For example, Figure 3 is the contour plots of w and u at time step 36,400, and Figure 4 is the contour plots of gauge pressure pg and subscale turbulent kinetic energy k. These snap shots do reveal the presence of wide range turbulent scales and the statistical homogeneity in the axial direction. As a fully developed pipe flow, the tangential and the radial velocity components must be statistically zero, and the gauge pressure (which does not include the mean pressure gradient) must be statistically constant. These conditions are in deed met by the numerical simulations, as shown by both the time histories and the contour plots.

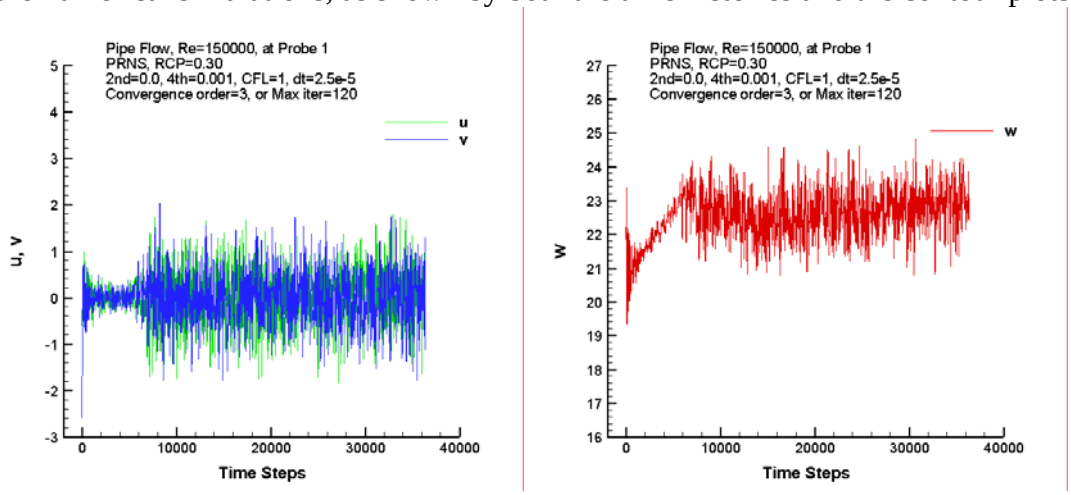

Figure 2: Time histories of velocity components at the centerline (Probe 1).

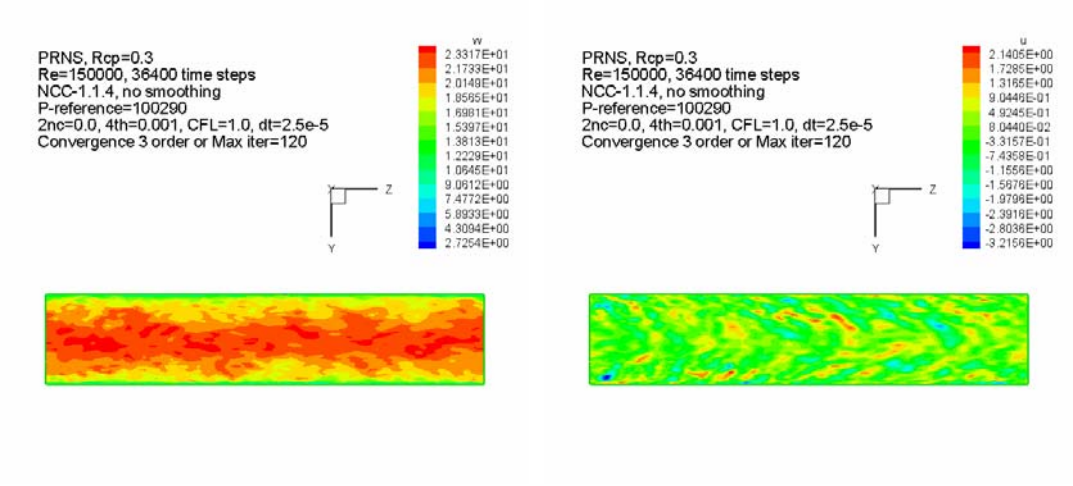

Figure 3: Snapshot contours of w and u at the time step 36400.

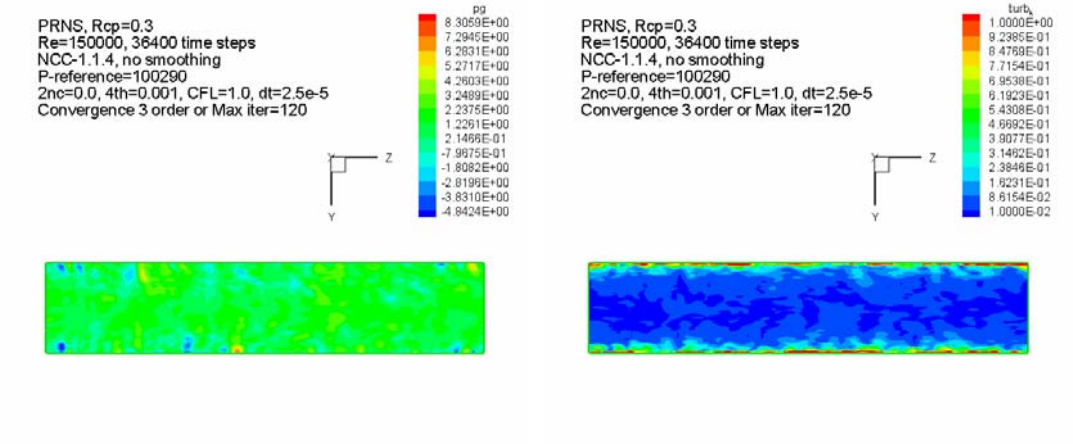

Figure 4: Snapshot contours of gauge pressure and subscale turbulent kinetic energy.

Examining the time power spectrum of turbulent fluctuations and the two-point correlations is another way to assess the quality of the numerical simulation. Figure 5 and Figure 6 present the power spectrum density (PSD) of the w component and its two-point (time) correlation at three locations (Probes 1, 6 and 14). The broadband feature of the PSD (i.e. more than two orders of energy variation from small scale to large scale) and the typical two-point correlation shapes (i.e. the correlation rapidly decreases as the time lag increases) indicate that the PRNS simulation with RCP = 0.3 does mimic the statistical features of a fully developed turbulence.

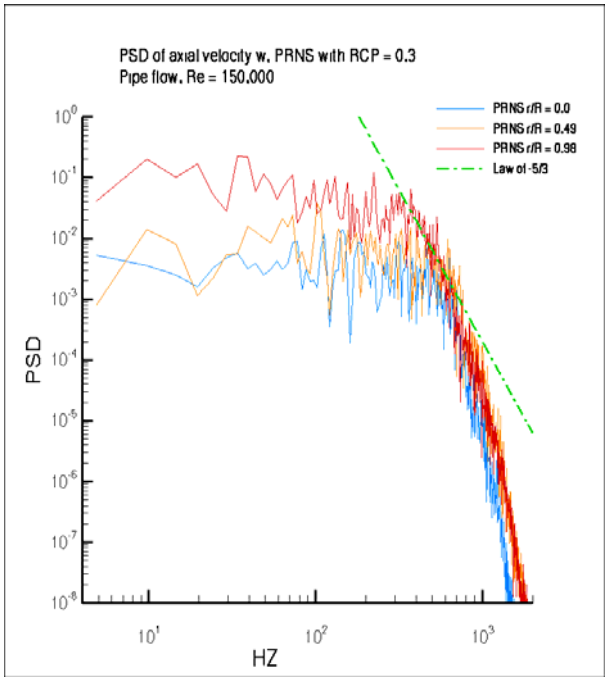

Figure 5: Power spectrum density of w component at Probes 1, 6 and 14.

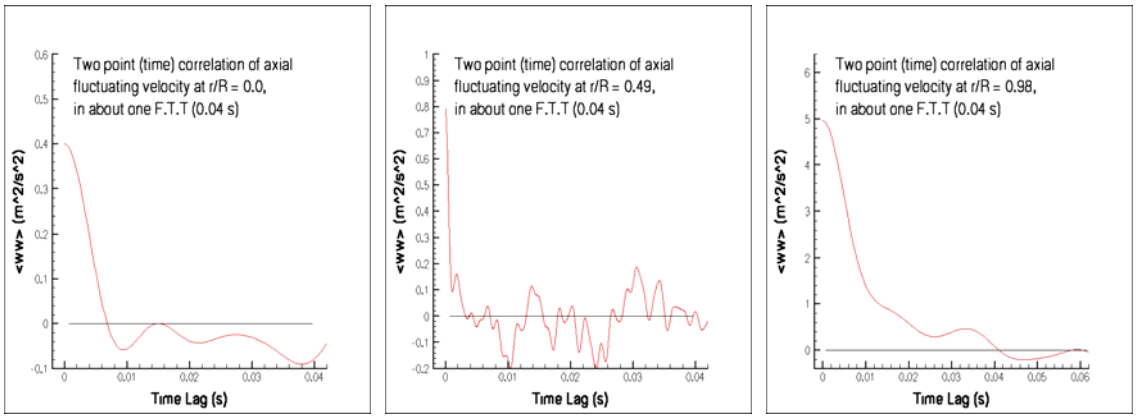

Figure 6: Two point (time) correlations of <ww> at Probes 1, 6 and 14.

There exists an experimental data of axial mean velocity profile at Reynolds number of 145,700, which is very close to 150,000. (Reference [20]). Figure 7 compares the PRNS results with the experimental data and the RANS results. As it can be seen, the result of PRNS compares reasonably well with the experimental data while the steady RANS result exhibits significant under-prediction.

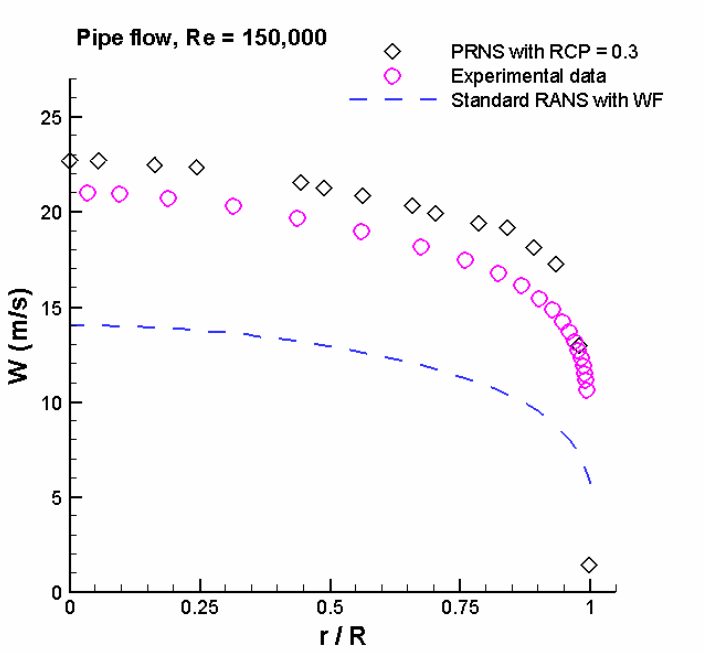

Figure 7: Comparison of W mean profiles between PRNS, RANS and experimental data.

To examine the behavior of PRNS at different values of RCP, we have also performed simulations with RCP = 0.2, 0.34, 0.4, 0.5, 0.8 and 1.0 using the same numerical setting. The results of these individual cases can be found in Appendix A. In the following, we summarize the major observations distilled from this parametric investigation.

In general, we find that, for a given grid resolution, there exists a minimum value of RCP (say 0.3) below which (say 0.2) the intended scale content of the operating subscale model cannot be properly supported by the resolution level of the given grid. In effect, this amounts to an attempt of using a coarse grid to execute a direct numerical simulation (DNS). The results will not be physically meaningful, and this is demonstrated by the results of the simulation with RCP = 0.2 (Section A.1). Although we still see a strong development of fluctuations, the operating subscale model does not play a role in their development, because the subscale turbulent kinetic energy appears to be erroneously small, i.e. k is of order 1.E-11, and the subscale eddy viscosity is nearly zero.

On the other hand, when RCP increases (e.g., RCP = 0.3, 0.34, 0.4… 1.0), the resolved part will change from fluctuations consisting of very large scale turbulence toward Reynolds-averaged mean value. This can be seen from Figure 8, the time history of the centerline axial velocity component (w), and Figure 9, the snapshot of the w contours at the end of each simulation. Figure 10 shows the instantaneous axial velocity w profiles from PRNS simulations with RCP = 0.3, 0.5, 0.8 and 1.0, also included is the experimental data for the mean profile. These figures indicate that PRNS with RCP = 0.3 can mimic the turbulent motion associated with a wide range of large scale turbulence, and can predict the mean profile reasonably well.

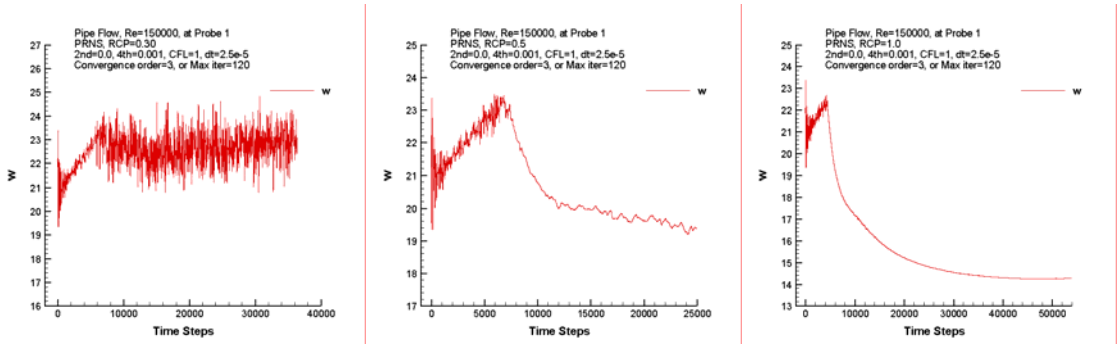

Figure 8: Time history of centerline w component with RCP = 0.3, 0.5 and 1.0.

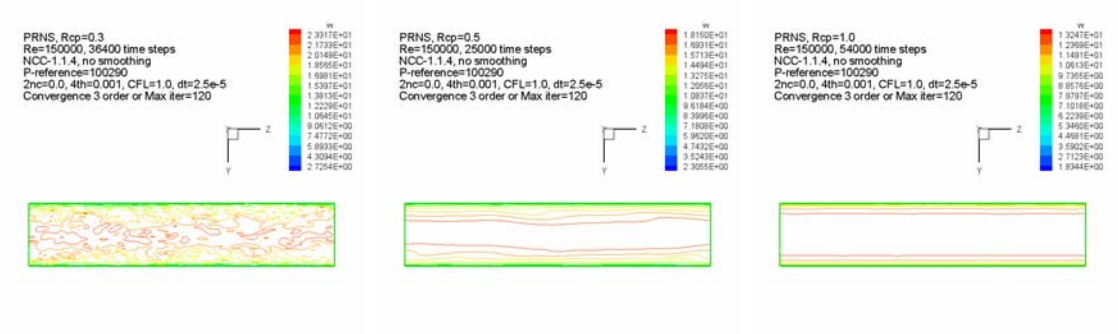

Figure 9: Contours of w component at center plane with RCP = 0.3, 0.5 and 1.0.

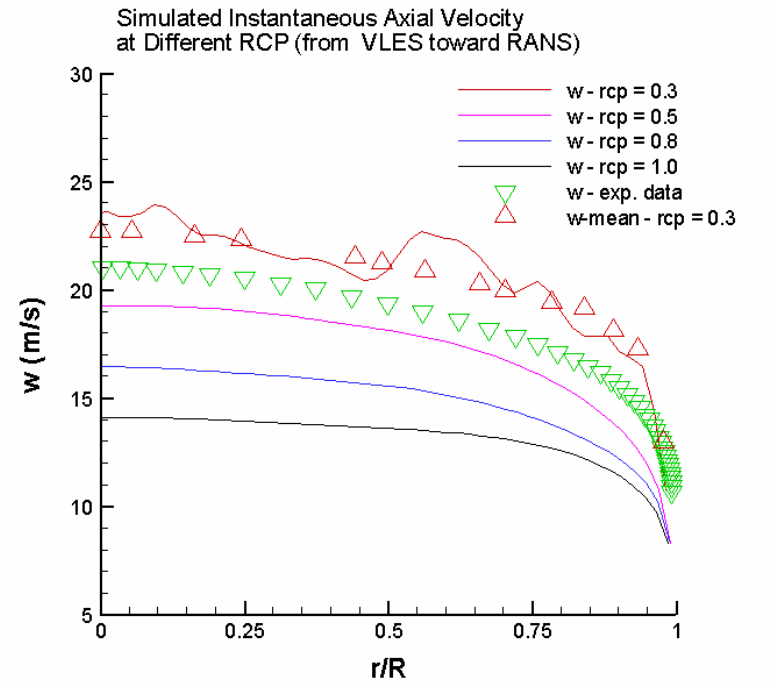

Figure 10: Instantaneous w profiles with RCP = 0.3, 0.5, 0.8 and 1.0.

The results shown in Figure 10 also indicate that the accuracy of the current subscale model becomes progressively worse as RCP increases, and, when RCP=1, the time-averaged profile coincides with the mean profile from the steady RANS calculation using a standard $k-\varepsilon$ model (see Section A.8). This is expected, because, when RCP = 1, the current PRNS is equivalent to an unsteady RANS simulation using a standard $k-\varepsilon$ model. It is desirable to further improve the current PRNS subscale model so that it will lead to better RANS results than those from the standard $k-\varepsilon$ mode. For example, a so called "Low-Reynolds number $k-\varepsilon$ model" ([28]) may be considered as a candidate for this purpose.

2.2 Turbulent Pipe Flow at Reynolds number 15,000

A pipe flow at Reynolds number 15,000 has been selected to represent turbulent pipe flows at lower Reynolds numbers. In these cases, physically, the turbulent fluctuations are relatively weak, and computationally, they are more susceptible to be damped by the numerical dissipation associated with the truncation errors and the added artificial dissipation. We have performed the PRNS simulations using RCP = 0.0, 0.2, 0.3, 0.34, 0.4, 0.5 and 1.0. The grid and the numerical setting are the same as those for Re=150,000, except that the time step is now dt = 4.E-04 (the flow is now slower) and a much smaller added fourth-difference dissipation (4^{th} = 0.00001) is used to further reduce the numerical damping. The detailed, individual results can be found in Appendix B (B.1-B.7). Generally speaking, in all of these simulations, the development of the initially induced fluctuations can not be sustained and the calculated flows do not evolve towards a fully developed turbulent flow.

In the case of RCP = 0.0, the simulation is performed without the use of subscale eddy viscosity. The results in Appendix B.1 indicate that the turbulent fluctuations have been damped out and the flow is evolving toward a laminar pipe flow.

In the case of RCP = 0.2, we see that the initially induced fluctuations are damped out sooner than in the case of RCP =0.0. This is apparently due to the effect of the invoked subscale eddy viscosity. As shown in Appendix B.2, all velocity fluctuations are damped out, and the subscale turbulent kinetic energy is practically zero. Therefore, the simulation is also evolving toward a laminar pipe flow.

When RCP = 0.3 or larger, the simulations appear to be quite different. The subscale turbulent kinetic energy is no longer vanishingly small, and the operating subscale eddy viscosity is more appreciable.

In the case of RCP = 0.3 (Appendix B.3), we see some sustained fluctuations. But clearly, it is not evolving toward a fully developed turbulent pipe flow. It seems that, at this particular value of RCP, the operating subscale eddy viscosity is small enough to still allow the presence of some large scale turbulence in the resolved field, but large enough to hinder their further development.

In the cases of RCP = 0.34, 0.4 and 0.5 (Appendix B.4, B.5, and B.6), we see that all fluctuations are again damped out, but the unresolved turbulent kinetic energy remains appreciably large. This suggests that the calculated solution is the "mean" of some under-developed turbulent flow, in which the dissipation effect of the operating subscale viscosity becomes unrealistically dominant.

In the case of RCP =1.0 (Appendix B.7), the PRNS simulation amounts to an unsteady RNAS simulation. The calculated solution is the Reynolds-averaged mean value. The accuracy of the PRNS results is the same as that of the steady RANS results using a standard $k-\varepsilon$ model.

It should be noted here that this Re=15,000 pipe flow had been previously simulated by PRNS using the NCC with RCP = 0.38. Although the same grid was used, the numerical setting was quite different, namely, the previous setting was not as computationally "clean" as the present one. It had allowed the round off error associated with the computation of the pressure gradient to become appreciable, it had adopted a lower order convergence criterion for the inner "pseudo-time" iteration, and it had used residual redistribution during the inner iteration. The net effect was that various, apparently random sources were injected into the simulation to promote the appearance of fluctuations in the calculated results. Somehow, the time-averaged results compared reasonably well with the experimental data (see Reference [8]), we now consider the good comparison as fortuitous. Nevertheless, this experience does suggest that, in addition to the eddy viscosity type of effect, physics-based sources type of effect need to be included in the subscale model to more faithfully mimic the interactions between the resolved and un-resolved turbulence scales, in particular, when the physical fluctuations involved are relatively weak, or when the local Reynolds number is relatively low. We have been exploring this idea, and some of the preliminary results are presented in the following section.

2.3 Preliminary Study of A Nonlinear Subscale Model

In Section 1.4, we have provided a nonlinear formulation of the subscale model for the unresolved turbulent stresses τ_{ij} , Equation (19), as well as the resulting source terms in the momentum equation and the energy equation, i.e., Equation (29) and Equation (37), respectively. Equation (19) may be rewritten as

$$\begin{aligned}\tau_{ij} - \frac{2}{3}\delta_{ij}\bar{\rho}k = &-2\,\mu_T\left(\tilde{s}_{ij} - \delta_{ij}\tilde{s}_{kk}/3\right)\\ &- A_3 f_3 \bar{\rho}\frac{k^3}{\varepsilon^2}\left(\tilde{s}_{ik}\tilde{\omega}_{kj} - \tilde{\omega}_{ik}\tilde{s}_{kj}\right)\\ &+ 2A_5 f_5 \bar{\rho}\frac{k^4}{\varepsilon^3}\left[\tilde{\omega}_{ik}\tilde{s}_{kj}^2 - \tilde{s}_{ik}^2\tilde{\omega}_{kj} + \tilde{\omega}_{ik}\tilde{s}_{km}\tilde{\omega}_{mj} - \tilde{\omega}_{kl}\tilde{s}_{lm}\tilde{\omega}_{mk}\delta_{ij} + II_s(\tilde{s}_{ij} - \delta_{ij}\tilde{s}_{kk}/3)\right].\end{aligned} \tag{40}$$

where μ_T is the subscale eddy viscosity defined by Equation (28). And, at this stage of the development, all the coefficients f_1, f_3 and f_5 are set equal to the resolution control parameter RCP.

The PRNS results presented in Sections 2.1 and 2.2 are obtained with a subscale model involving only μ_T, the nonlinear part that reflects the effects of anisotropy and rotation has been ignored. As mentioned before, this nonlinear part leads to additional source term in the momentum equation for the resolved turbulence, and this source term may play an important role when the unresolved scales become larger or when the flows are at lower Reynolds numbers.

To explore this idea, we have included the nonlinear terms in the subscale model and repeated the PRNS simulation of the pipe flow at Reynolds number 15,000. The results are very encouraging. The detailed results for the case of RCP = 0.3 can be found in the Appendix C.1. They indicate that the fluctuations of velocity components are now being sustained and evolving towards a fully developed state. This is clearly due to the new source terms from the nonlinear part of τ_{ij}.

The effect of nonlinear subscale model on the PRNS simulations for flows at relatively large Reynolds numbers has been examined by using the pipe flow at Reynolds number 150,000 with RCP = 0.3. For this Reynolds number, we employed the existing flow field previously established with the linear subscale model as the starting condition, and the simulation was then performed with the nonlinear subscale model. We have not found much dramatic changes between the two simulations, except that the subscale turbulent kinetic energy as well as the subscale eddy viscosity appears to be stronger in some regions. The detailed results can be founded in Appendix C.2.

A more extensive study of the effects of the nonlinear subscale model is under way, and the results will be reported elsewhere.

3 Preliminary Applications

To illustrate the intended applications for the PRNS approach, we include here some sample results previously published in References [8] and [27].

3.1 Non-Reacting Flow in A Single Injector Flame Tube

This injector has been used in an industrial combustor. The flow field inside a single injector flame tube has many important features occurring inside a real combustor, such as massive separation, strong swirling and recirculation. This flow has been studied both experimentally and numerically [29].

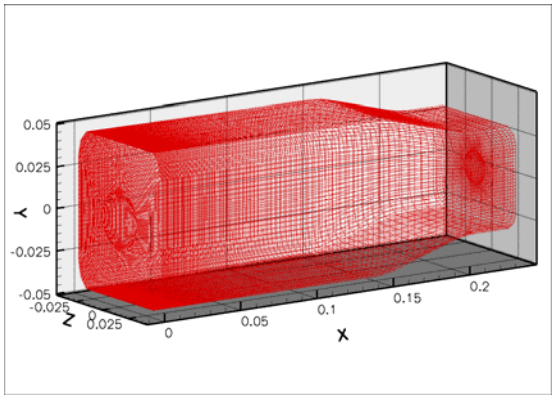

Figure 11: Computational domain for RANS and PRNS simulations.

Figure 11 shows the computational domain. The combustion chamber is a rectangular box. A highly swirling jet is injected from a circular inlet. The Reynolds number based on the inlet axial velocity and diameter is about 3,200,000. A grid of 495,000 elements was used in the simulation. At the inlet, only the mean profiles of velocities, density and temperature are specified. At the outlet, simple extrapolation is used to minimize the possible unphysical reflections. Figures 12 and 13 are the instantaneous contours of the axial velocity and the vorticity magnitude, respectively. They are obtained from three different values of *Rcp* : 1.0, 0.46, and 0.38. Figures 14 and 15 illustrate the instantaneous features of the kinetic energy of the unresolved scales and the effective eddy viscosity ($\mu + \mu_T$). These results demonstrate that the characteristics of simulation will change from RANS towards LES as the RCP reduces from 1.0. Figure 16 gives the comparison between several instantaneous centerline axial velocity distributions with the mean value provided by LES data. Apparently, the simulation with RCP = 0.38 and a relatively coarse grid captured many features of LES. Figure 17 shows the time history of the axial velocity fluctuation and its power spectrum at a centerline location inside the recirculation region. The broadband feature of the power spectrum clearly indicates that a wide range of large-scale turbulence has been captured by PRNS.

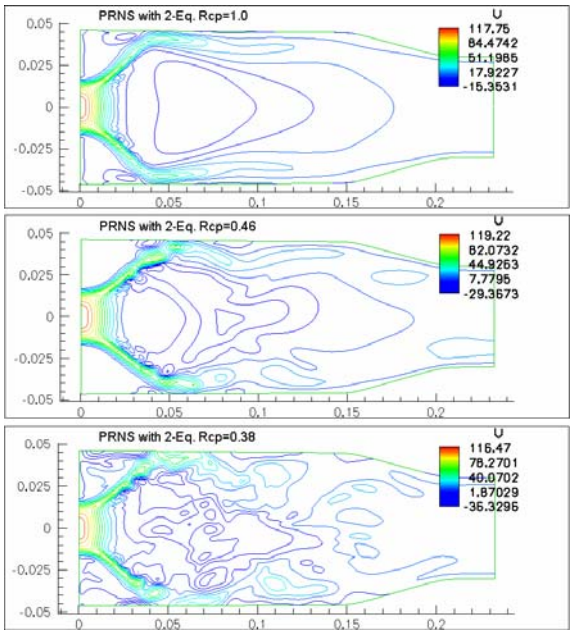

Figure 12: Contours of axial velocity

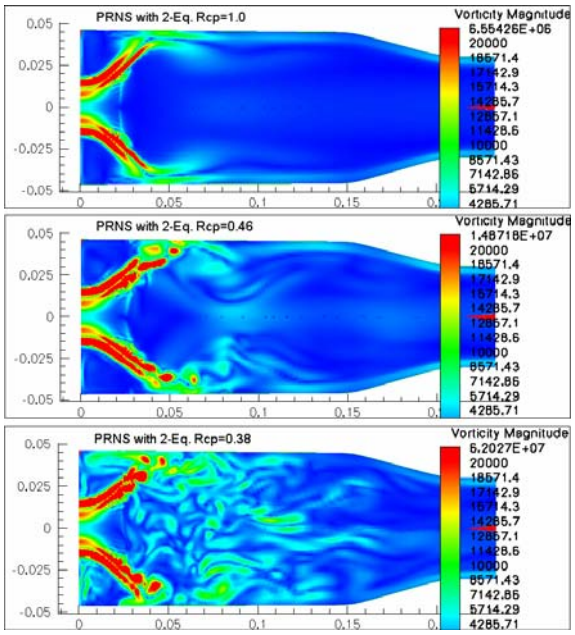

Figure 13: Contours of vorticity magnitude.

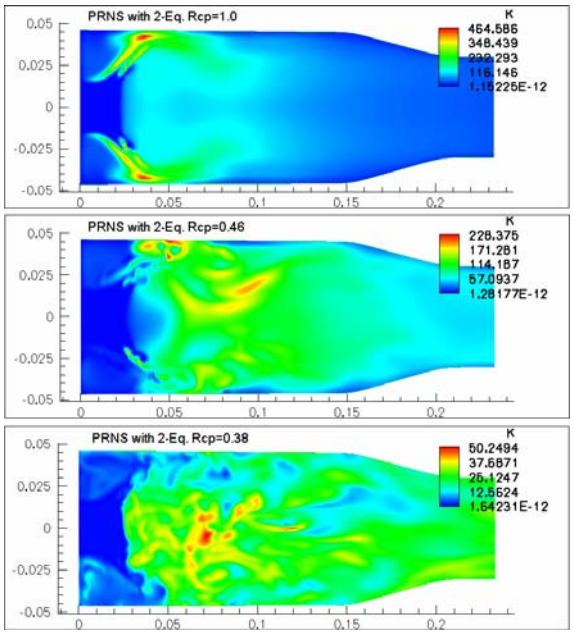

Figure 14: Unresolved kinetic energy.

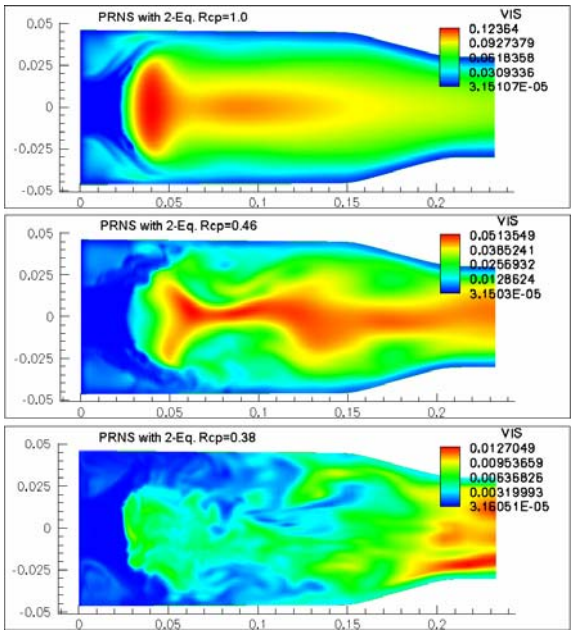

Figure 15: Subscale eddy viscosity.

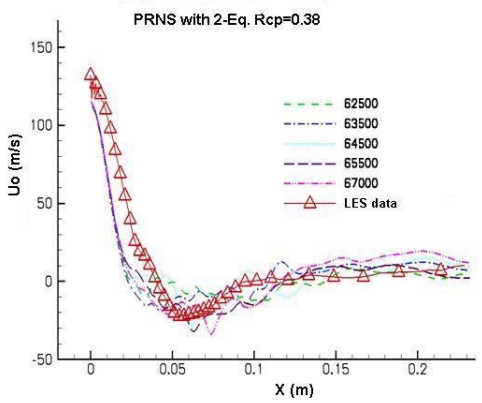

Figure 16: Axial velocity profiles.

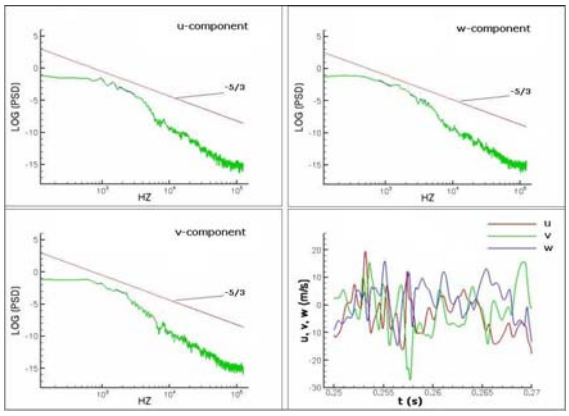

Figure 17: Velocities and power spectrum.

3.2 Reacting Flow in a Lean Direct Injection (LDI) Hydrogen Combustor

The so called C4 configuration was one of the experimental LDI hydrogen combustors [30] studied at NASA GRC. It was designed to study the effects of fuel/air mixing on the combustion, especially on the NOx emission. In general, better mixing of fuel and air will improve the combustion as well as reduce the NOx emission. To assist the experimental studies, we had carried out numerical simulations using both RANS and PRNS approaches.

The geometry for the C4 configuration is shown in Figure 18. It consists of seven converging-diverging nozzles, the fuel (hydrogen) is injected into the upper part of each nozzle perpendicularly through four fine fuel tubes, the air from the inlet flows to nozzles and meets with the high speed hydrogen jets, the mixture of air and hydrogen then flows through the converging-diverging nozzles into the combustor. The studies were focused on the effectiveness of fuel/air mixing and its effect on combustion. An unstructured tetrahedral grid was used for this complex geometry. The total number of cells is about 3.5 millions. The same grid has been used for both RANS and PRNS simulations.

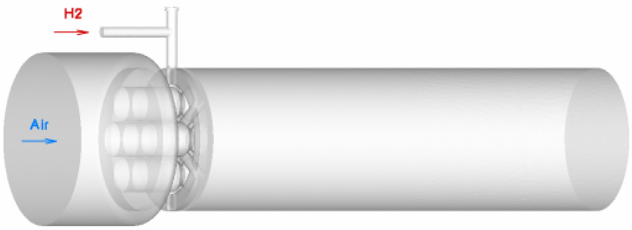

Figure 18: The configuration of a LDI hydrogen combustor.

RANS Simulation of the C4 LDI Hydrogen Combustor

We started with the steady RANS simulation of a non-reacting flow using the nonlinear k-ε RANS model [15]. The aim was to examine the global features of the fuel/air mixing. Subsequently, we switched the combustion on to perform the steady RANS simulation of the reacting flow. The combustion model used in this simulation was a one based on the eddy dissipation concept [31]. The inlet and outlet boundary conditions were set according to the experimental studies. The mass flow rate and temperature for air at the inlet were 0.40012 kg/s and 700.212 K; the mass flow rate and temperature for hydrogen at its inlet were 0.00482 kg/s and 588.555 K. The outlet back pressure was set to 622,040 Pa.

Results of steady non-reacting RANS simulation

The global flow feature is indicated in Figure 19, which is a contour plot of the axial velocity at a center plane. Figure 20 shows the vorticity magnitude at the same plane. Figure 21 is the distribution of the hydrogen mass fraction in the lateral cross section at the nozzle throat. Figure 22 is the distribution of the hydrogen mass fraction at a different lateral section located at the exit of the nozzles, i.e., the entrance of the combustor. These fuel mass fraction plots can be used to assess how well the mixing is achieved by the design of this particular C4 configuration.

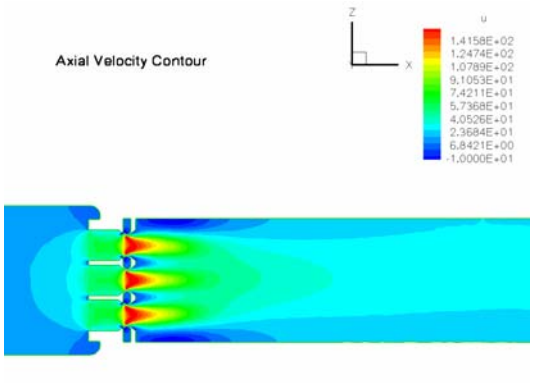

Figure 19: Axial velocity (RANS).

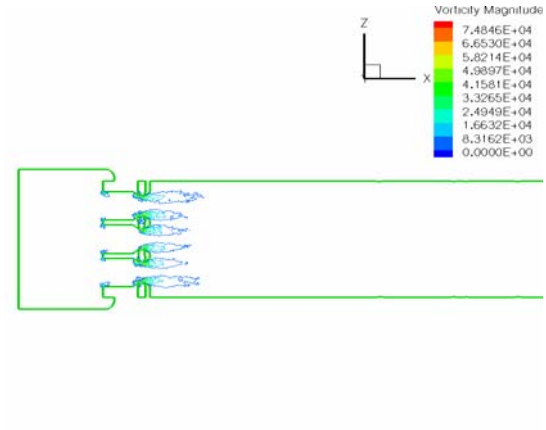

Figure 20: Vorticity Magnitude

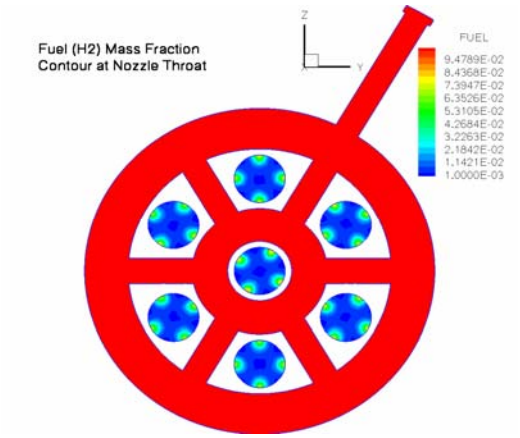

Figure 21: Fuel mass fraction at nozzle throat.

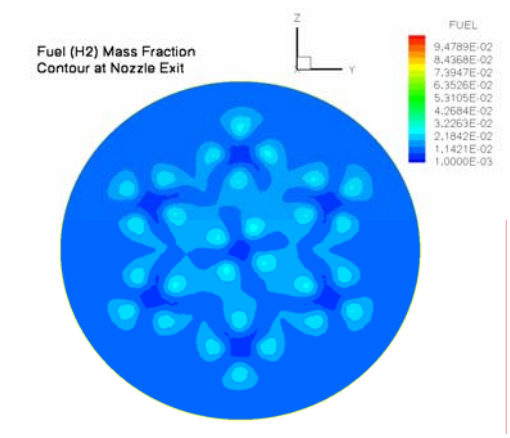

Figure 22: Fuel mass fraction at nozzle exit.

Results of steady reacting RANS simulation

As mentioned before, a simple turbulent combustion model, namely, the Magnussen model [31] was used to obtain a global picture of the flame structures. Figures 23 and 24 are the contour plots of axial velocity and vorticity magnitude at the center plane. We observed that the axial velocity and the vorticity are much larger and stronger than that revealed in the non-reacting simulation. Figure 25 is the distribution of temperature at the center plane, and Figure 26 is the temperature contour in the neighborhood of a nozzle. These temperature distributions indicate that the combustion occurs quite close to the exit of the nozzles.

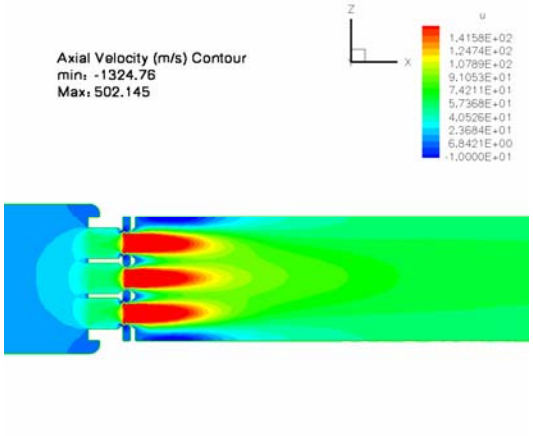

Figure 23: Contour of axial velocity.

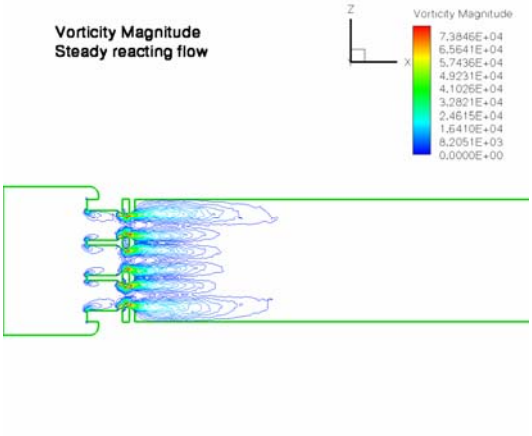

Figure 24: Contour of vorticity magnitude.

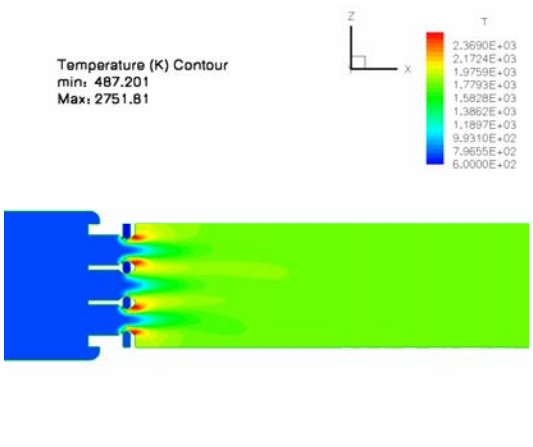

Figure 25: Temperature at center plane.

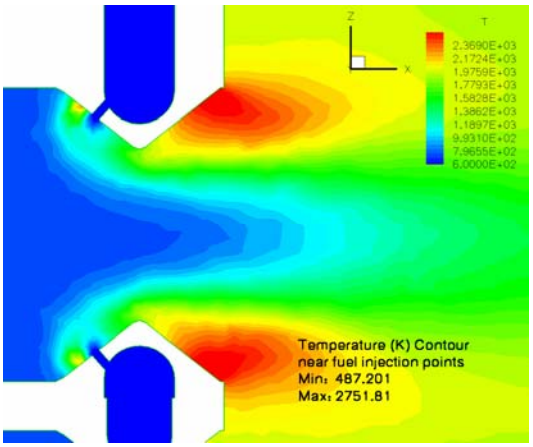

Figure 26: Temperature near the injection

PRNS Simulation of the C4 LDI Hydrogen Combustor

A very large eddy simulation using PRNS was carried out using the steady RANS results of the reacting flow as the initial condition. The resolution control parameter was RCP = 0.38.

Figures 27 and 28 are the snapshots of the contours of the axial velocity and the vorticity magnitude, which indicate the presence of unsteady, large scale flow structures that are absent from the corresponding RANS simulation (see Figures 23 and 24). Figure 29 shows the instantaneous temperature contours at the center plane. Figure 30 is the temperature distribution in a nozzle. These figures also show a very different flame structures from that provided by the RANS simulation (see Figures 28 and 29). We also noticed that the maximum flame temperature, 2543 K, as predicted by PRNS near the exit of the nozzles, is lower over 200 degrees than that predicted by RANS.

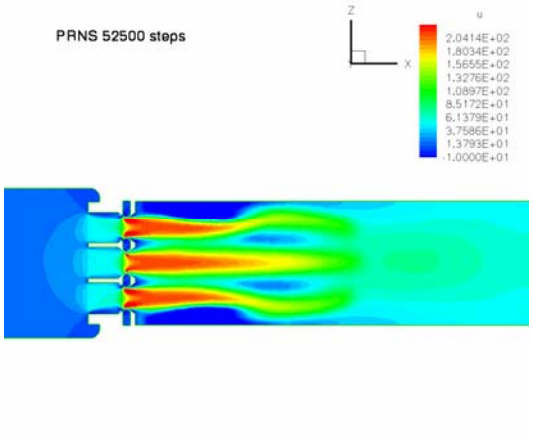

Figure 27: Contour of axial velocity.

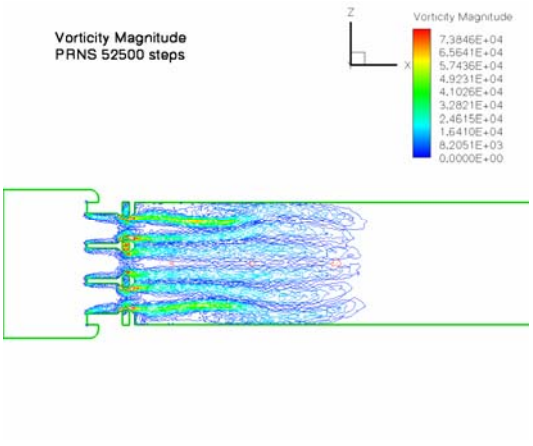

Figure 28: Contour of vorticity magnitude.

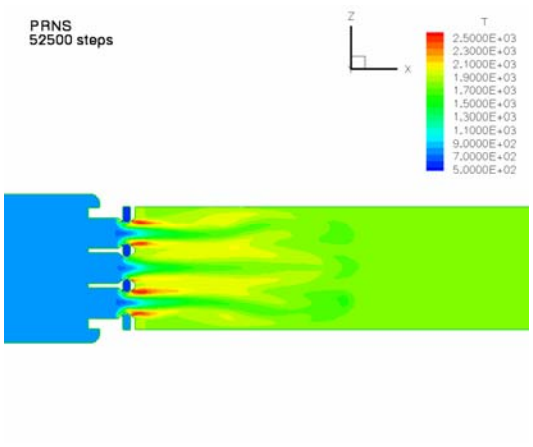

Figure 29: Temperature at the center plane

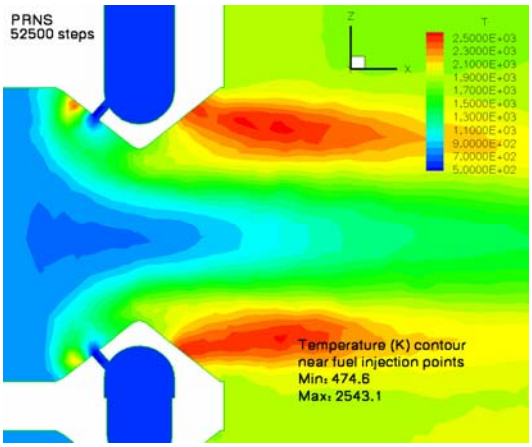

Figure 30: Temperature near the injection.

The RANS and PRNS simulations yield different features. RANS can quickly provide a global picture of the combusting flow, and can be used as the initial condition for the PRNS simulation. The explicit presence of the unsteady, large flow structures in the calculation will then improve the fidelity of the combustion simulation. By leveraging the strengths of these two complimentary approaches, higher fidelity analysis of turbulent combustion in realistic combustor and operating conditions can then be routinely conducted at reasonable computational costs.

III. Findings and Recommendations

The partially resolved numerical simulation (PRNS) approach for the very large eddy simulation (VLES) has been implemented into the National Combustion Code (NCC). Under the present effort, the fundamentals of the PRNS have been assessed by systematically examining the computed results of the fully developed pipe flows at different Reynolds numbers. The benefits of the PRNS for computing the practical combustor flows have been demonstrated by two representative cases. The major findings and recommendations emerging from the current investigation are:

1. Major Findings

- PRNS is effective in bridging the fidelity and the computing resource gaps between the traditional RANS and LES approaches. This feature should be particularly attractive to the researchers and designers working in an engineering environment. So far, our experience suggests that, with care, typical RANS type grid resolution can support PRNS to successfully perform the very large eddy simulation.

- PRNS has been verified to be a unifying approach for simulating the turbulent flows. It enables the computations evolving from the RANS toward VLES by controlling the value of the resolution parameter RCP.
- Successful VLES simulations have been obtained with RCP between 0.3 and 0.4 for a very wide range of the flow Reynolds numbers.
- Numerical setting in the NCC code, in fact, in any CFD code, must be "clean" enough such that the effects of the operating physical model are not appreciably polluted by the effects of the numerical artifacts. We have found a baseline setting for NCC to perform PRNS computations.
- In lower Reynolds number flows, the physical, turbulent fluctuations are relatively weak, and they are more susceptible to the damping effects of both the numerical errors and the eddy viscosity of the subscale model. Additional physics-based sources are helpful in computationally sustaining the development of these weak fluctuations in the PRNS calculations.
- A nonlinear formulation of the subscale model for unresolved turbulent stresses has been proposed. Its linear part accounts for the dissipation effect of the unresolved turbulence via the eddy viscosity, and its nonlinear part reflects the effects of anisotropy and rotation. The results of a preliminary evaluation indicate that the nonlinear part can play a significant role in sustaining the large scale turbulence, and its importance becomes more apparent in the case of lower Reynolds number flow.
- Current RANS with standard $k-\varepsilon$ model in the NCC tends to under predict the mean axial velocity of the fully developed pipe flow.

2. Recommendations

- Comprehensive evaluation of the current nonlinear subscale model and its further development are needed to buttress the PRNS approach for the VLES of practical combustor flows.
- A better RANS model is needed as the parent of the PRNS subscale model to improve the prediction capability of PRNS when the value of RCP approaches one.
- Systematic study of the effects of grid quality and grid resolution on the PRNS simulation must be conducted.
- Development of turbulent combustion models which are consistent with the scale resolution level of the PRNS approach is required for the predictive simulation of advanced combustion systems using the PRNS.

References

1. Georgiadis, N. J., Iwan, J., Alexander D., and Reshotko, E., "Development of A Hybrid RANS/LES Method for Compressible Mixing Layer Simulations," AIAA Paper 2001-0289, 2001.
2. Fan T.C., Tian, M., Edwards, J. R., Hassan, H. A., and Baurle, R. A., "Validation of A Hybrid Reynolds-Averaged /Large-Eddy Simulation Method for Simulating Cavity Flameholder Configuration," AIAA Paper 2001-2929, 2001.
3. Menter, F.R., Kuntz, M., and Bender, R., "A Scale-adaptive Simulation Model for Turbulent Flow Predictions," AIAA Paper 2003-0767, 2003.
4. Spalart, P.R., "Strategies for Turbulent Modeling and Simulations," Int. J. Heat and Fluid Flow Vol. 21, 2000, pp. 252-263.
5. Speziale, C.G., "Turbulence Modeling for Time-Dependent RANS and VLES: A Review," AIAA J., Vol.36, No.2, 1998, pp. 173-184.
6. Arunajatesan, S., and Sinha, N., "Unified Unsteady RANS-LES Simulations of Cavity Flow Fields," AIAA Paper 2001-0516, 2001.
7. Batten, P., Goldberge, U., and Chakravarthy, S., "LNS – An Approach Towards Embedded LES," AIAA Paper 2002-0427, 2002.
8. Liu, N.-S. and Shih, T.-H., "Turbulent Modeling for Very Large-Eddy Simulation," AIAA Journal, Vol. 44, No. 4, April 2006.
9. Liu, N.-S., Shih, T.-H., and Wey, T., "Comprehensive Combustion Modeling and Simulation: Recent Progress at NASA Glenn Research Center," ISABE Paper 2007-1268, 2007.
10. Liu, N.-S., "On the Comprehensive Modeling and Simulation of Combustion Systems," AIAA Paper 2001-0805, 2001.
11. Ajmani, K. and Chen, K.-H., "Unsteady-Flow Computations for the NCC," AIAA Paper 2001-0972, 2001.
12. Chen, K-H., Norris, A.T., Quealy, A., and Liu, N.-S., "Benchmark Test Cases for the National Combustion Code," AIAA Paper 1998-3855, 1998.
13. Ryder, R.C., "The Baseline Solver for the National Combustion Code," AIAA Paper 1998-3853, 1998.
14. Quealy, A., Ryder, R.C., Norris, A.T., and Liu, N.-S., "National Combustion Code: Parallel Implementation and Performance," AIAA Paper 2000-0336, 2000.
15. Raju, M. S., "On the Importance of Chemistry/Turbulence Interactions in Spray Computations," Numerical Heat Transfer, Part B: Fundamentals, No. 5, Vol. 41, pp. 409-432, 2002.
16. Shih, T.-H., Chen, K.-H., and Liu, N.-S., "A Non-Linear $k-\varepsilon$ Model for Turbulent Shear Flows," AIAA Paper 1998-3983, July 1998.
17. Shih, T.-H., Povinelli, L. A., and Liu, N.-S., "Application of Generalized Wall Function for Complex Turbulent Flows," Journal of Turbulence, Vol. 4, April 2003, pp 1.-16.
18. Ferziger, J. H., and Peric, M., *Computational Methods for Fluid Dynamics*, Springer-Verlag Berlin Heidelberg 1996.
19. Kim, W. W., Menon, S., and Mongia, H. C., "Large Eddy Simulation of a Gas Turbine Combustor Flow," Combust. Sci. and Tech., 1999, Vol. 143, pp. 25-62.

20. Zagarola, M.V., and Smith, A.J., "Experiments in High Reynolds Number Turbulent Pipe Flow," Phys. Rev. Lett. 78, 1997.
21. Smagorinsky, J., "General Circulation Experiments with the Primitive Equations," Month. Weath. Rev., Vol.93, pp. 99-165.
22. Shih, T.-H., Zhu, J., Liou, W., Chen, K-H., Liu, N-S., and Lumley, J.L., "Modeling of turbulent swirling flows," NASA, 1997, TM 113112.
23. Shih, T.-H., Liou, W.W., Shabbir, A., Yang, Z., and Zhu, J., "A New $k-\varepsilon$ Eddy Viscosity Model for High Reynolds Number Turbulent Flows," Computers Fluids, Vol. 24, N0. 3, 1995, pp. 227-238.
24. Shih, T.-H., "Constitutive Relations and Realizability of Single-Point Turbulence Closures" Turbulence and Transition Modelling, Chapter 4., Edited by Hallback, M., Henningson, D.S., Johansson, A.V. and Alfredsson, P.H., KLUWER ACADEMIC PUBLISHERS, 1996.
25. Shih, T.-H., "Some developments in computational modeling of turbulent flow," Fluid Dynamic Research 20 (1997) 67-96.
26. Shih, T.-H., Liu, N.-S.: A Strategy for Very Large Eddy Simulation of Complex Turbulent Flows. *AIAA 2006-175, 44th AIAA Aerospace Sciences Meeting and Exhibit* 9-12 Jan. 2006, Reno, Nevada.
27. Shih, T.-H. and Liu, N.-S., "Modeling of Internal Reacting Flows and External Static Stall flows Using RANS and PRNS," Flow, Turbulence and Combustion, July 18, 2007.
28. Yang, Z. and Shih, T.-H., "A $k-\varepsilon$ model of Near Wall Turbulence," NASA TM 105283, 06, 1991.
29. Kim, W-W., Menon, S., and Mongia, H.C., "Large Eddy Simulation of Gas Turbine Combustor Flow," Combust. Sci. and Tech., Vol. 143, 1999, pp. 25-62.
30. Marek, C. J., Smith, T. D., and Kundu, K., "Low Emission Hydrogen Combustors for Gas Turbines Using Lean Direct Injection," AIAA 2005-3776, July 2005.
31. Magnussen, B. F., and Mjertager, B. H., "On Mathematical Modeling of Turbulent Combustion," 16th Symp. (Int.) on Combustion, The Combustion Institute, Pittsburgh, pp. 719-729, 1976.

Appendix A: Effects of the Resolution Control Parameter on the PRNS Solutions (Re=150,000)

A.1 PRNS with RCP = 0.2

History of velocity components at probe 1 and probe 14:

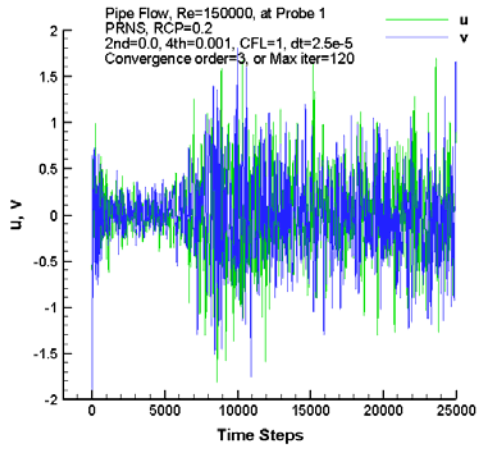

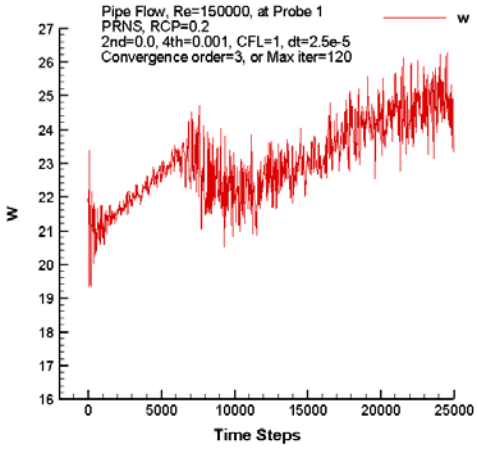

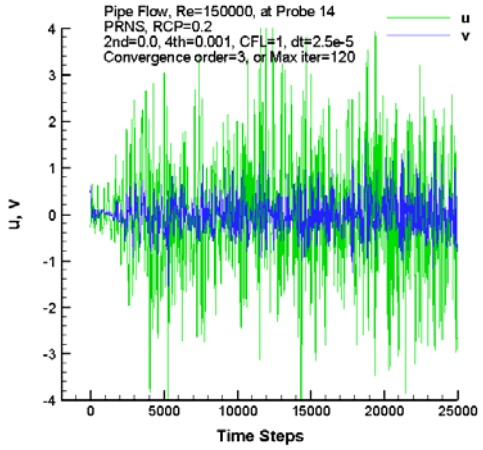

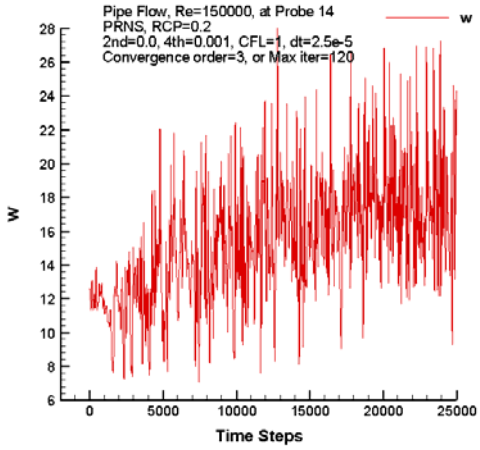

History of subscale turbulent kinetic energy at probes 1 and 14:

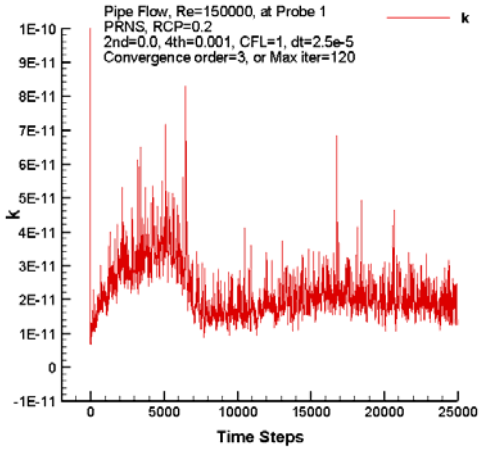

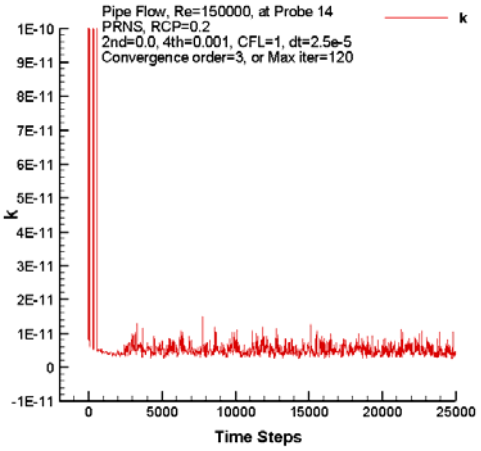

Contours of w, u, v, pg, k, $\mu + \mu_T$ at the time step 25,000:

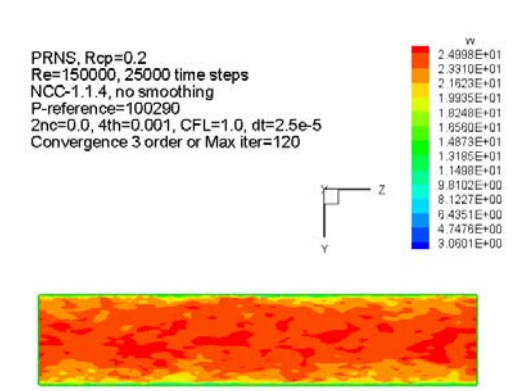

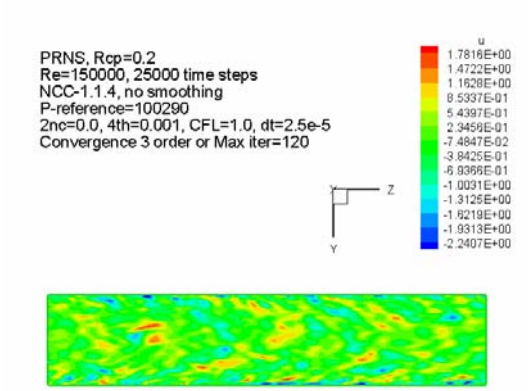

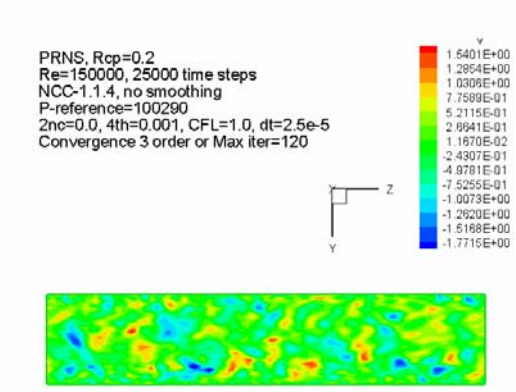

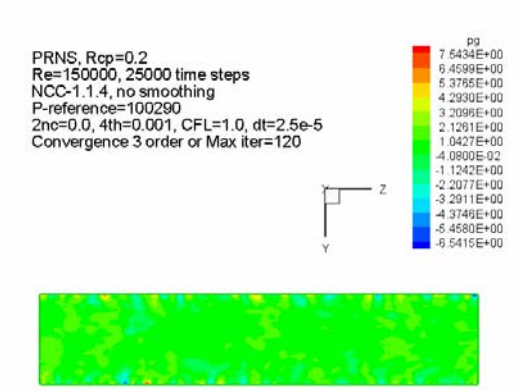

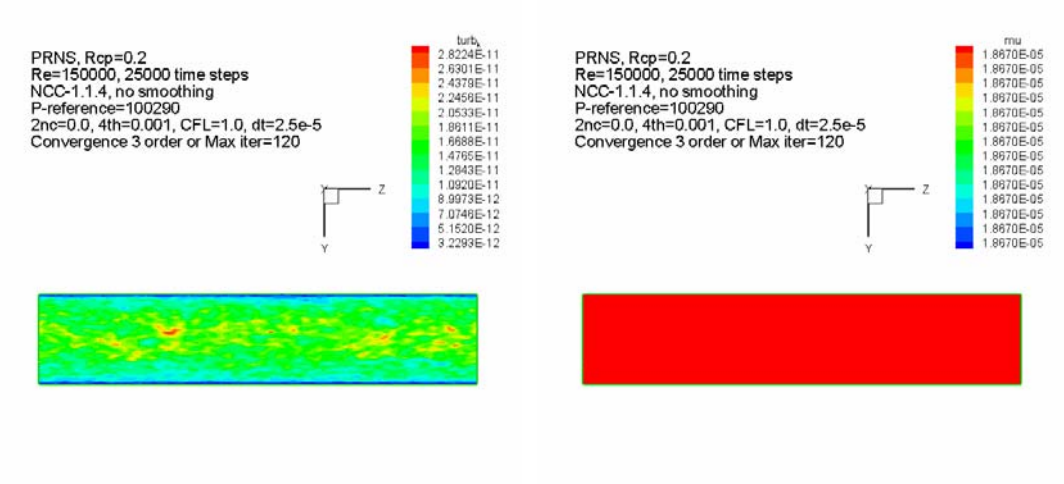

A.2 PRNS with RCP = 0.3

History of velocity components at probe 1 and probe 14:

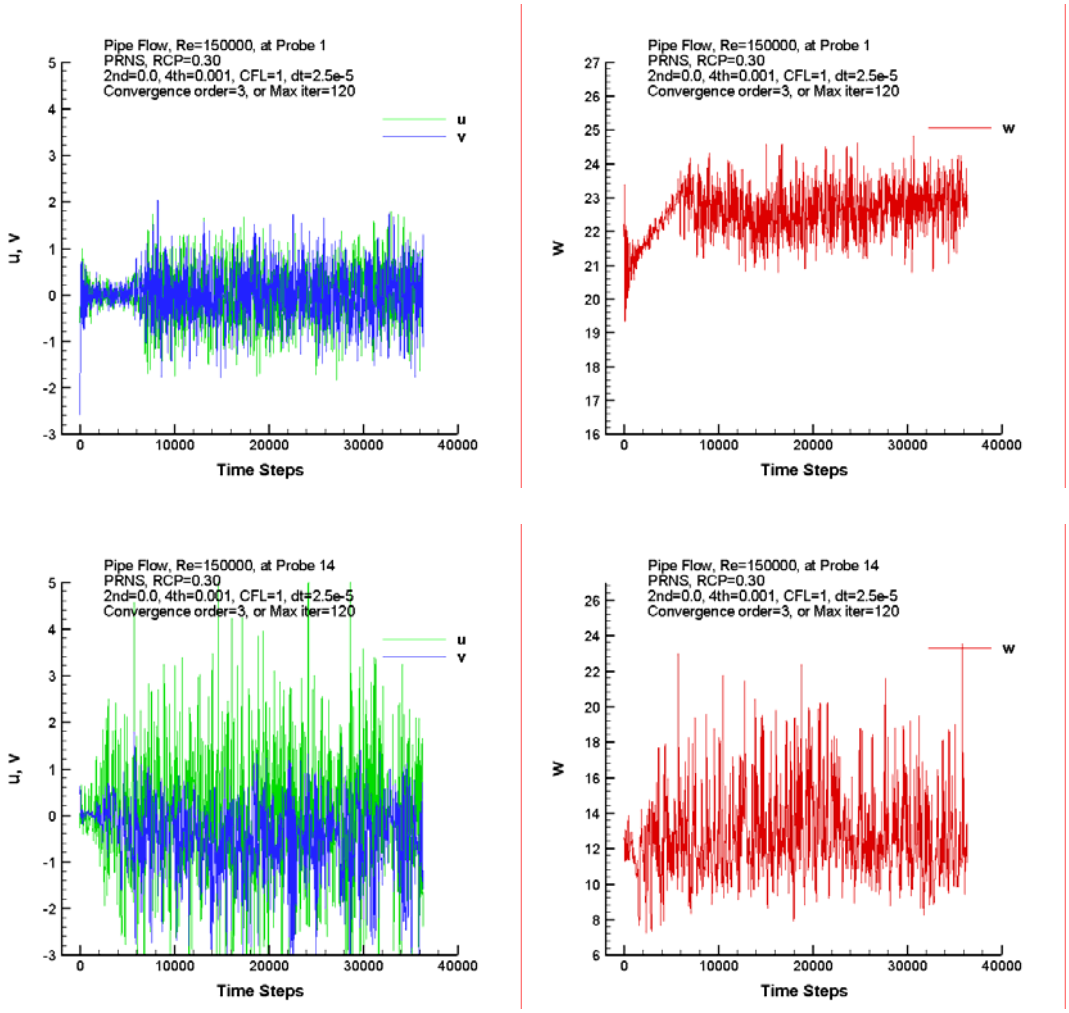

History of subscale turbulent kinetic energy at probes 1 and 14:

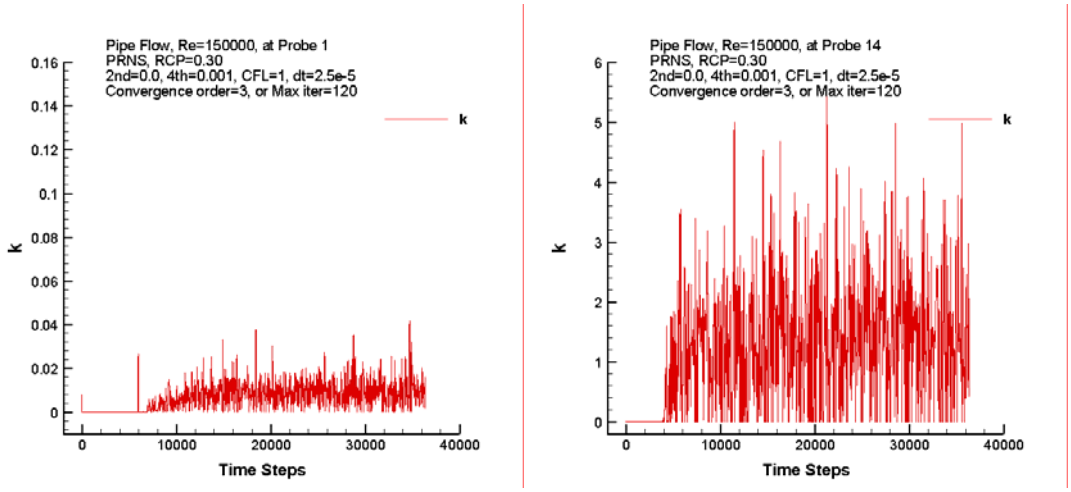

Contours of w, u, v, pg, k, $\mu + \mu_T$ at the time step 36,400:

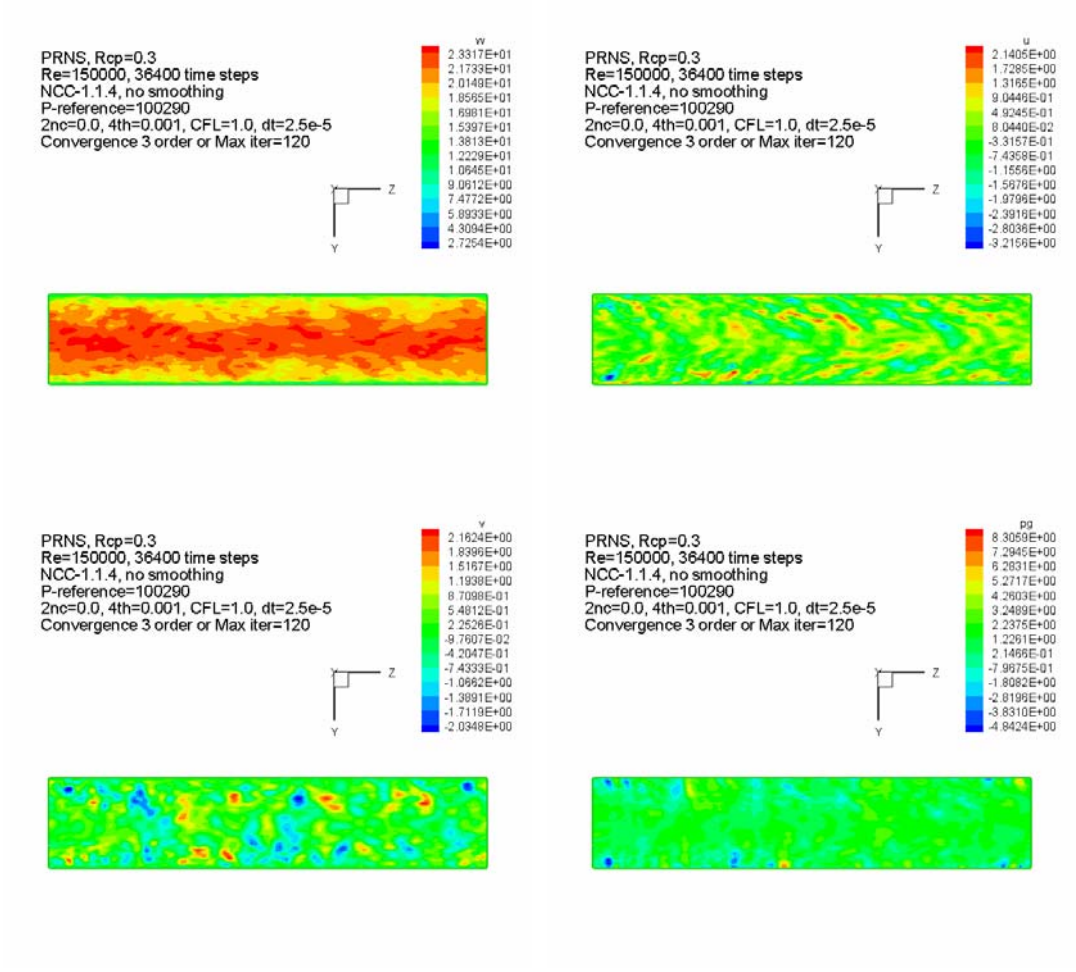

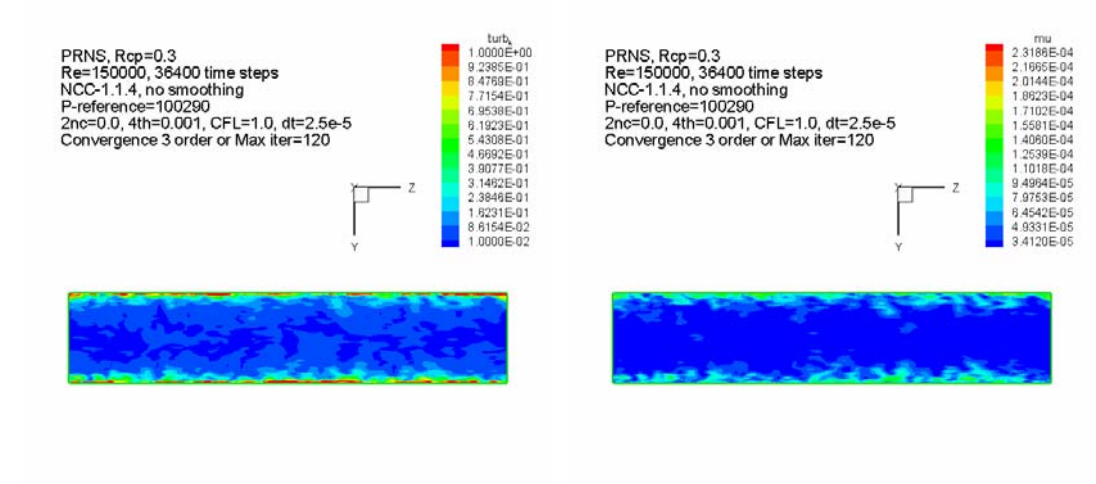

Power spectrum and two-point correlations:

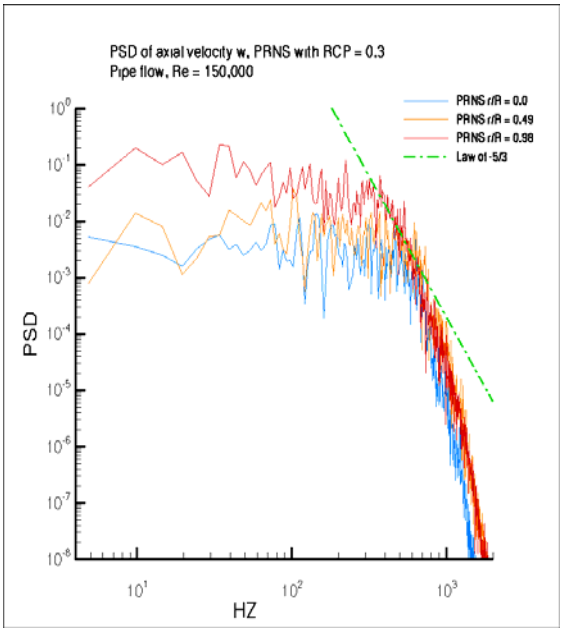

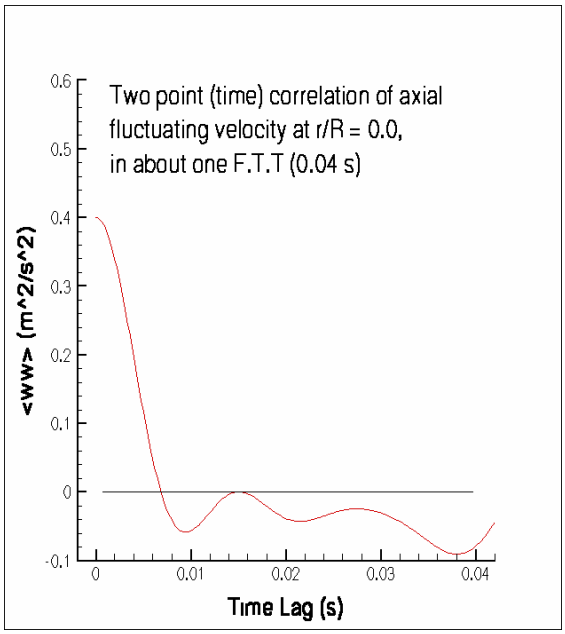

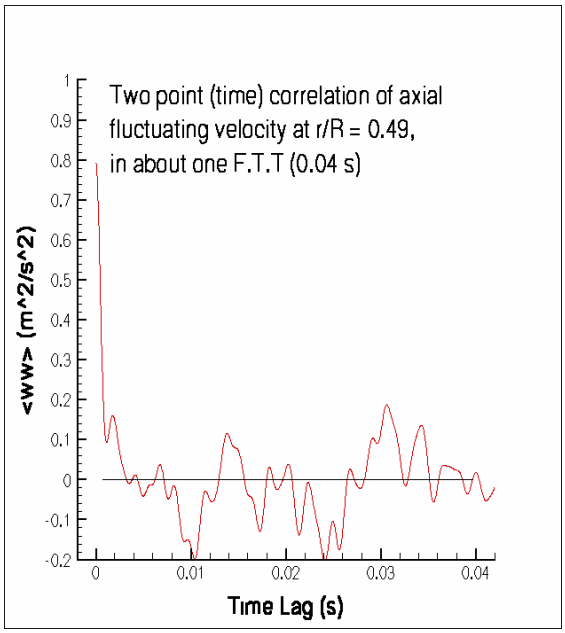

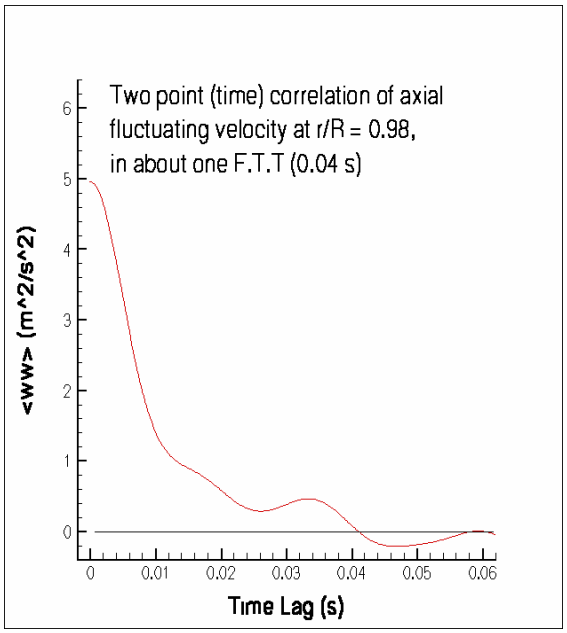

Comparison with RANS and experimental data:

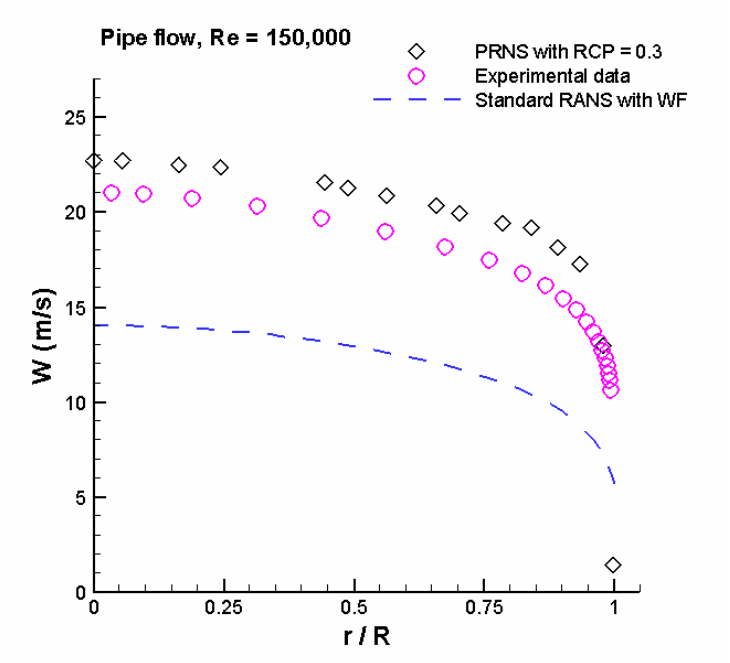

A.3 PRNS with RCP = 0.34

History of velocity components at probe 1 and probe 14:

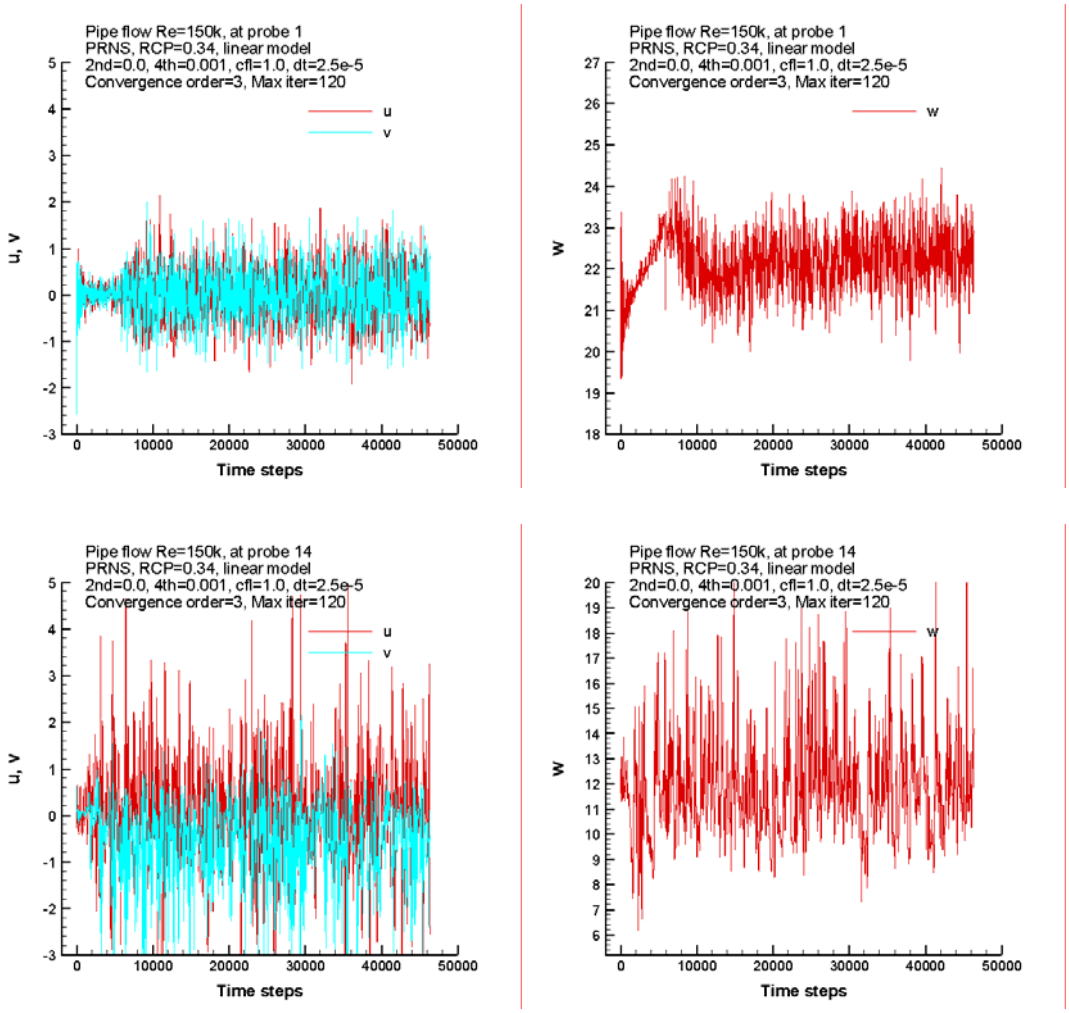

History of subscale turbulent kinetic energy at probes 1 and 14:

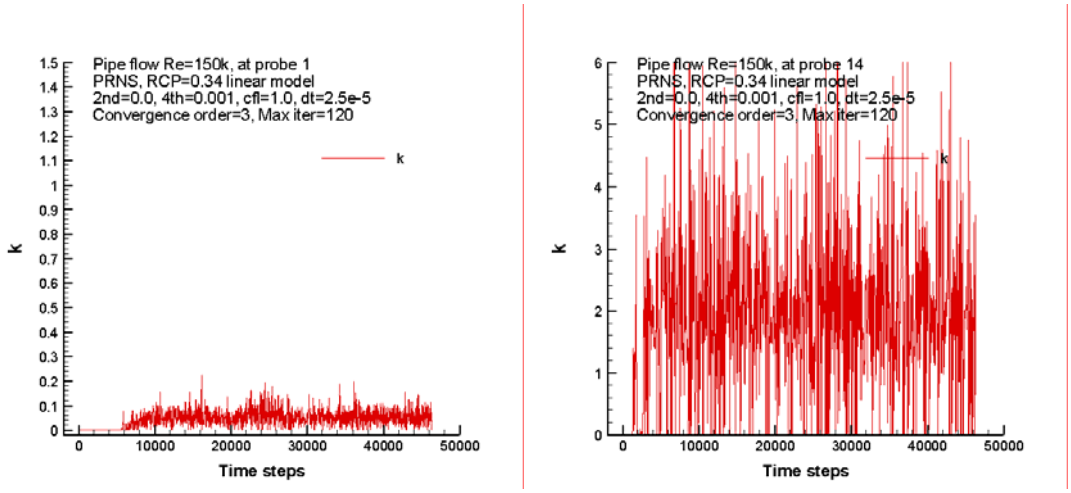

Contours of w, u, v, pg, k, $\mu + \mu_T$ at the time step 46,400:

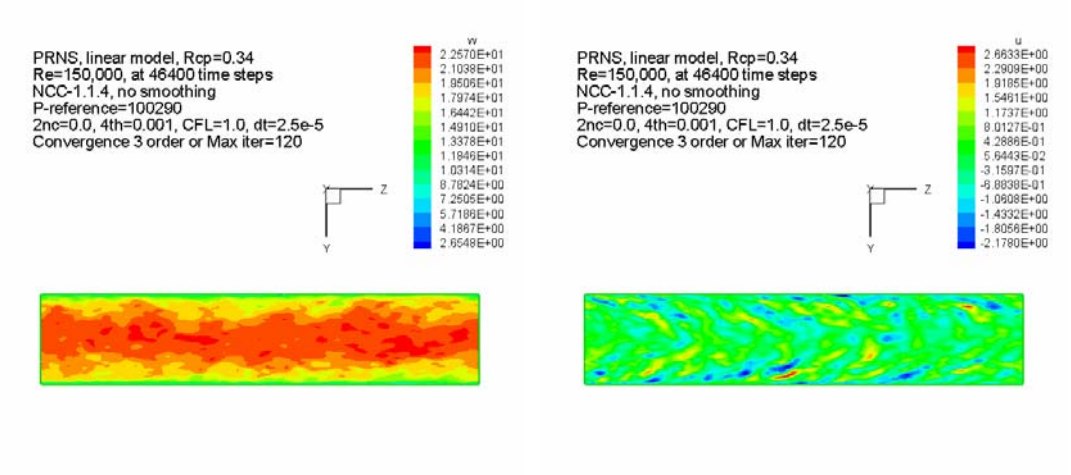

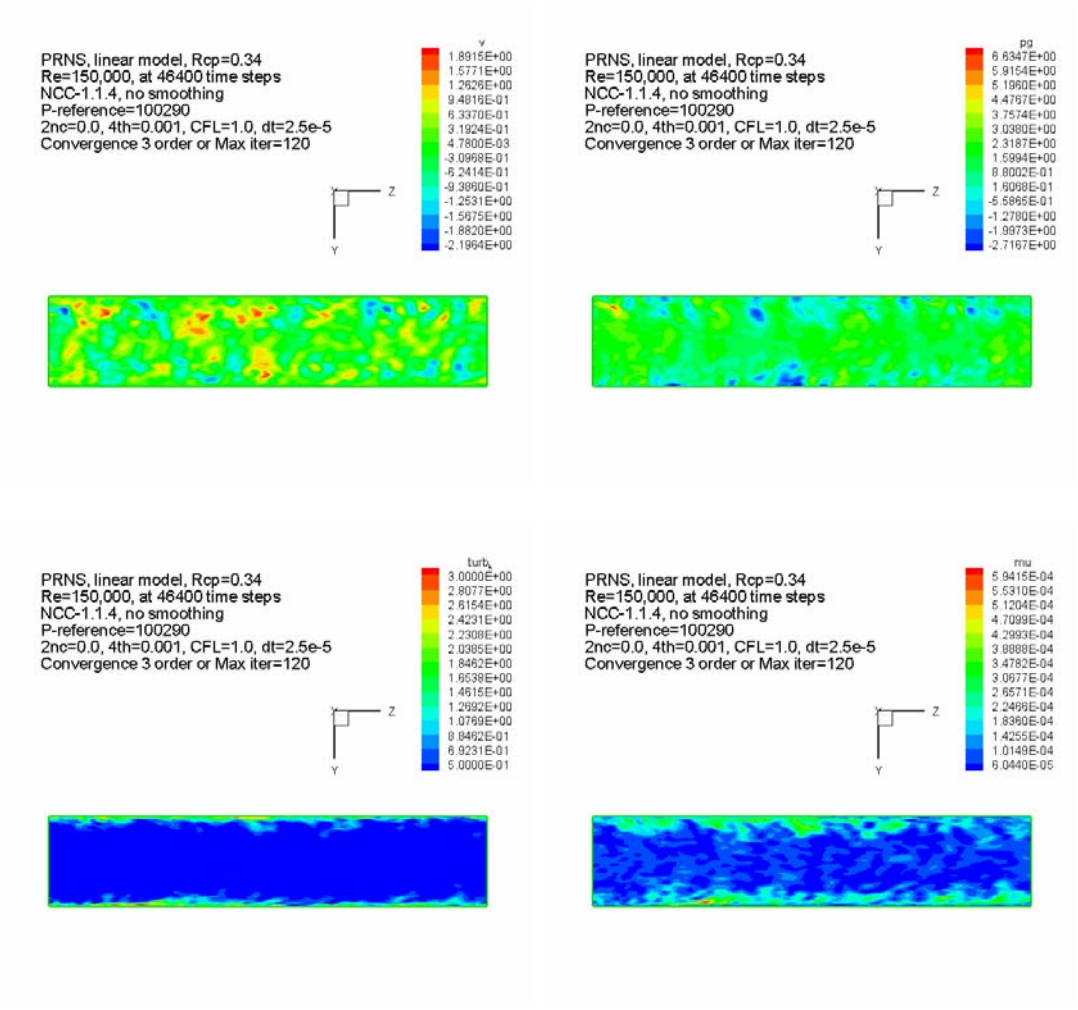

A.4 PRNS with RCP = 0.4

History of velocity components at probe 1 and probe 14:

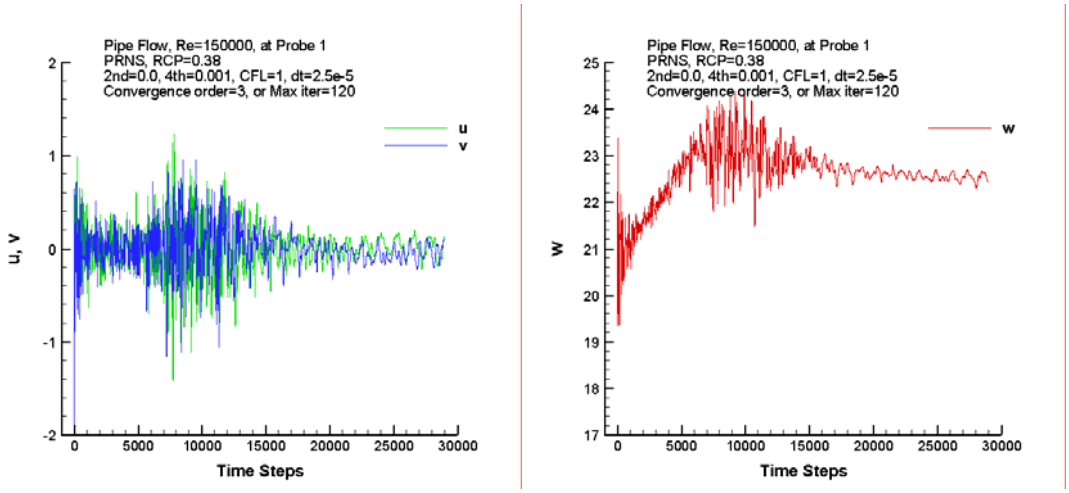

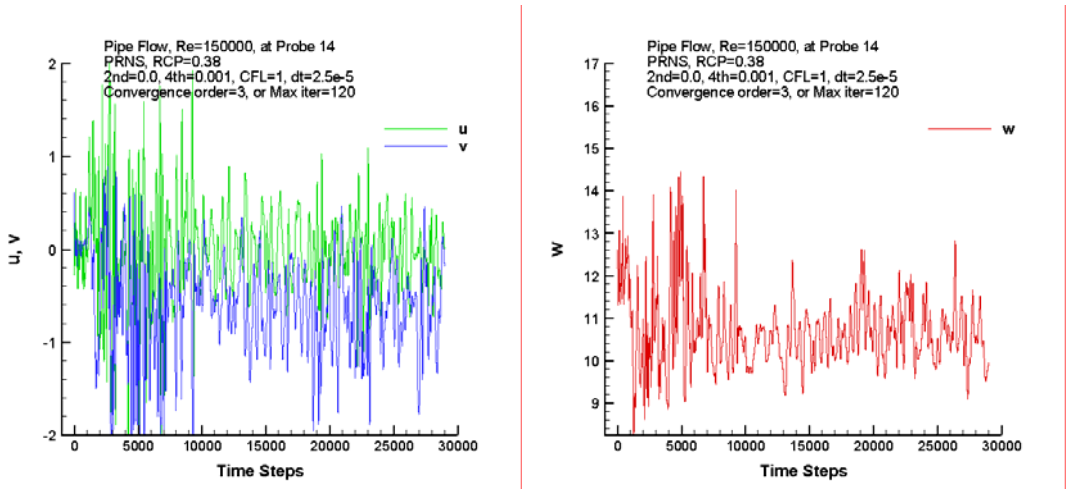

History of subscale turbulent kinetic energy at probes 1 and 14:

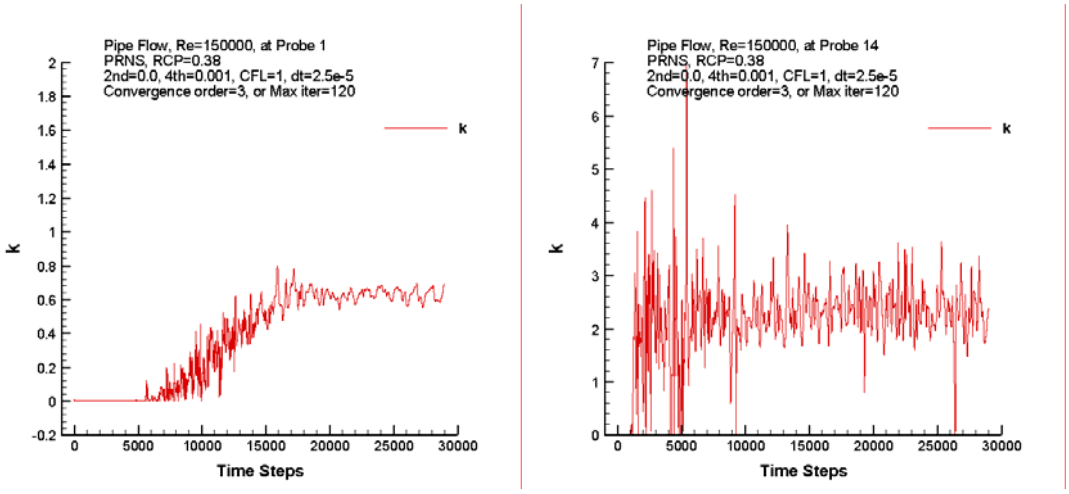

Contours of w, u, v, pg, k, $\mu + \mu_T$ at the time step 29,000:

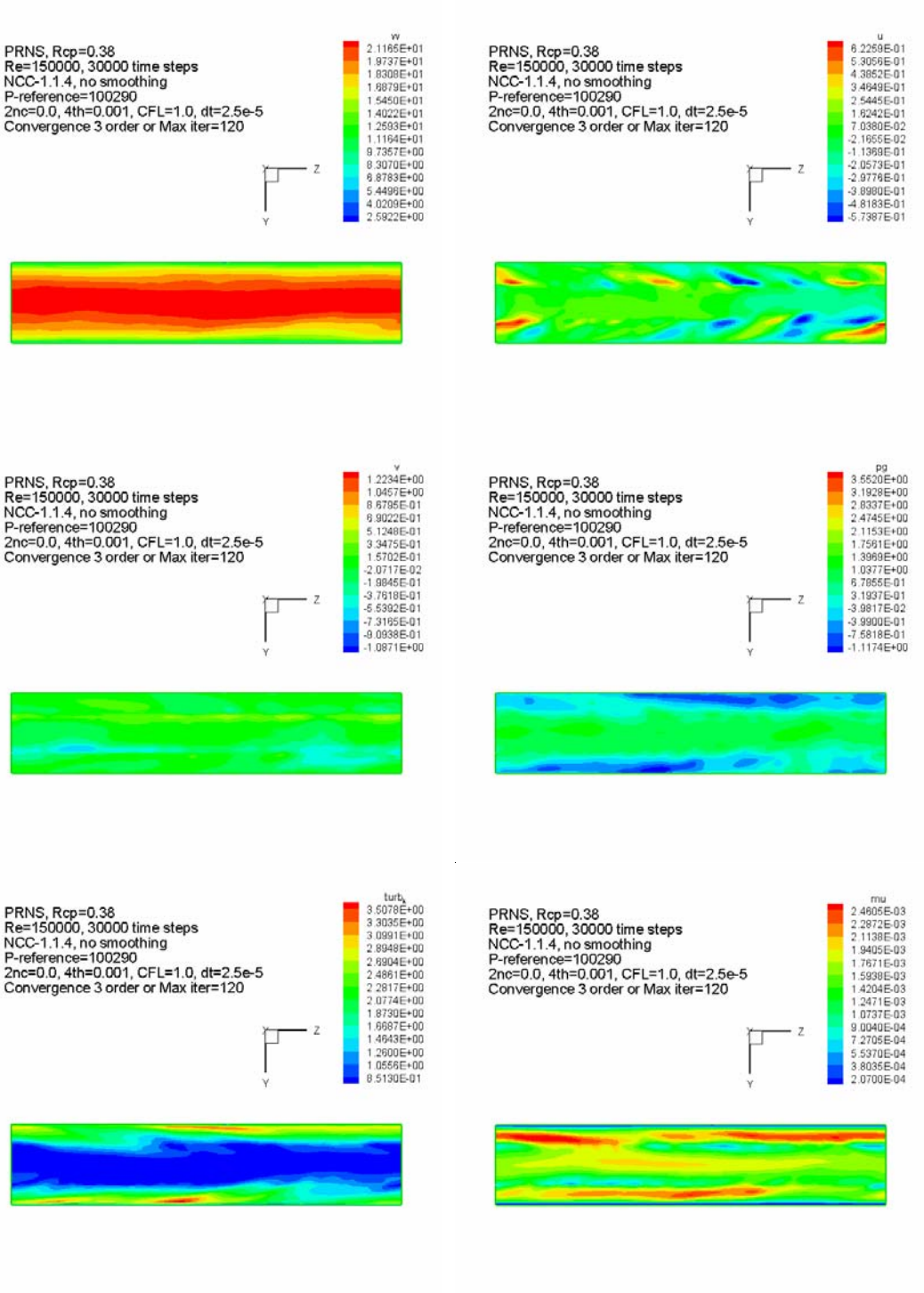

A.5 PRNS with RCP = 0.5

History of velocity components at probe 1 and probe 14:

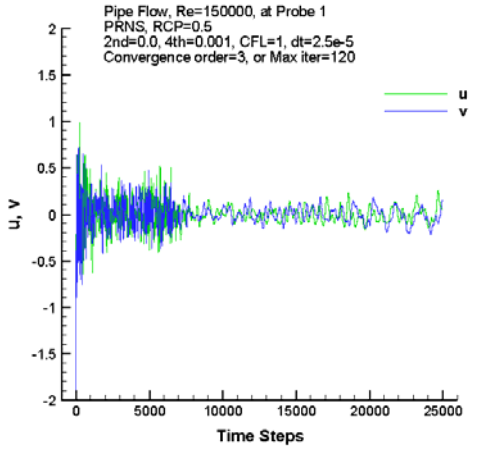

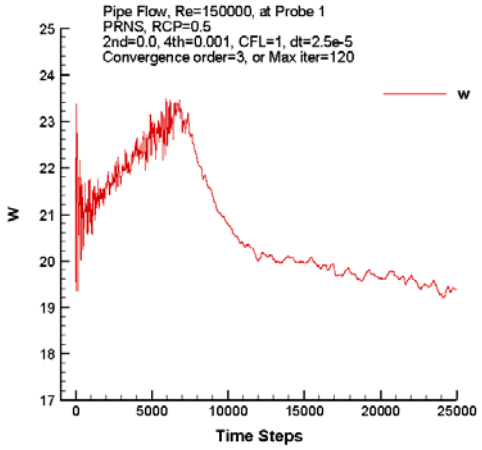

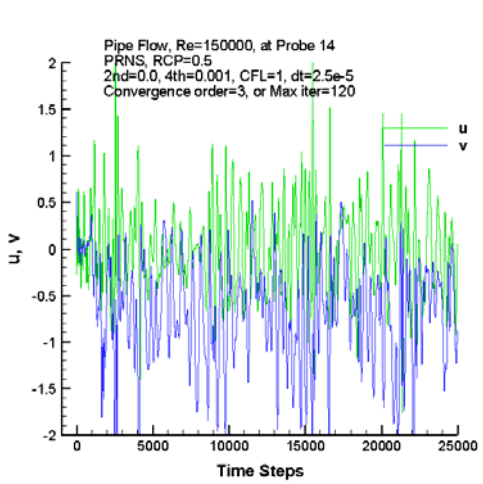

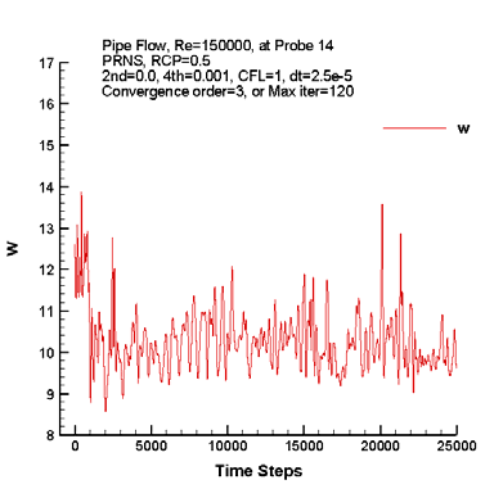

History of subscale turbulent kinetic energy at probes 1 and 14:

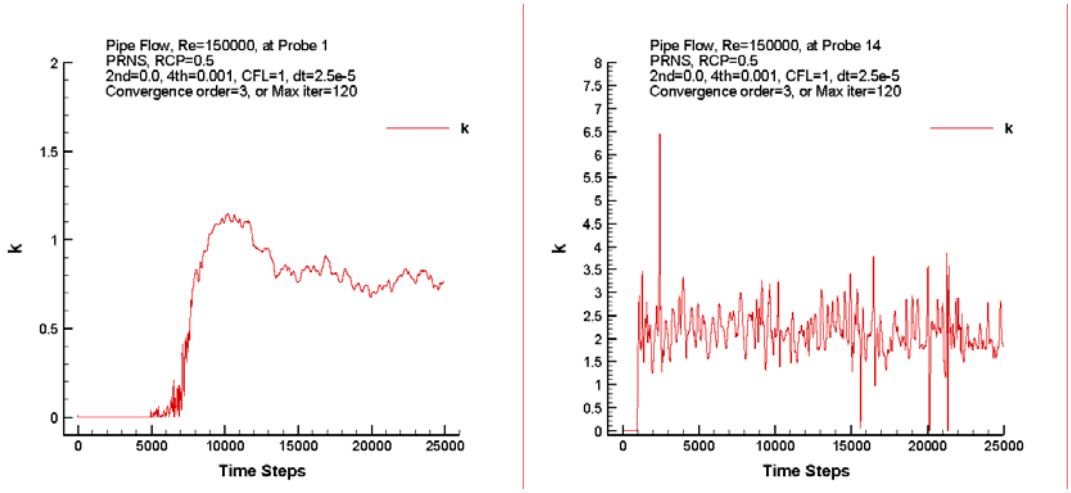

Contours of w, u, v, pg, k, $\mu + \mu_T$ at the time step 25,000:

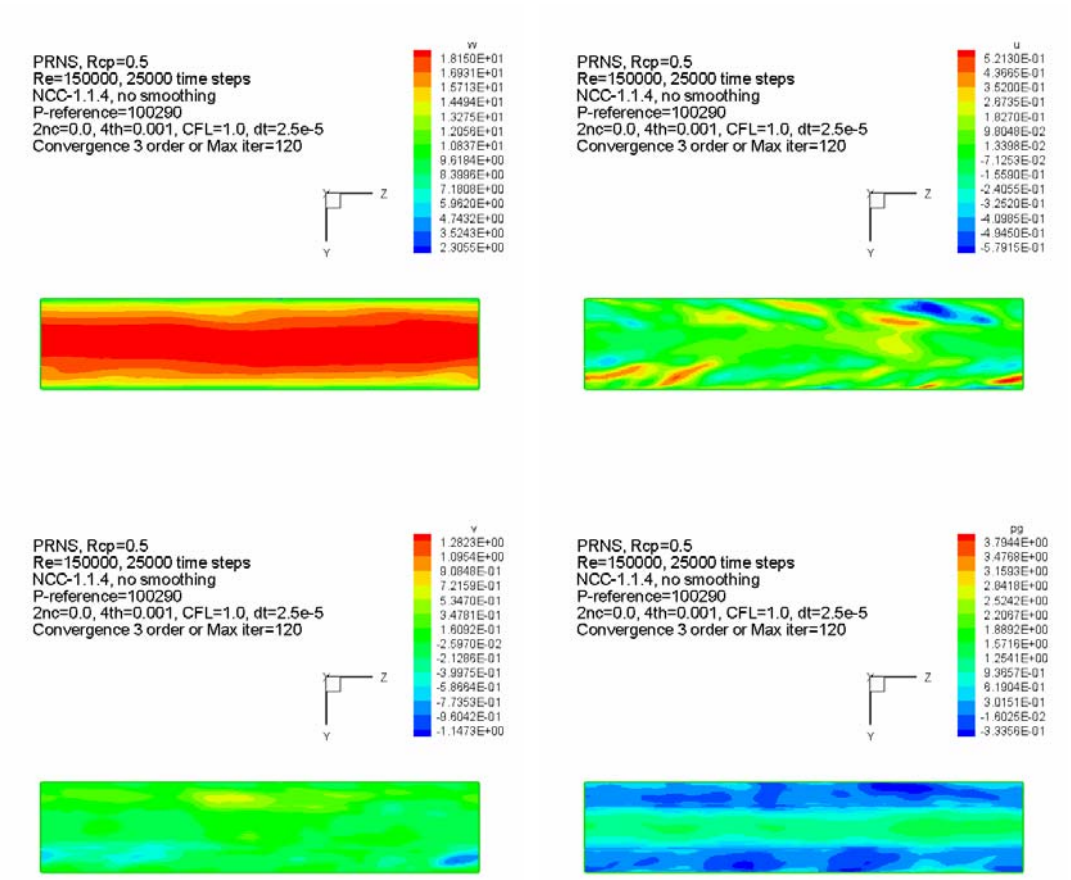

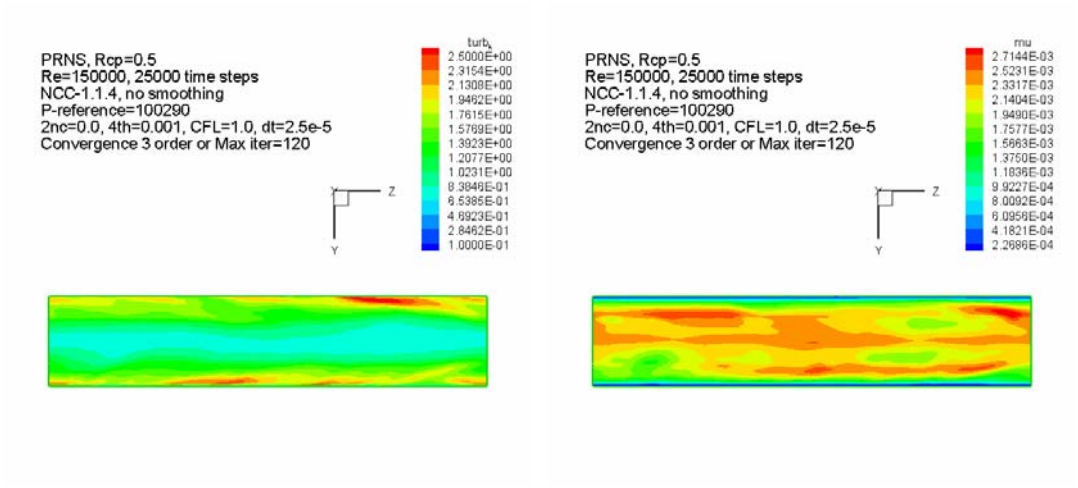

A.6 PRNS with RCP = 0.8

History of velocity components at probe 1 and probe 14:

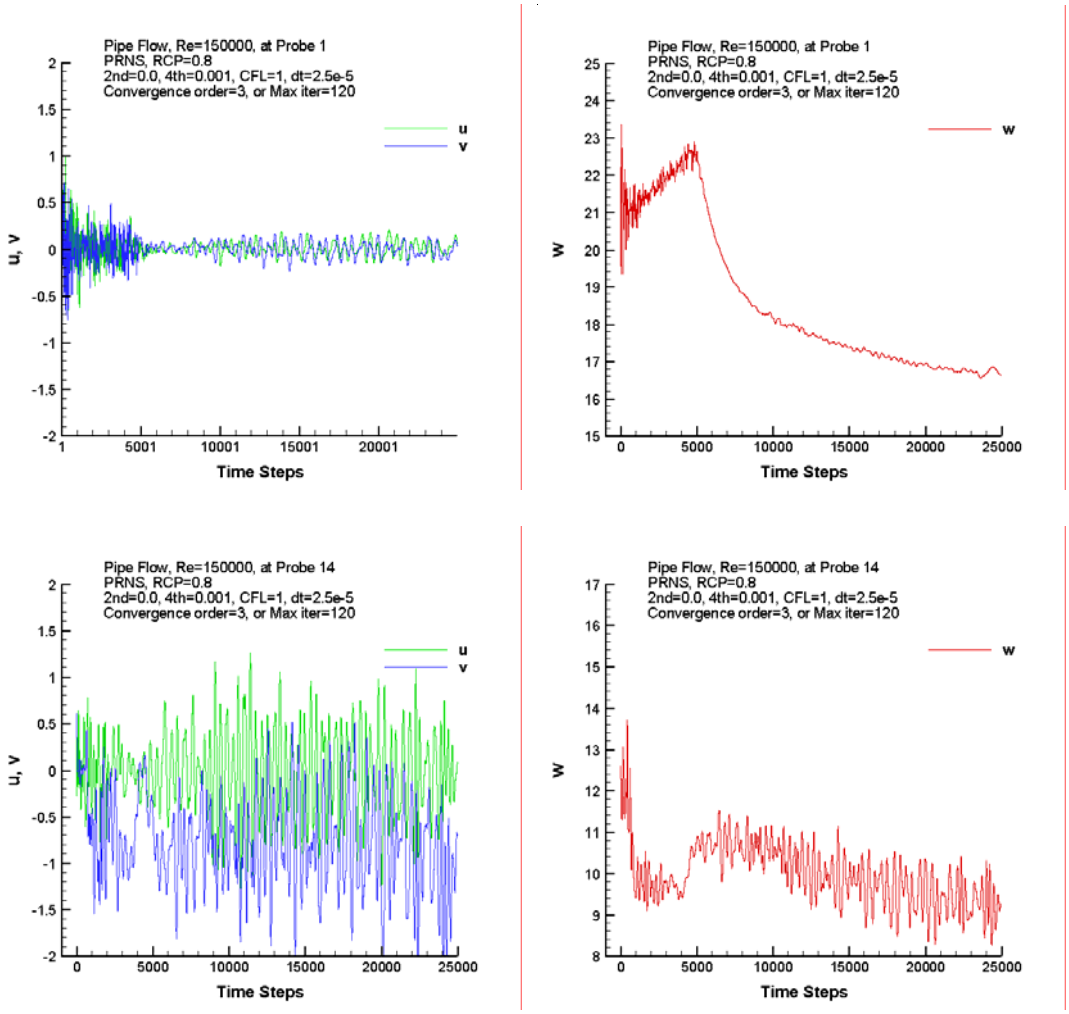

History of subscale turbulent kinetic energy at probes 1 and 14:

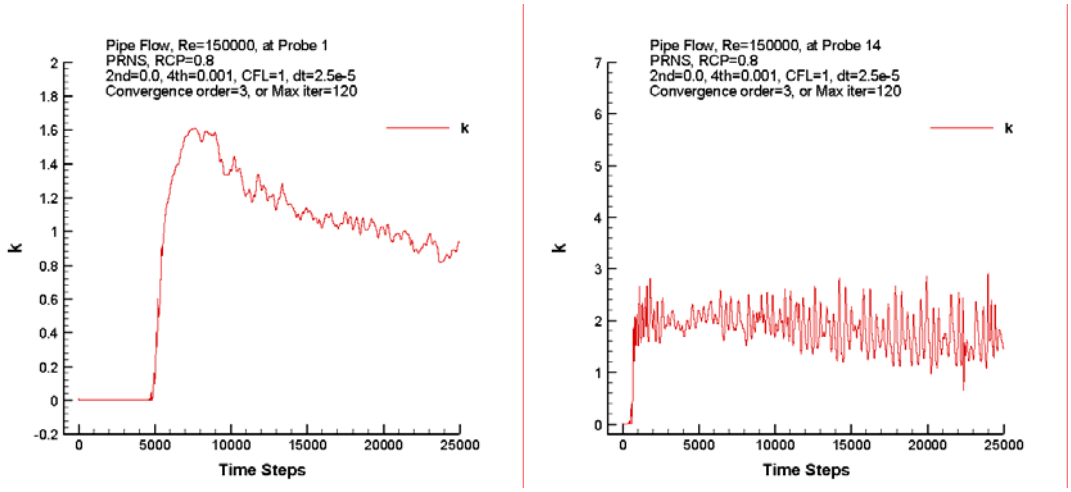

Contours of w, u, v, pg, k, $\mu + \mu_T$ at the time step 25,000:

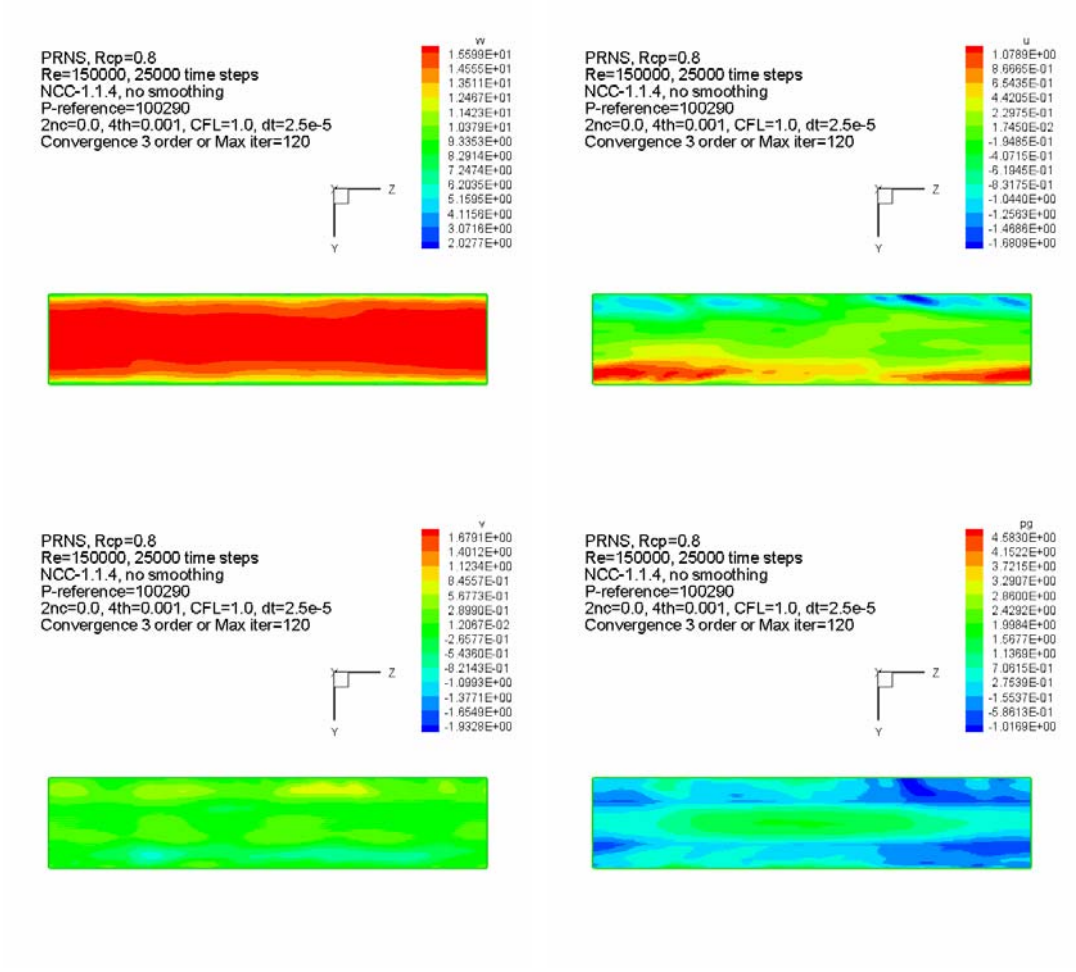

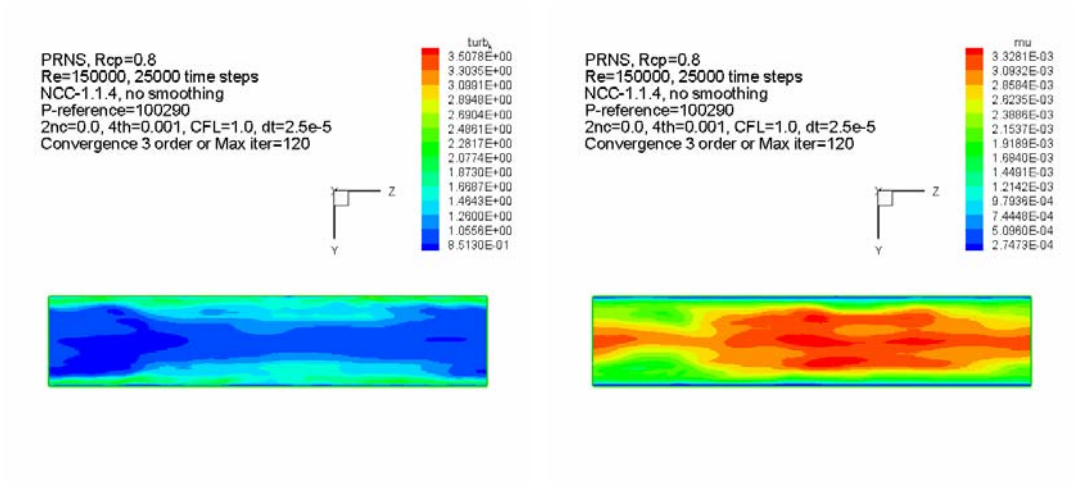

A.7 PRNS with RCP = 1.0

History of velocity components at probe 1 and probe 14:

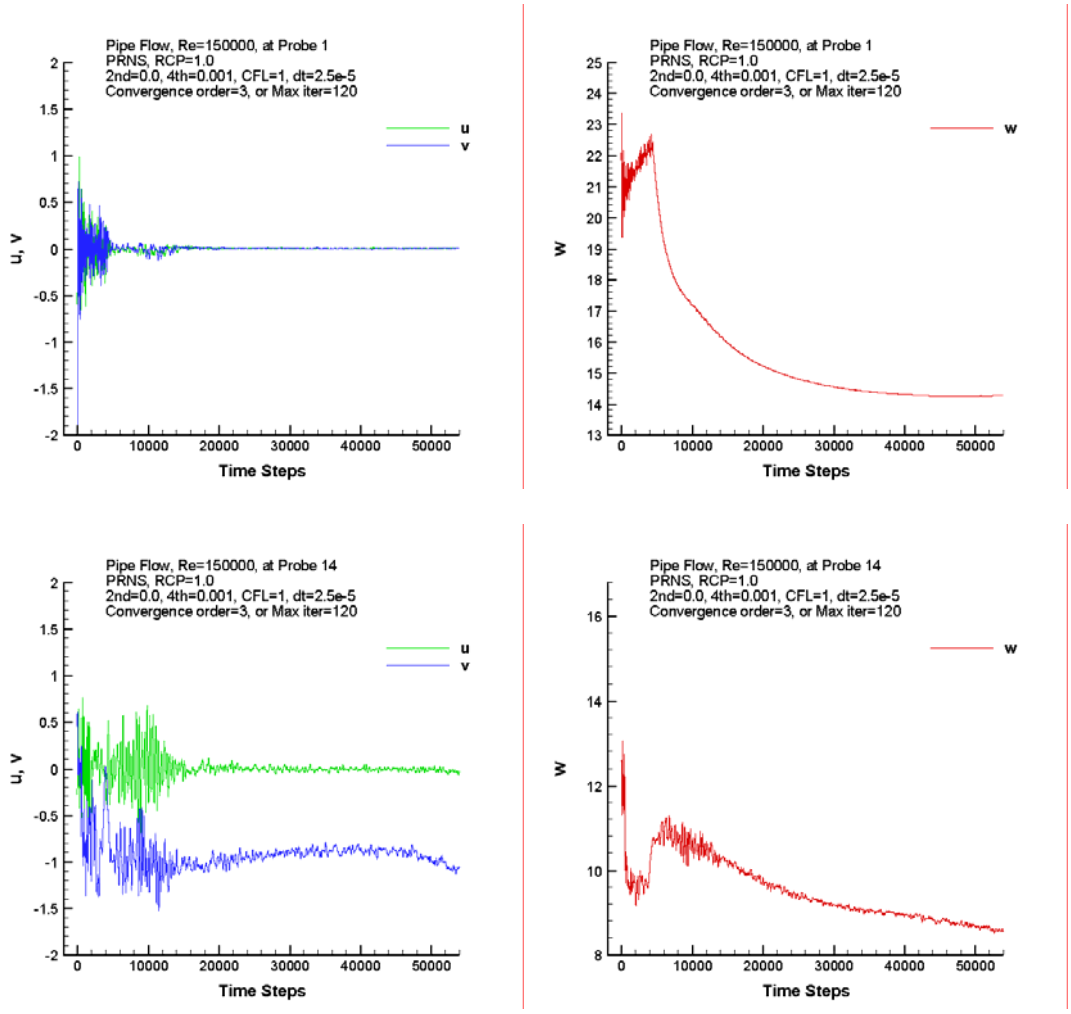

History of subscale turbulent kinetic energy at probes 1 and 14:

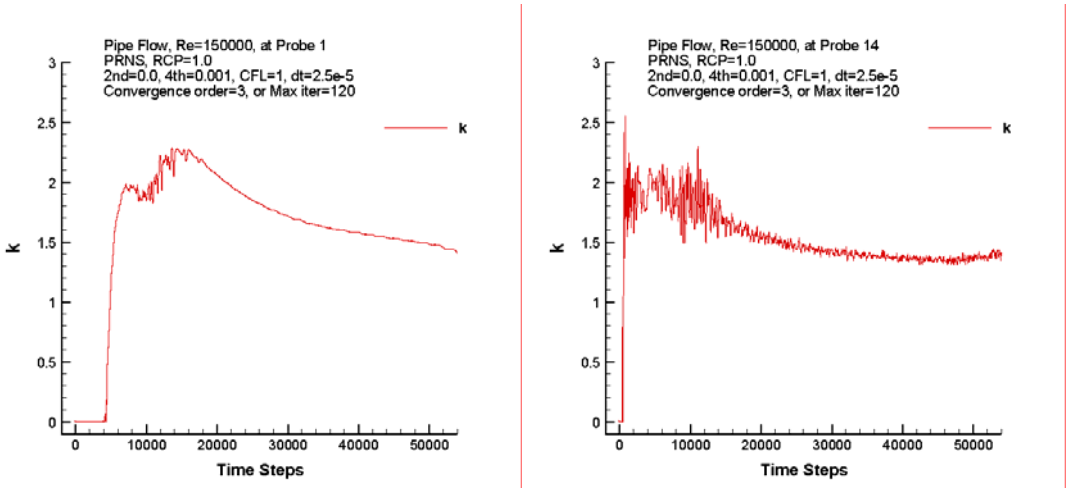

Contours of w, u, v, pg, k, $\mu + \mu_T$ at the time step 54,000:

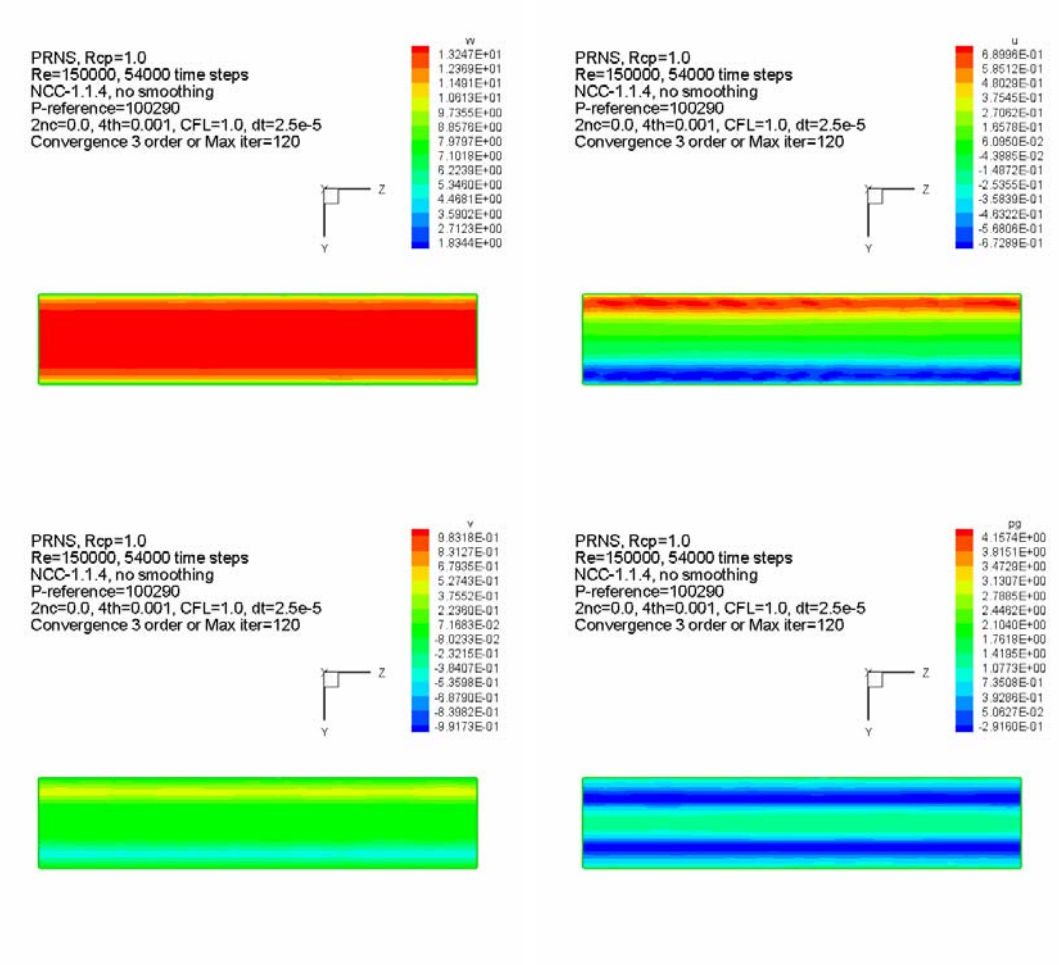

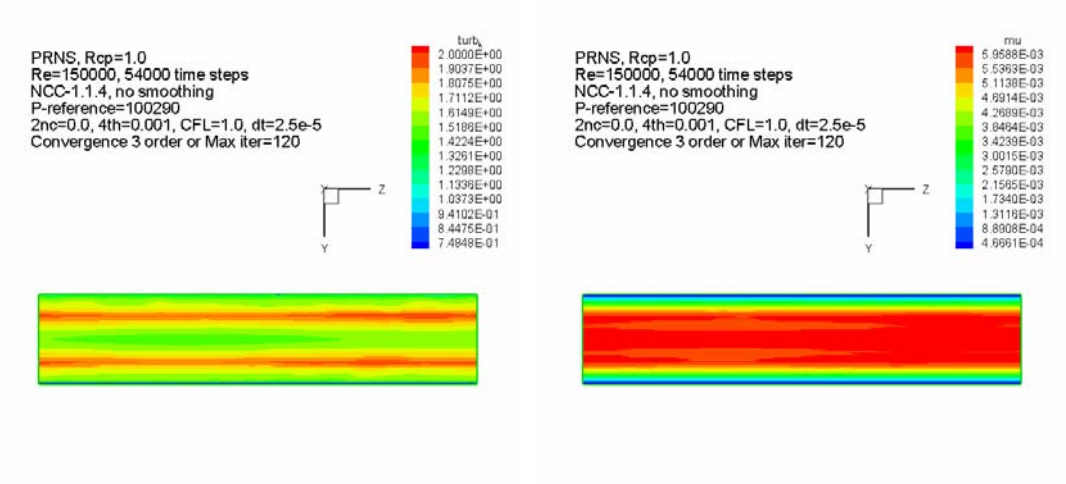

A.8 Steady RANS simulation

Iteration history of velocity components at probe 1 and probe 14:

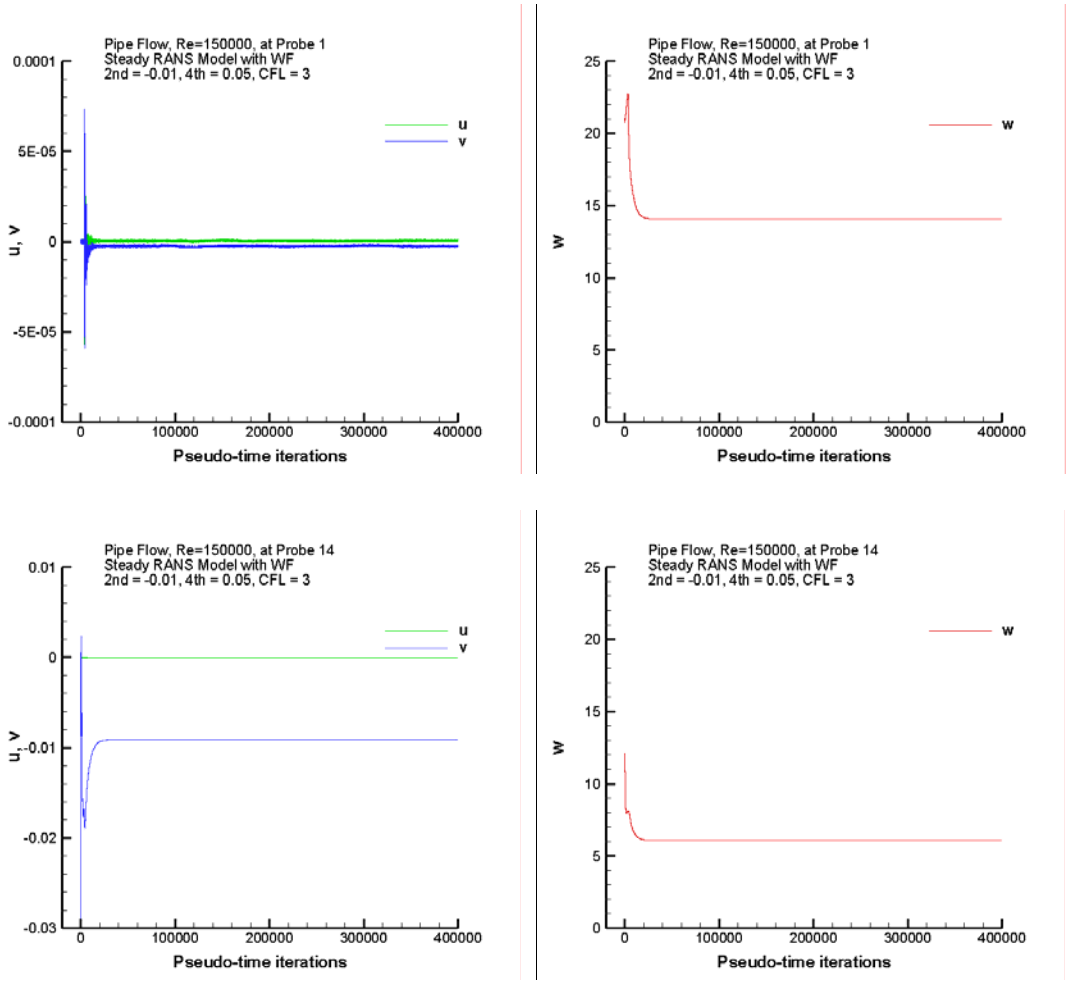

Iteration history of turbulent kinetic energy at probes 1 and 14:

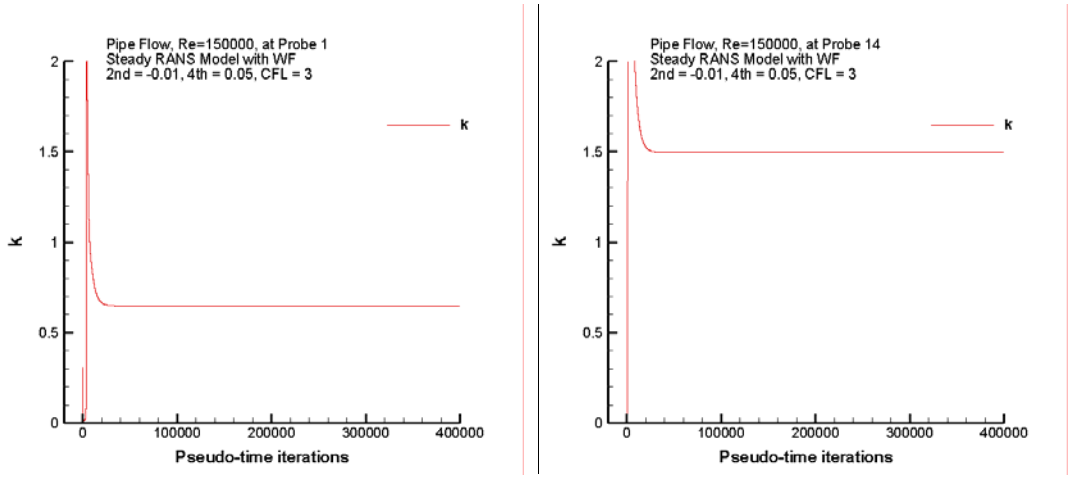

Contours of w, u, v, pg, k, $\mu + \mu_T$ at the iteration number 400,000:

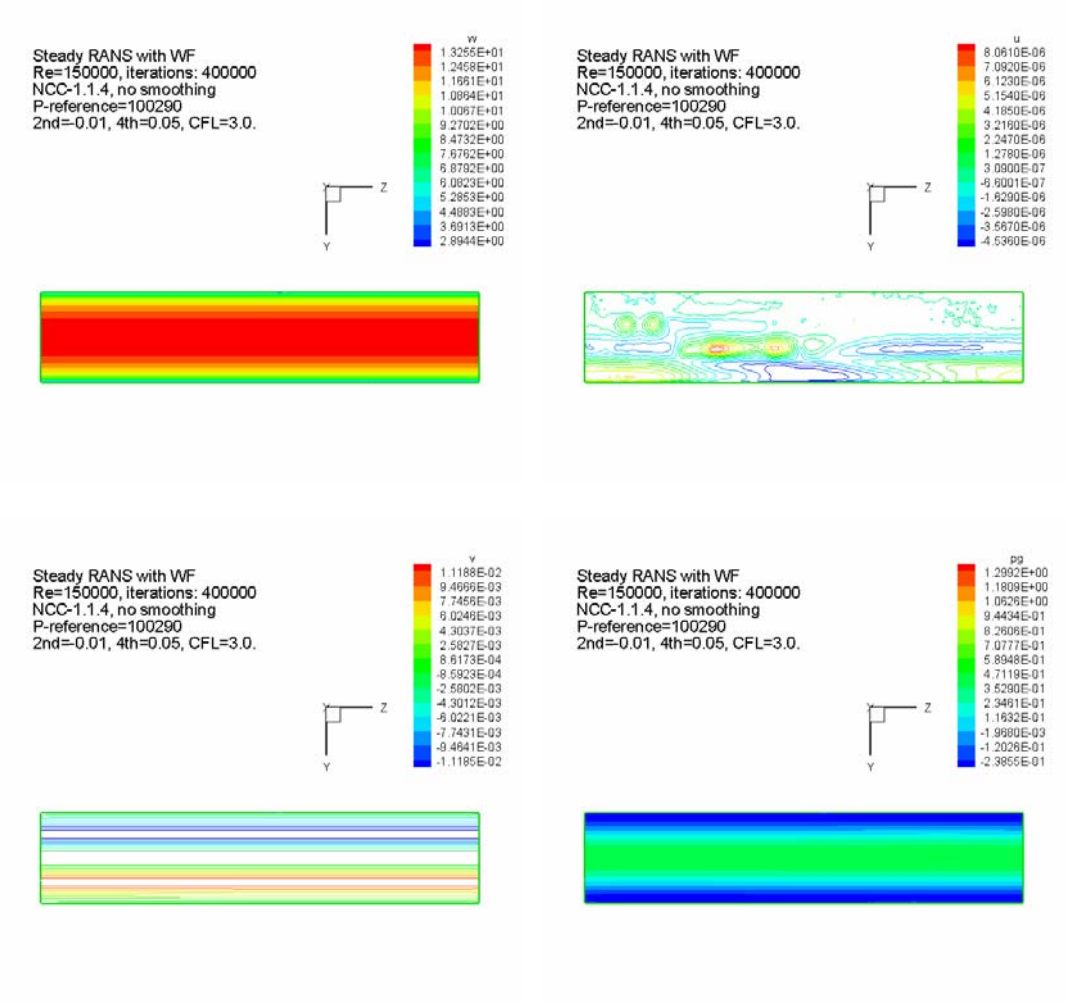

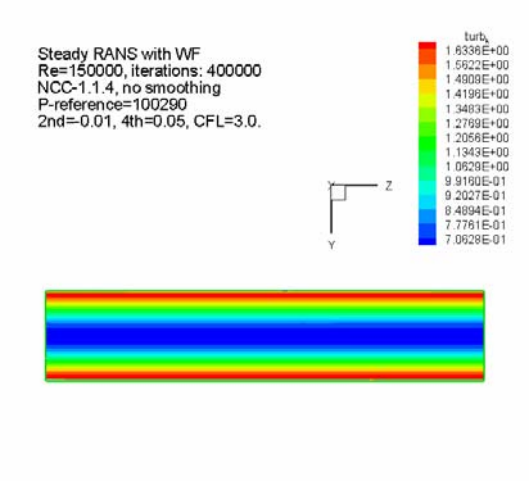

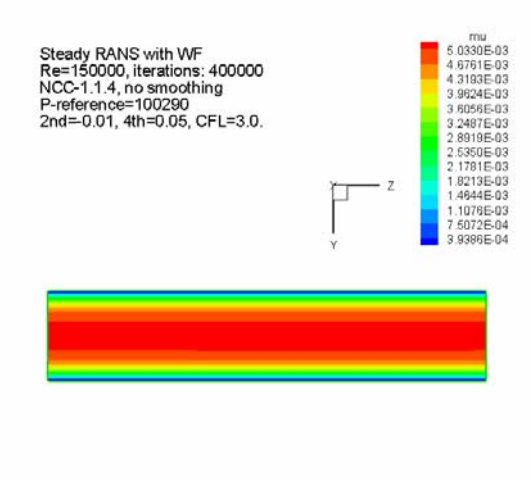

Radial profiles of w, u, v, k and $\mu + \mu_T$ ***:***

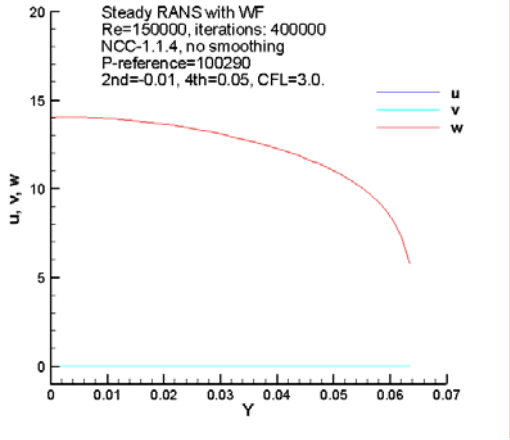

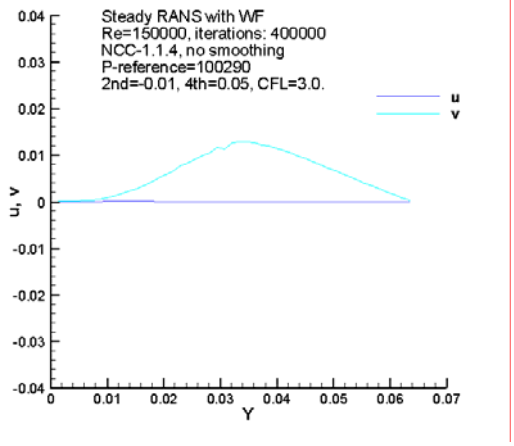

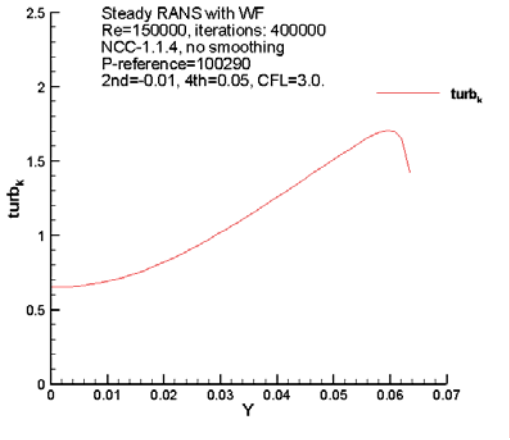

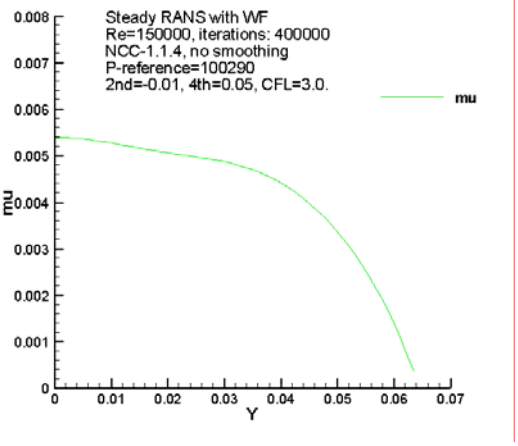

Appendix B: Effects of the Resolution Control Parameter on the PRNS Solutions (Re=15,000)

B.1 PRNS with RCP = 0.0

History of velocity components at probe 1 and probe 14:

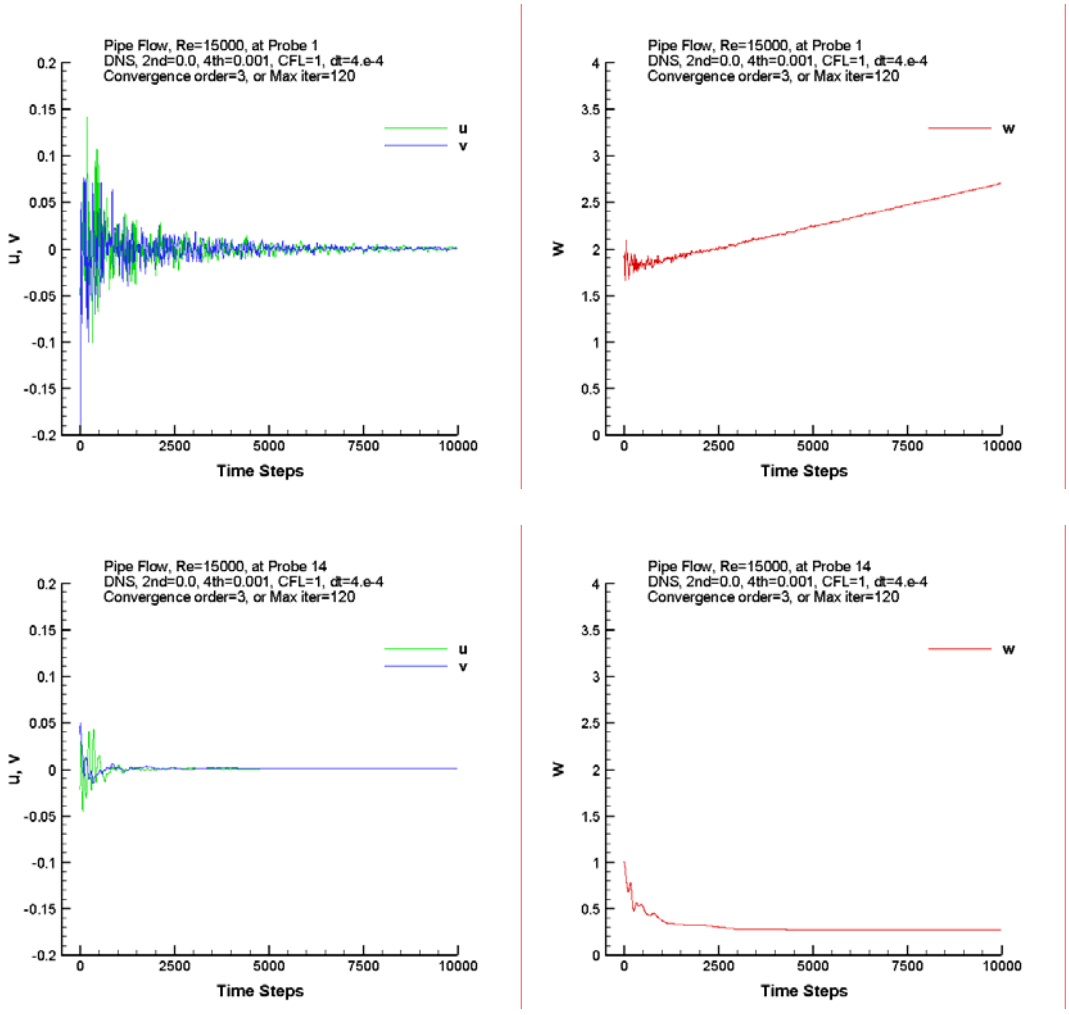

Contours of w, u, v, pg at the time step 10,000:

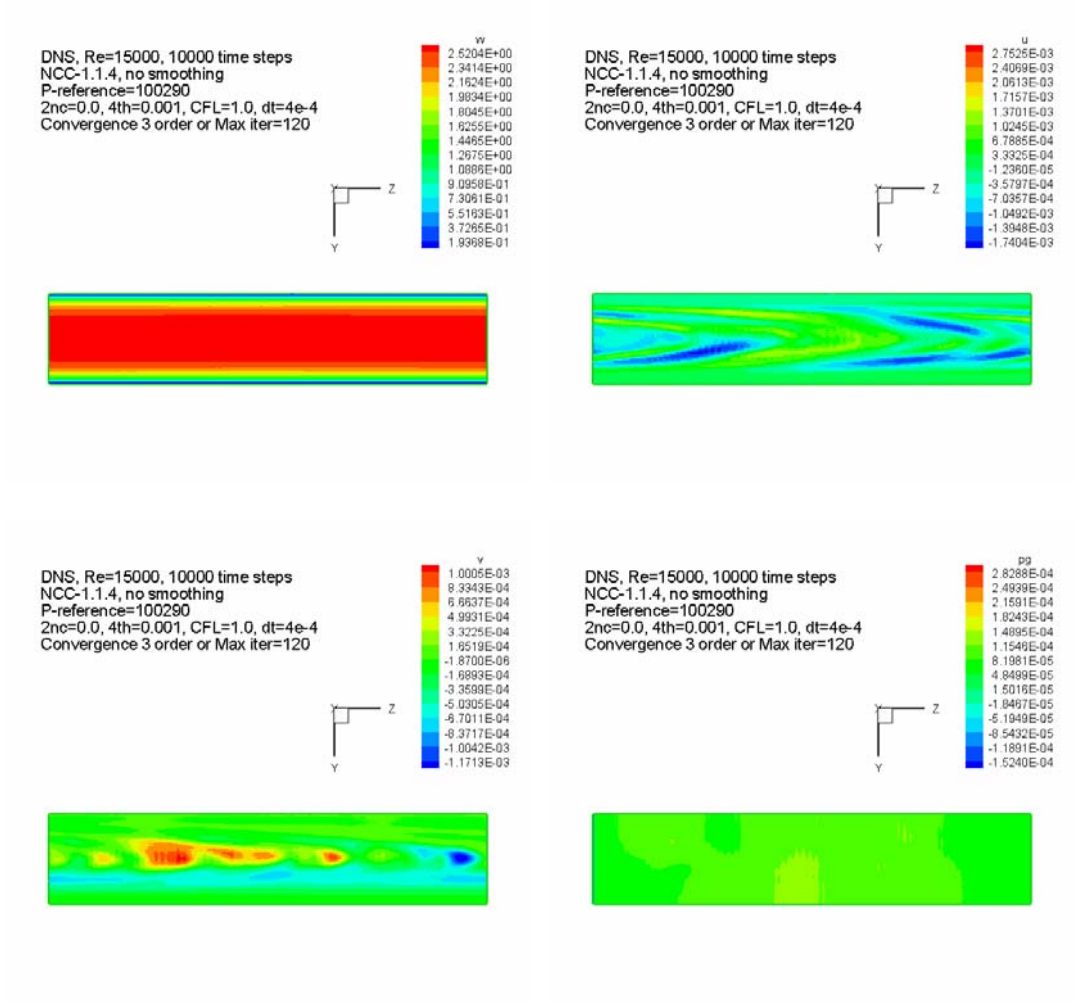

B.2 PRNS with RCP = 0.2

History of velocity components at probe 1 and probe 14:

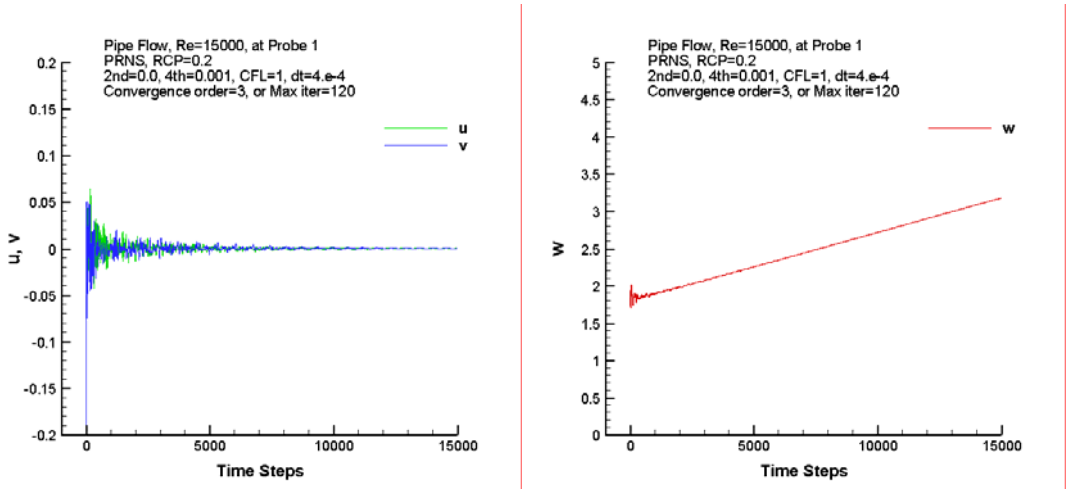

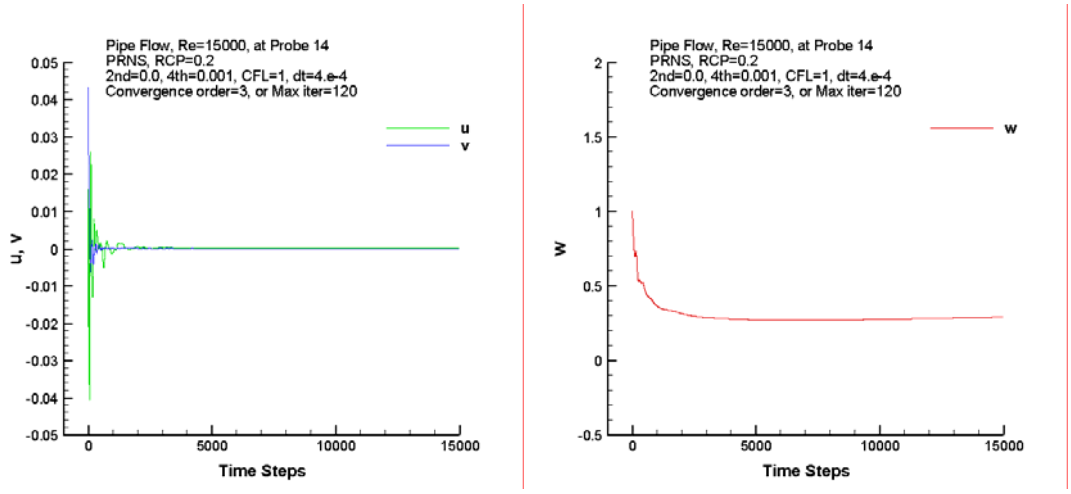

History of subscale turbulent kinetic energy at probes 1 and 14:

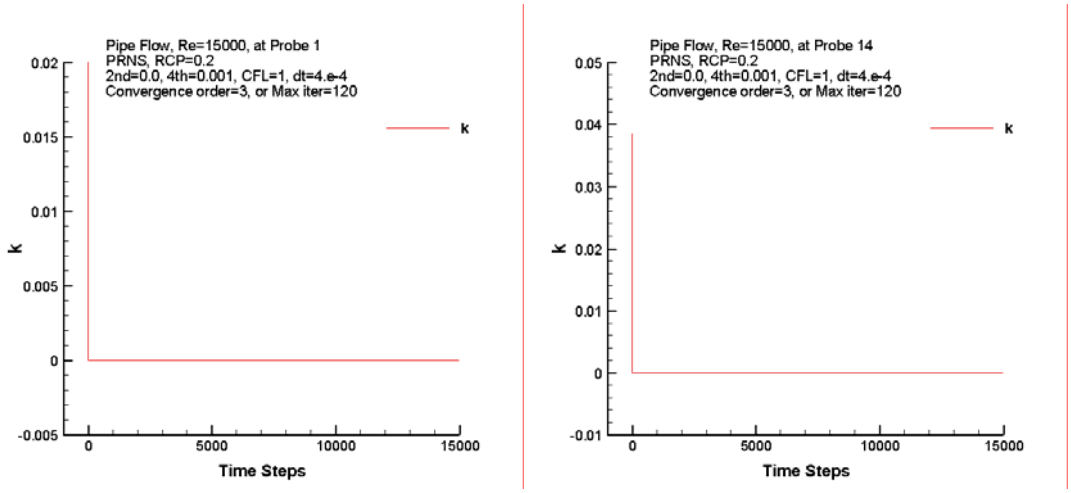

Contours of w, u, v, pg, k, $\mu + \mu_T$ at the time step 15,000:

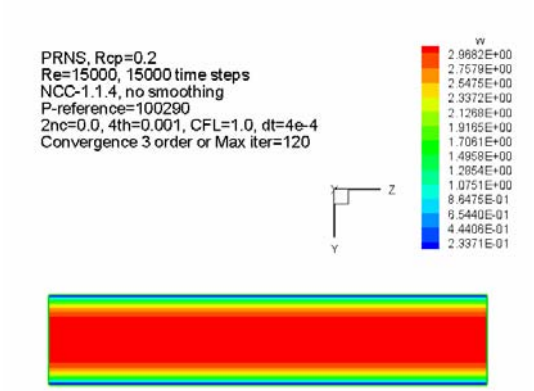

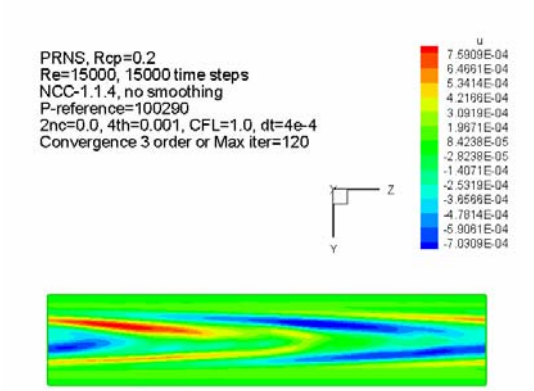

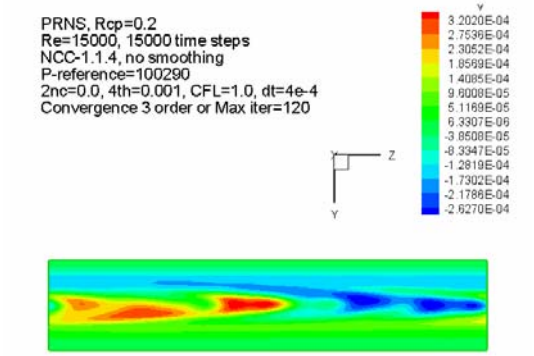

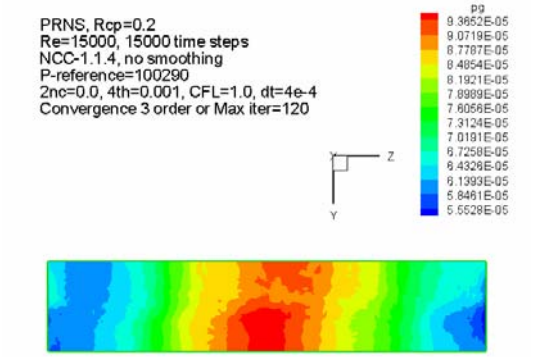

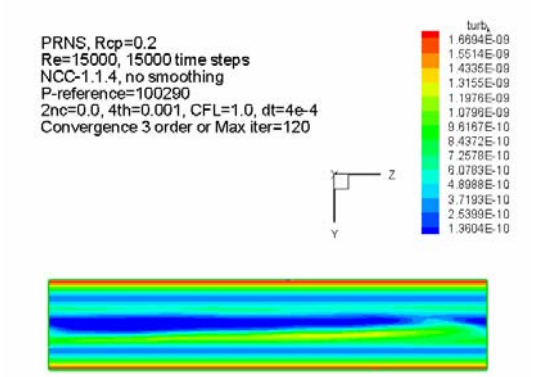

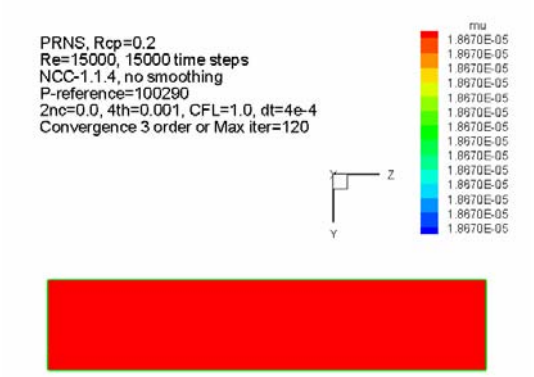

B.3 PRNS with RCP = 0.3

History of velocity components at probe 1 and probe 14:

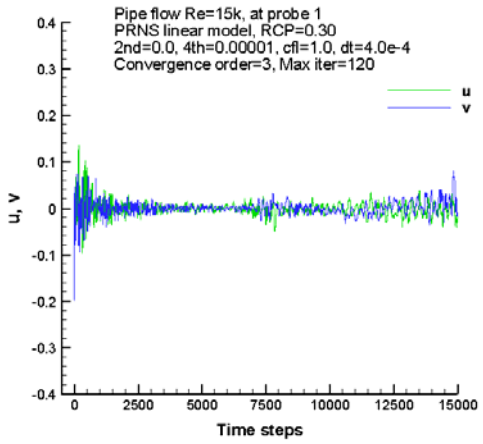

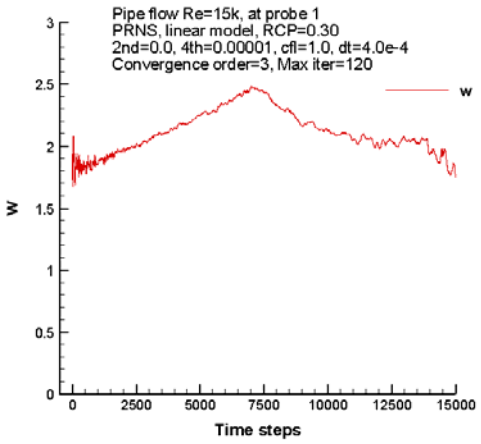

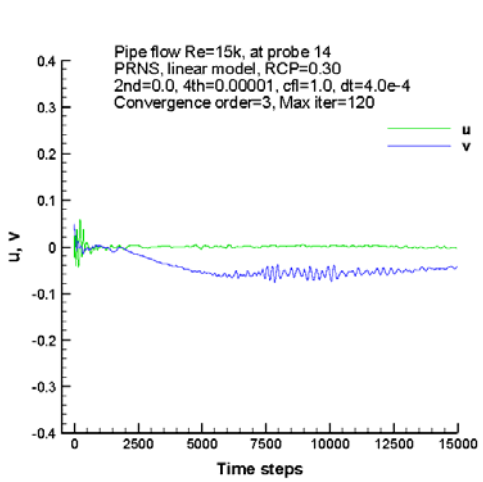

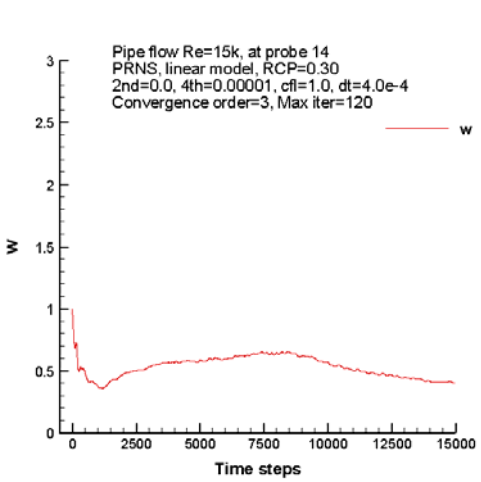

History of subscale turbulent kinetic energy at probes 1 and 14:

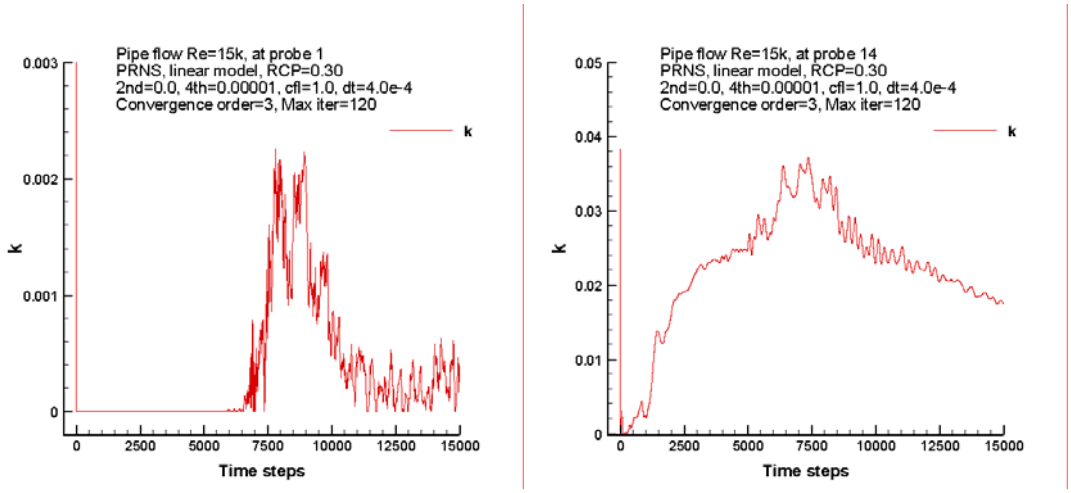

Contours of w, u, v, pg, k, $\mu + \mu_T$ at the time step 15,000:

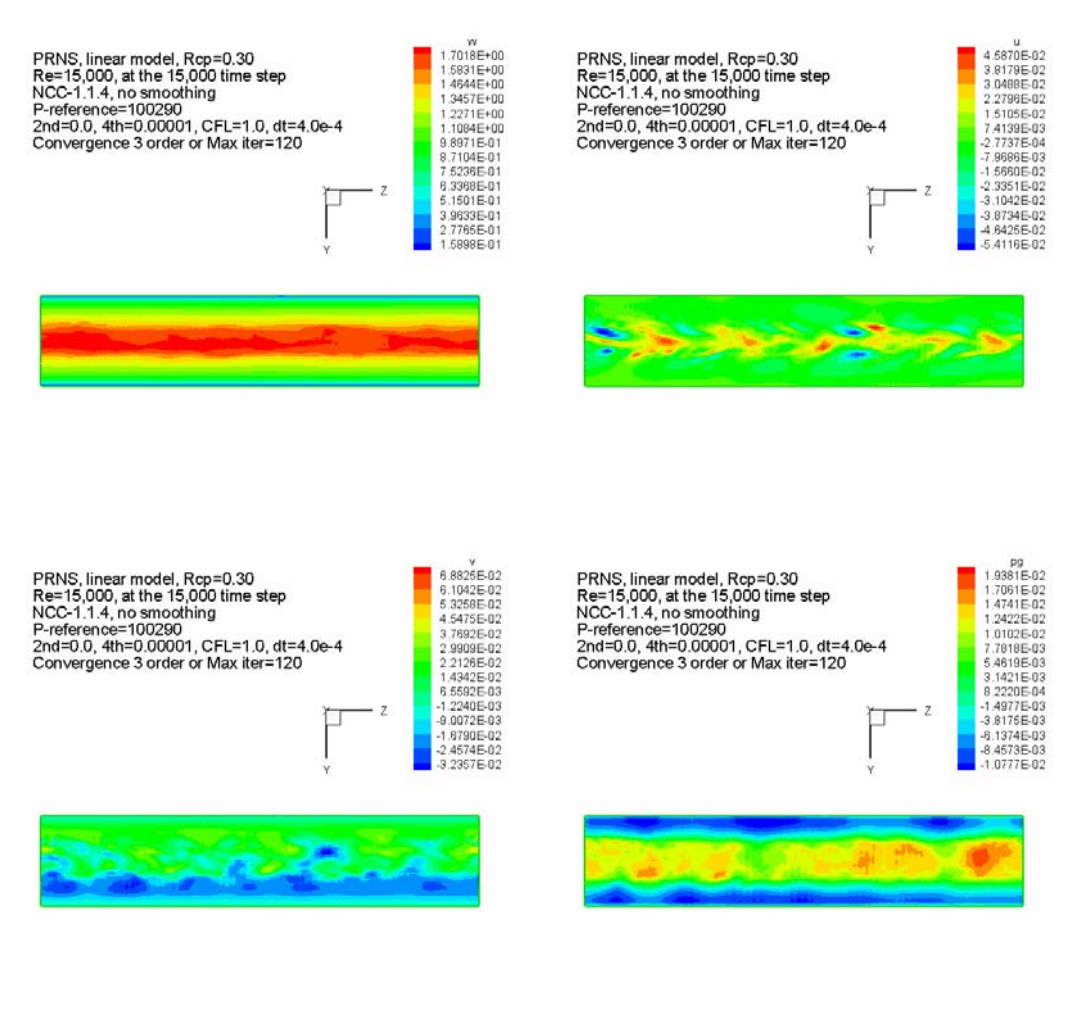

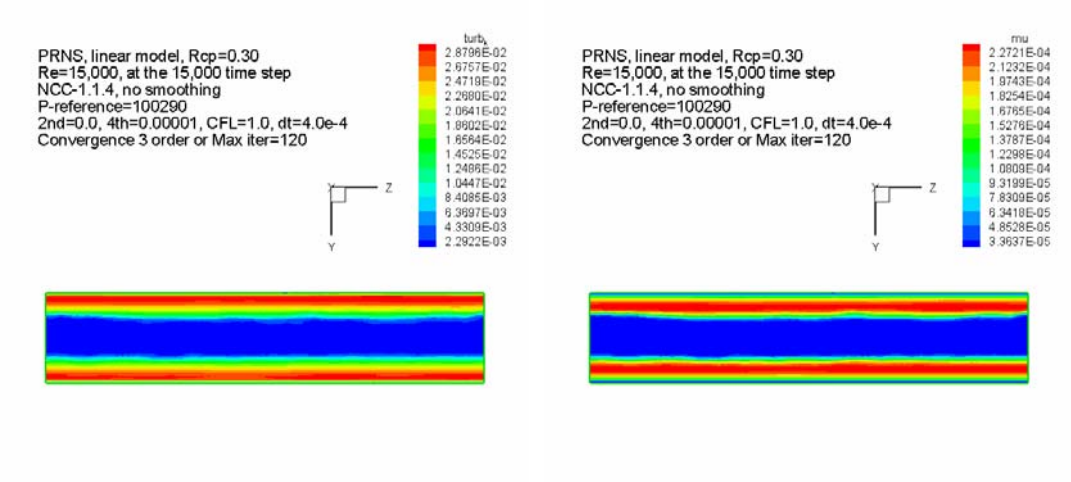

B.4 PRNS with RCP = 0.34

History of velocity components at probe 1 and probe 14:

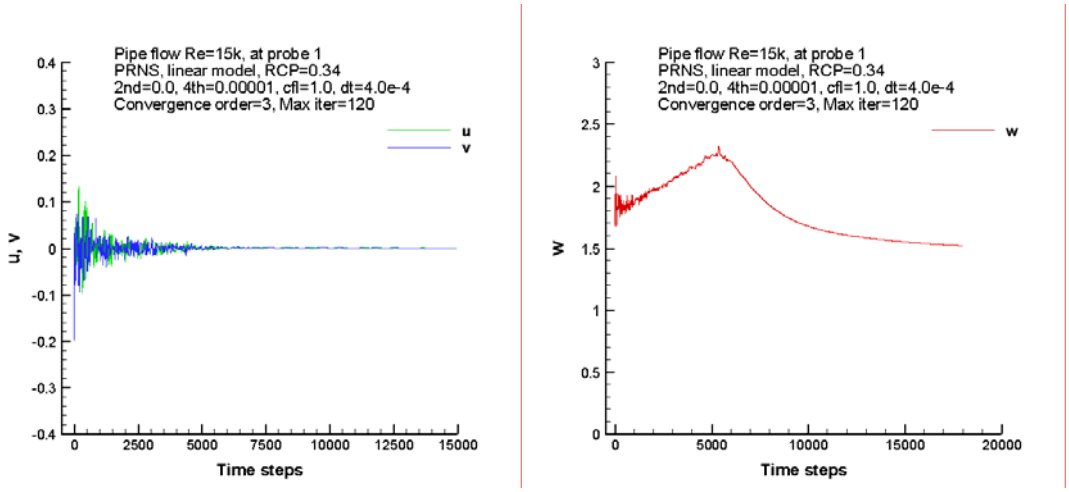

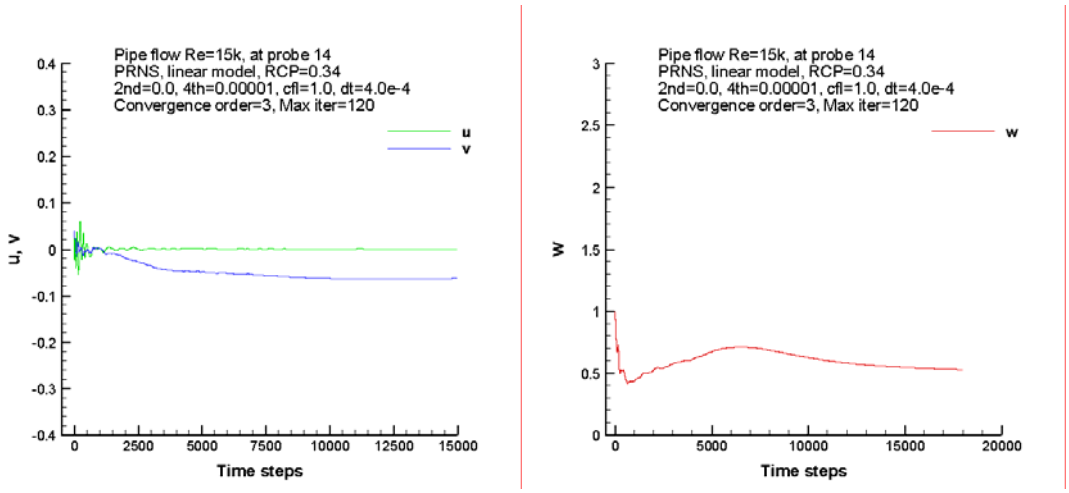

History of subscale turbulent kinetic energy at probes 1 and 14:

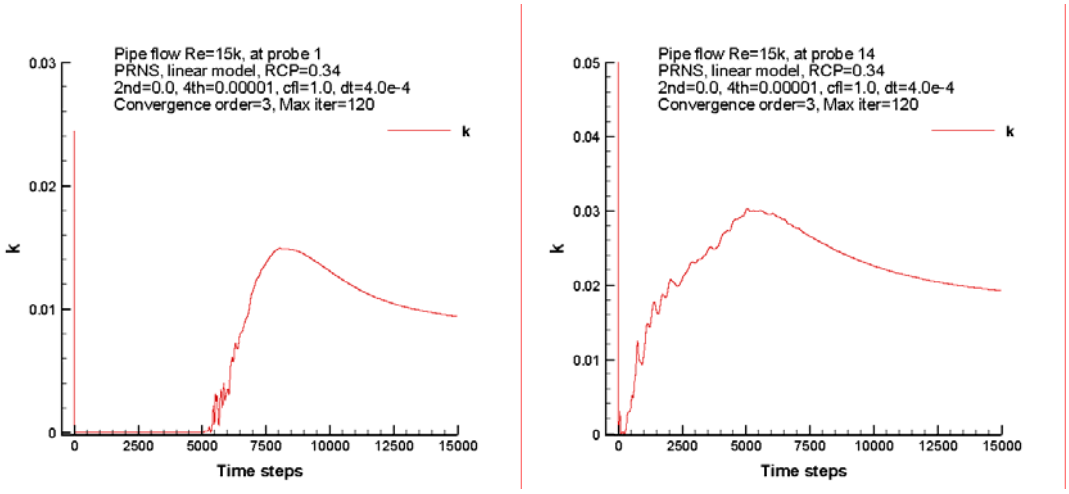

Contours of w, u, v, pg, k, $\mu + \mu_T$ at the time step 15,000:

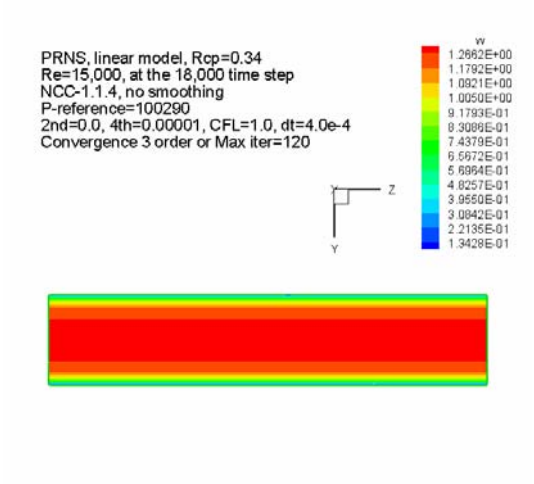

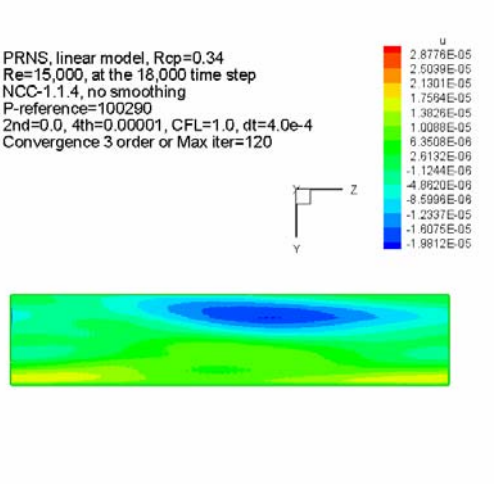

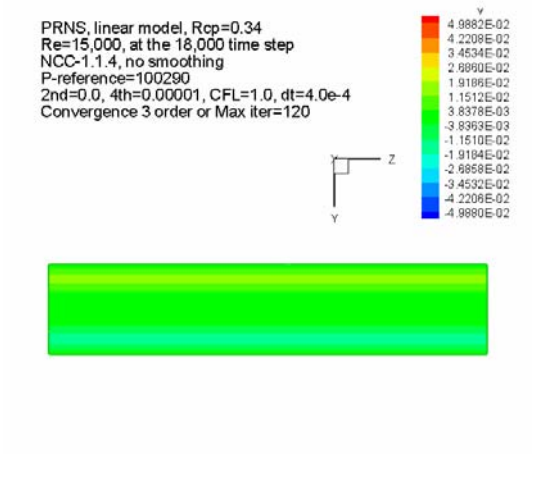

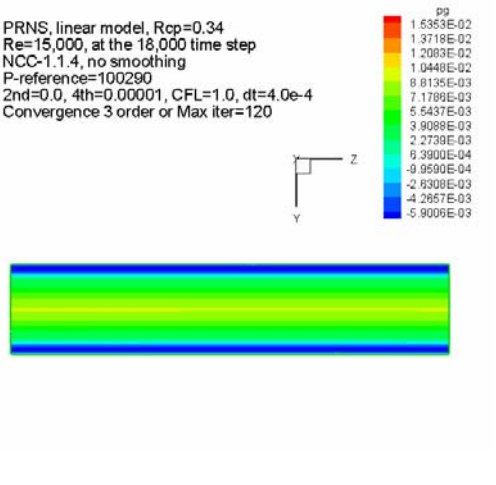

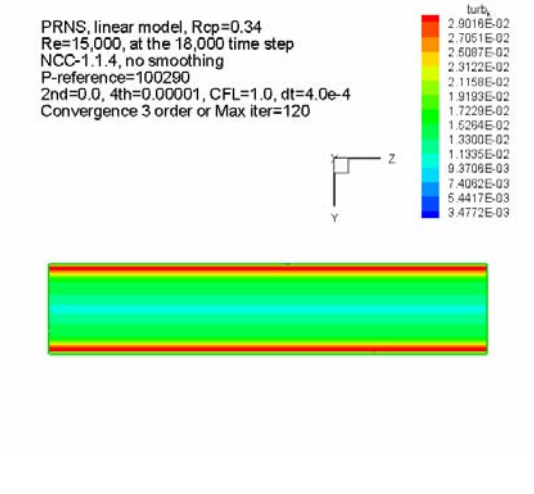

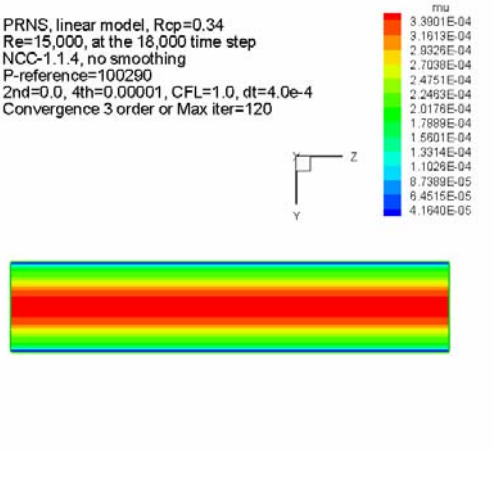

B.5 PRNS with RCP = 0.4

History of velocity components at probe 1 and probe 14:

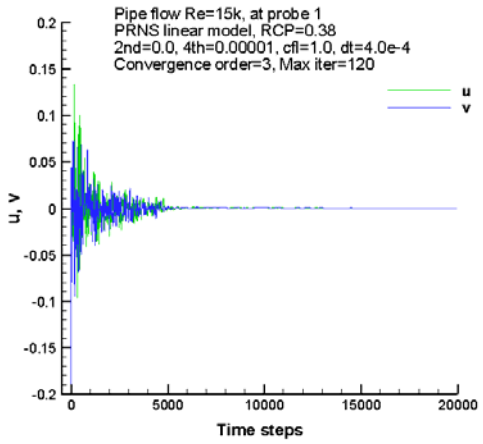

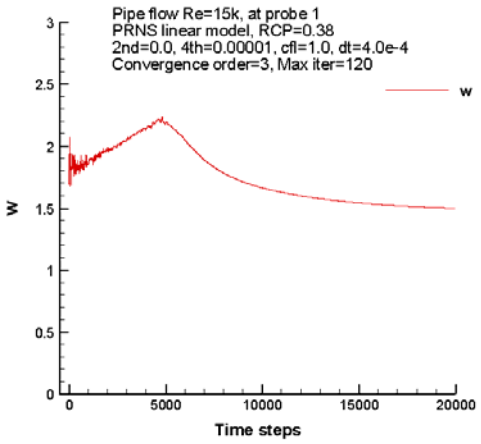

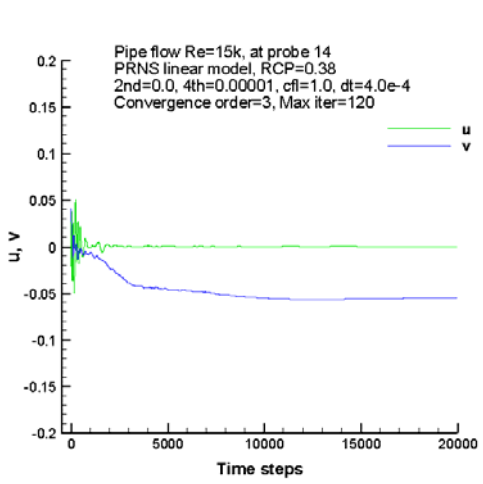

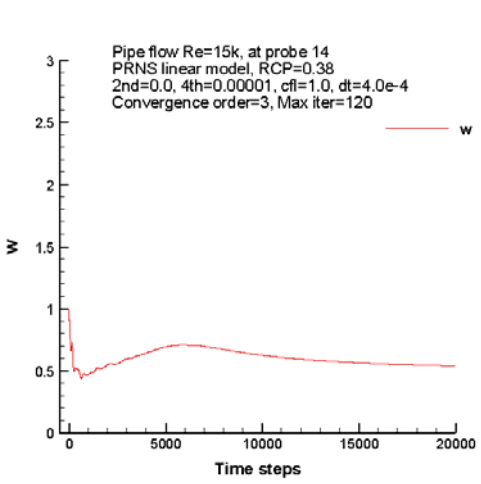

History of subscale turbulent kinetic energy at probes 1 and 14:

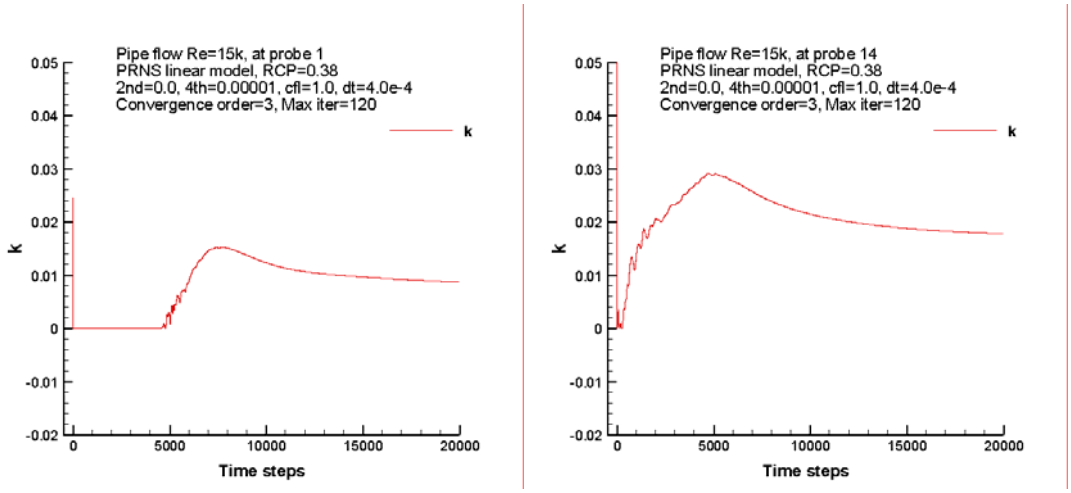

Contours of w, u, v, pg, k, $\mu + \mu_T$ at the time step 20,000:

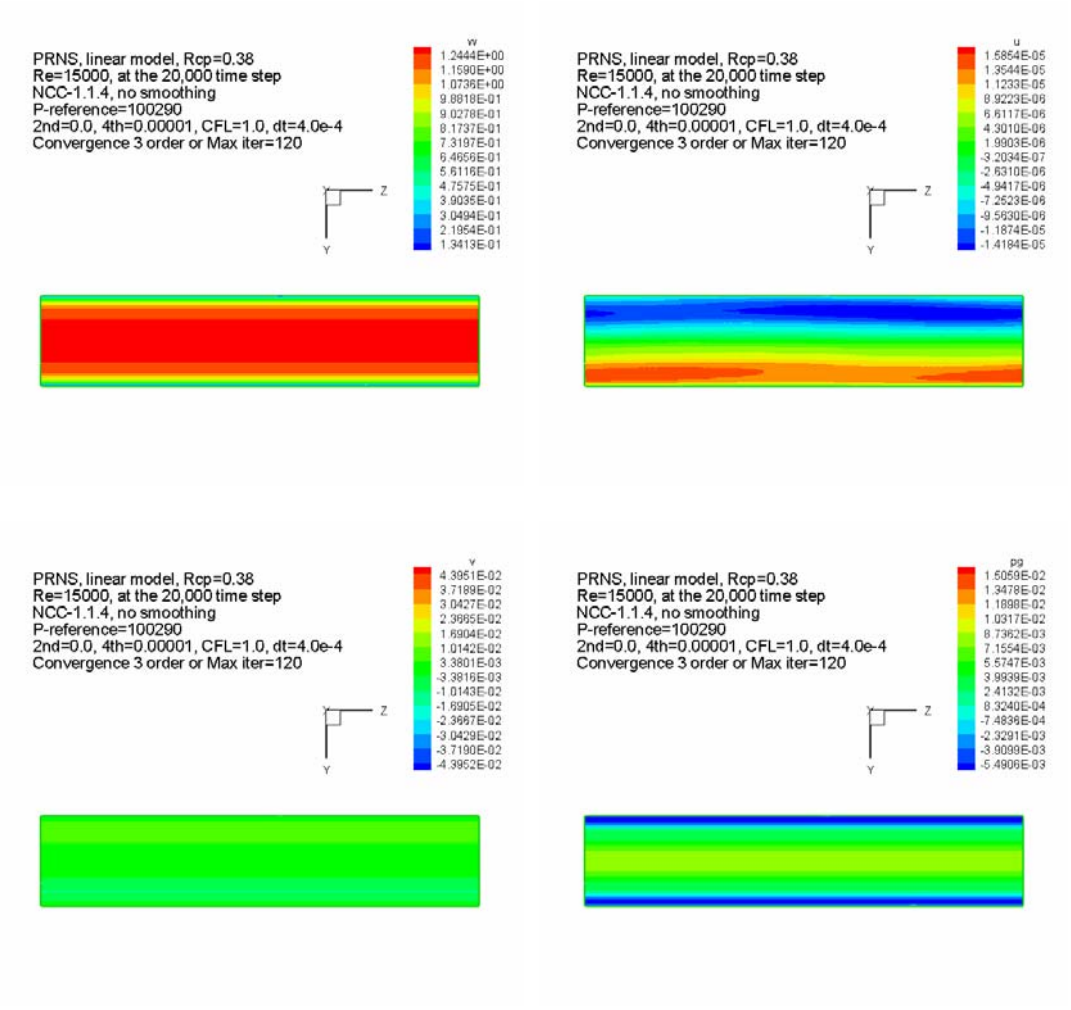

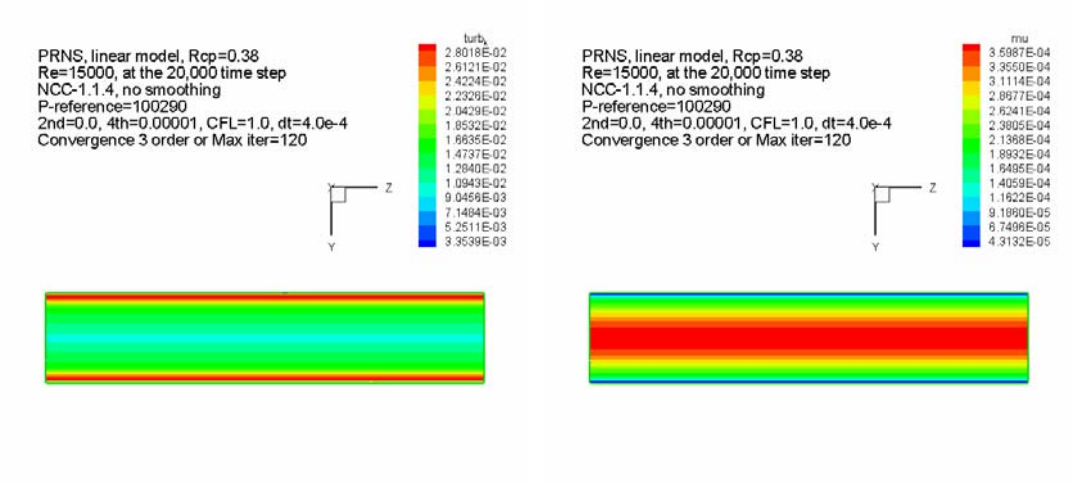

B.6 PRNS with RCP = 0.5

History of velocity components at probe 1 and probe 14:

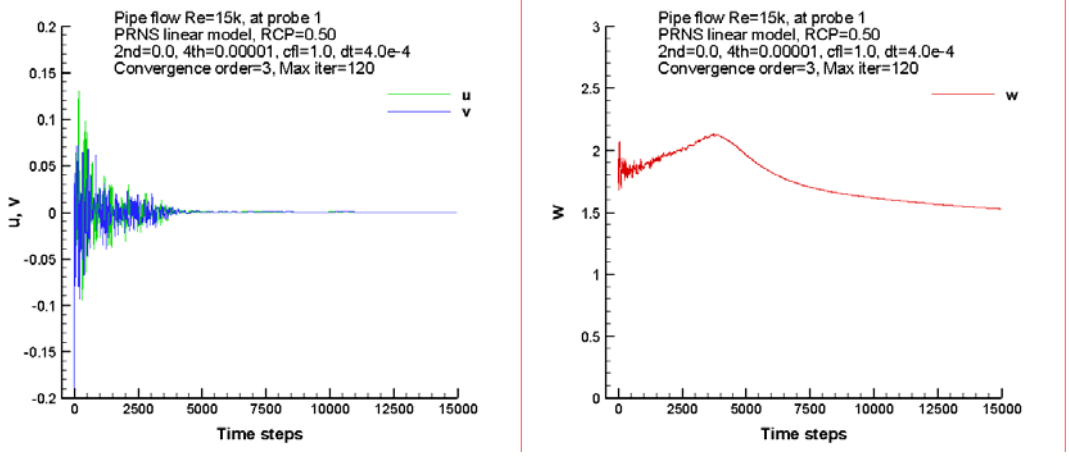

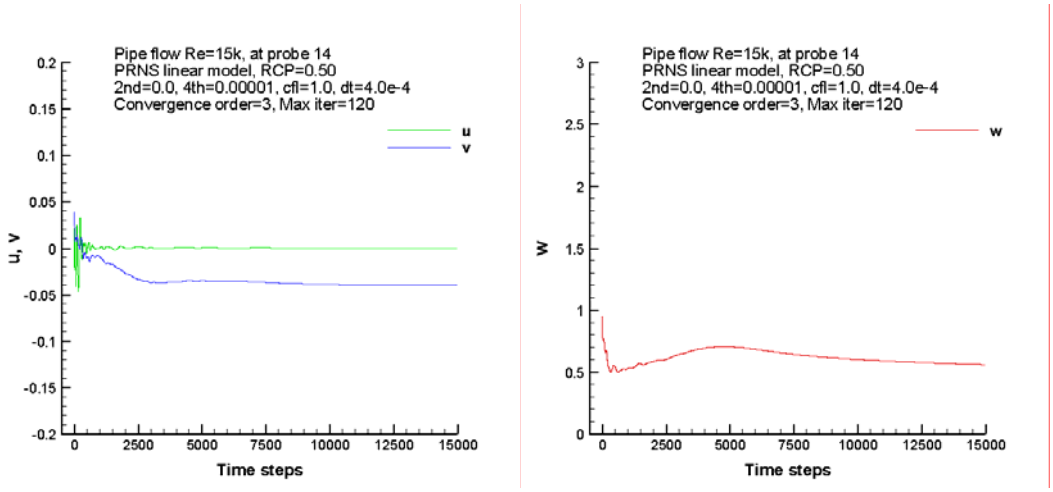

History of subscale turbulent kinetic energy at probes 1 and 14:

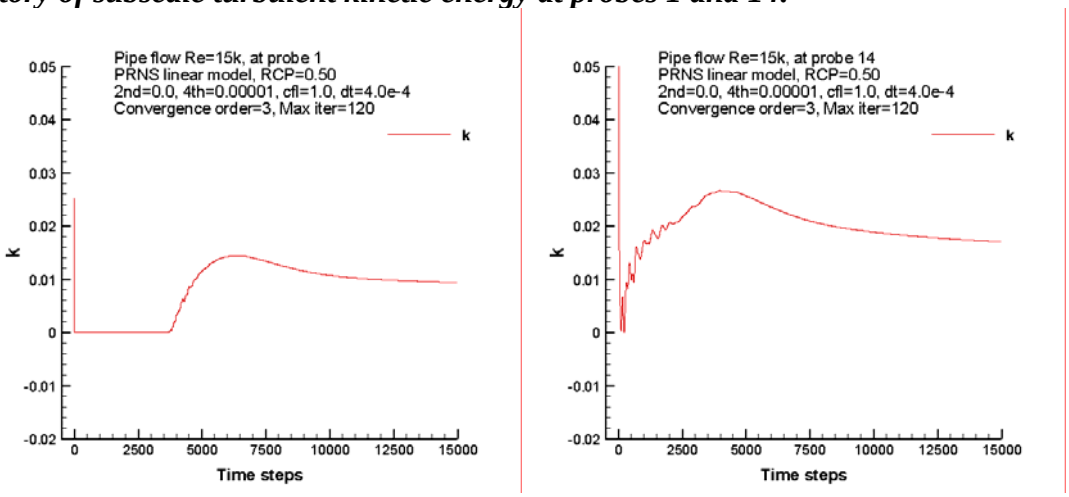

Contours of w, u, v, pg, k, $\mu + \mu_T$ at the time step 15,000:

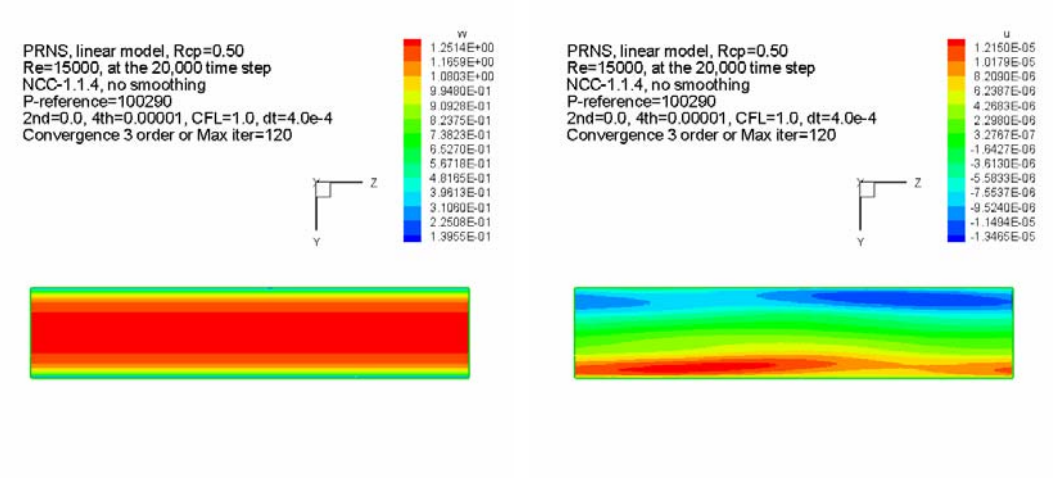

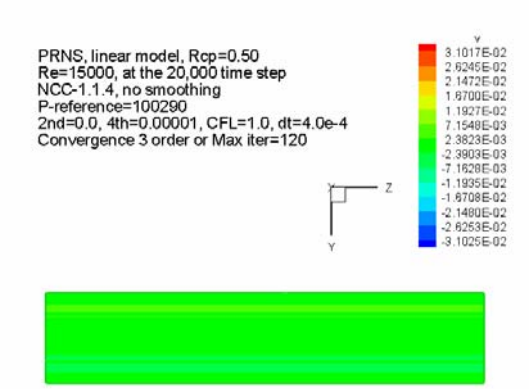
PRNS, linear model, Rcp=0.50
Re=15000, at the 20,000 time step
NCC-1.1.4, no smoothing
P-reference=100290
2nd=0.0, 4th=0.00001, CFL=1.0, dt=4.0e-4
Convergence 3 order or Max iter=120
Y
3.1017E-02
2.6245E-02
2.1472E-02
1.6700E-02
1.1927E-02
7.1548E-03
2.3823E-03
-2.3903E-03
-7.1628E-03
-1.1935E-02
-1.6708E-02
-2.1480E-02
-2.6253E-02
-3.1025E-02
Z
Y

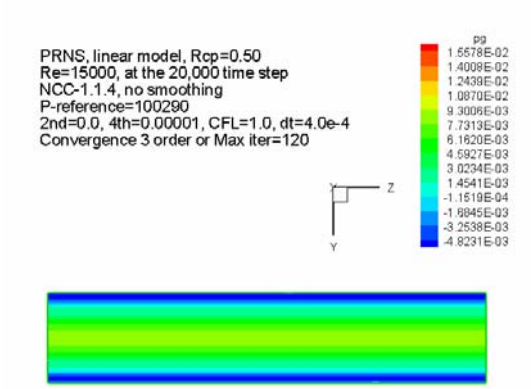
PRNS, linear model, Rcp=0.50
Re=15000, at the 20,000 time step
NCC-1.1.4, no smoothing
P-reference=100290
2nd=0.0, 4th=0.00001, CFL=1.0, dt=4.0e-4
Convergence 3 order or Max iter=120
pg
1.5578E-02
1.4008E-02
1.2438E-02
1.0870E-02
9.3006E-03
7.7313E-03
6.1620E-03
4.5927E-03
3.0234E-03
1.4541E-03
-1.1519E-04
-1.6845E-03
-3.2538E-03
-4.8231E-03
Z
Y

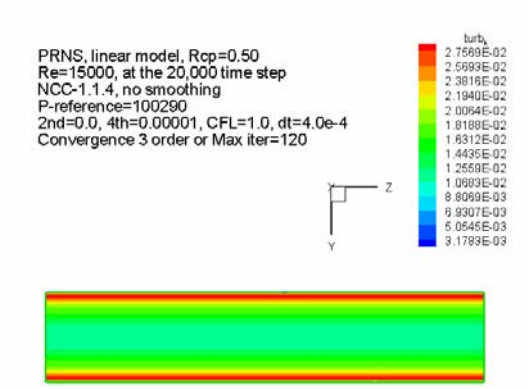
PRNS, linear model, Rcp=0.50
Re=15000, at the 20,000 time step
NCC-1.1.4, no smoothing
P-reference=100290
2nd=0.0, 4th=0.00001, CFL=1.0, dt=4.0e-4
Convergence 3 order or Max iter=120
turb
2.7569E-02
2.5693E-02
2.3816E-02
2.1940E-02
2.0064E-02
1.8188E-02
1.6312E-02
1.4435E-02
1.2559E-02
1.0683E-02
8.8069E-03
6.9307E-03
5.0545E-03
3.1783E-03
Z
Y

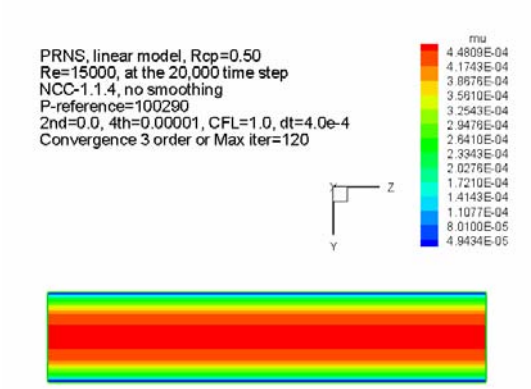
PRNS, linear model, Rcp=0.50
Re=15000, at the 20,000 time step
NCC-1.1.4, no smoothing
P-reference=100290
2nd=0.0, 4th=0.00001, CFL=1.0, dt=4.0e-4
Convergence 3 order or Max iter=120
mu
4.4809E-04
4.1743E-04
3.8676E-04
3.5610E-04
3.2543E-04
2.9476E-04
2.6410E-04
2.3343E-04
2.0276E-04
1.7210E-04
1.4143E-04
1.1077E-04
8.0100E-05
4.9434E-05
Z
Y

B.7 PRNS with RCP = 1.0

History of velocity components at probe 1 and probe 14:

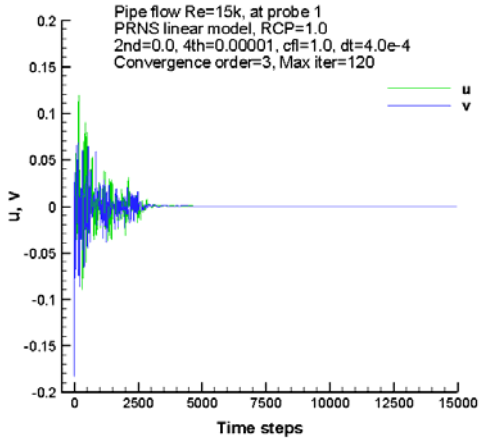

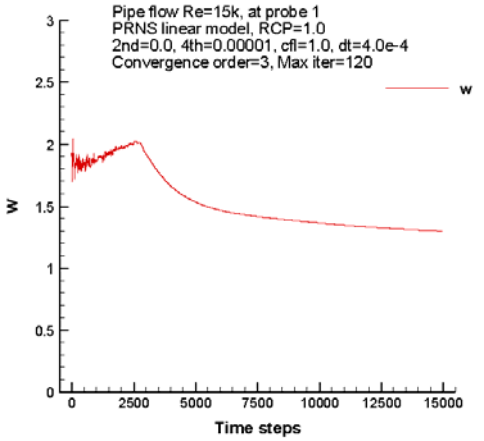

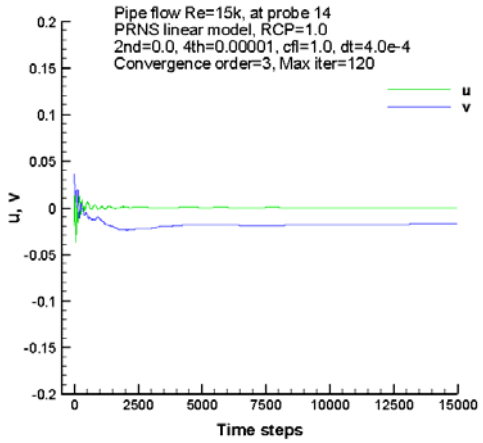

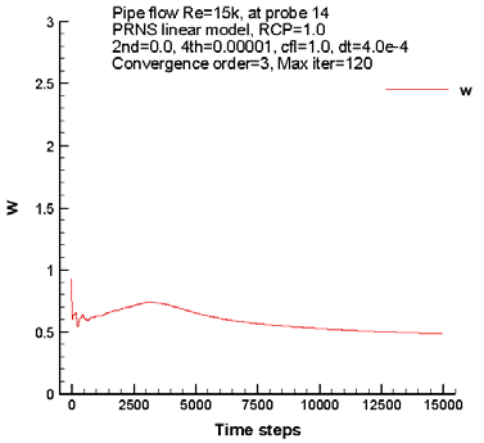

History of subscale turbulent kinetic energy at probes 1 and 14:

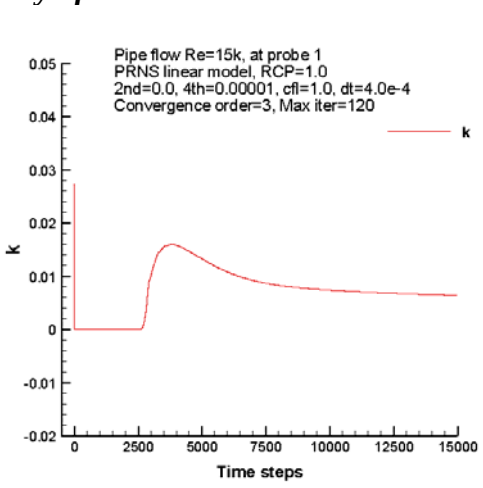

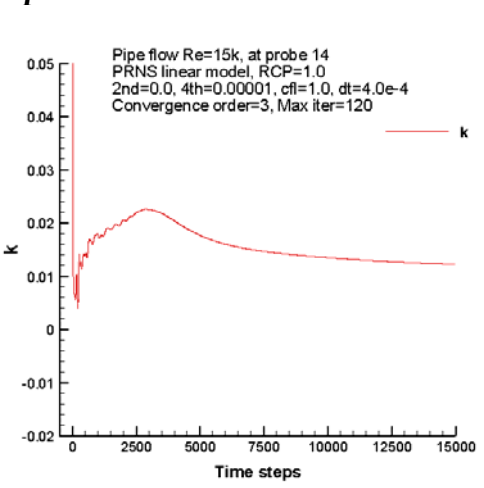

Contours of w, u, v, pg, k, $\mu + \mu_T$ ***at the time step 15,000:***

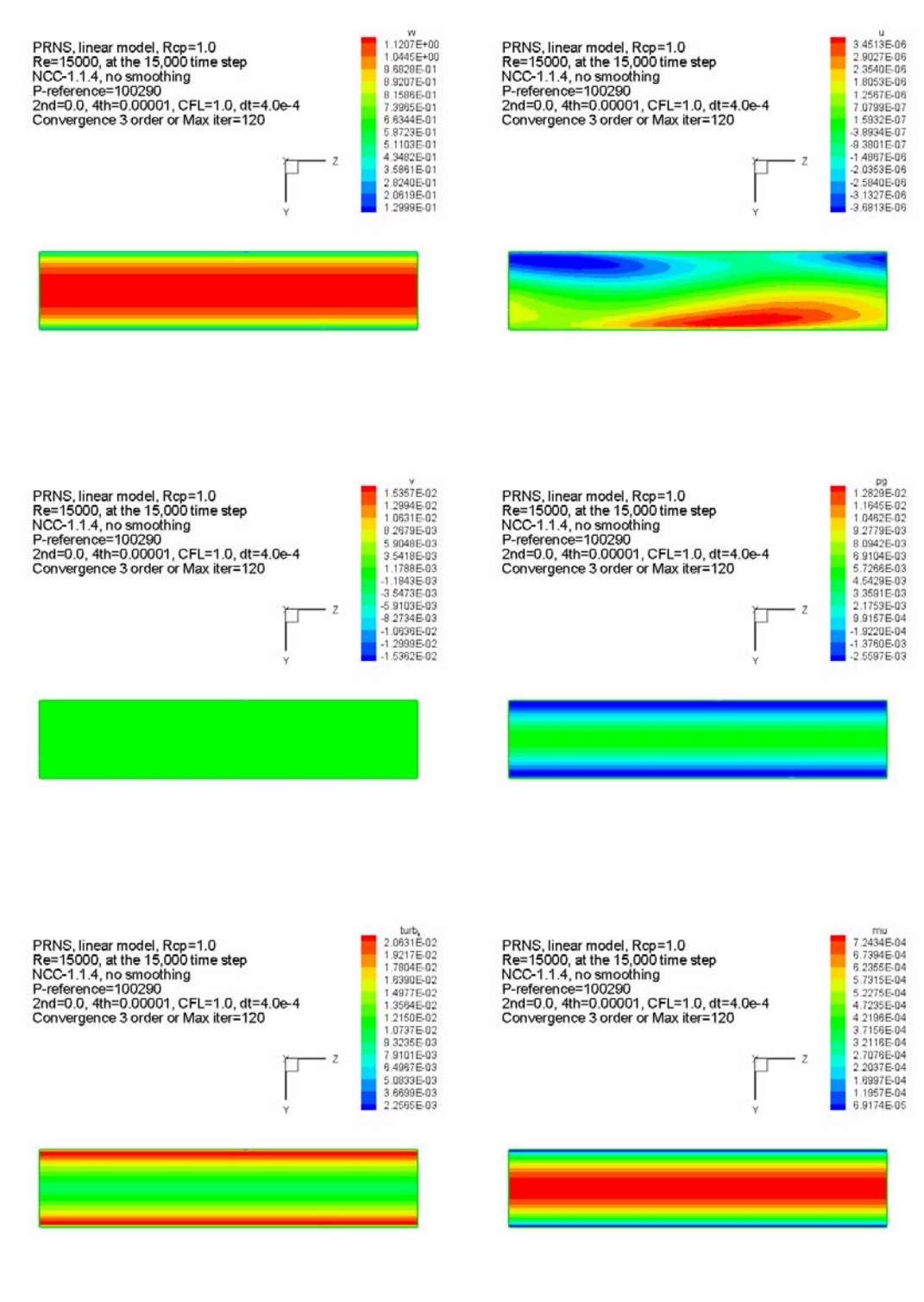

Appendix C: Effects of anisotropy and rotation in the subscale model

C.1 Nonlinear PRNS with RCP = 0.3 at Reynolds number 15,000

History of velocity components at probe 1 and probe 14:

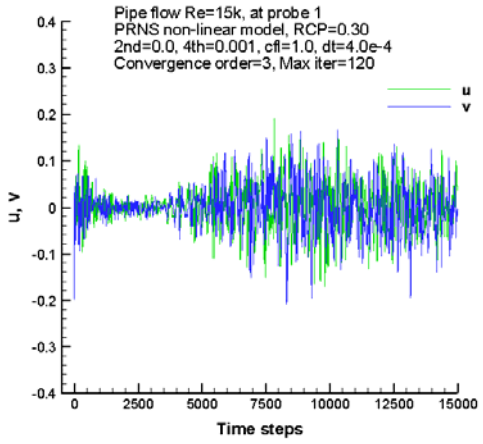

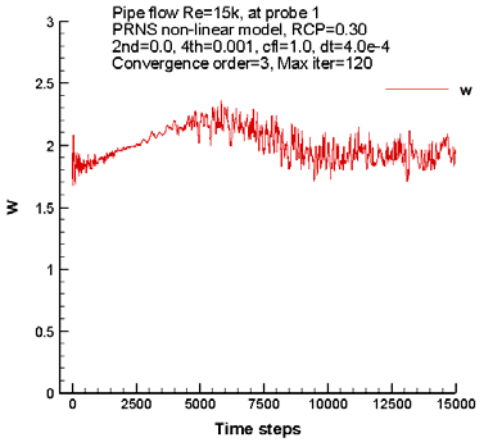

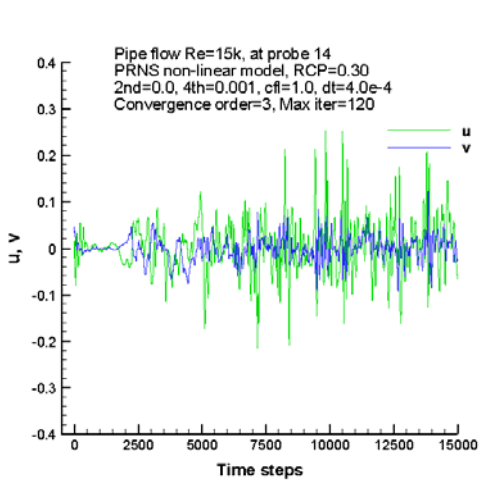

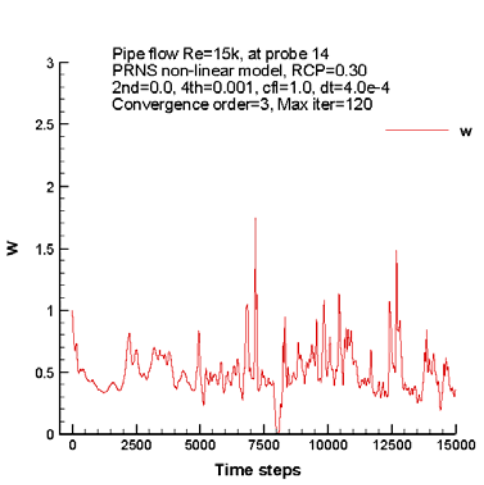

History of subscale turbulent kinetic energy at probes 1 and 14:

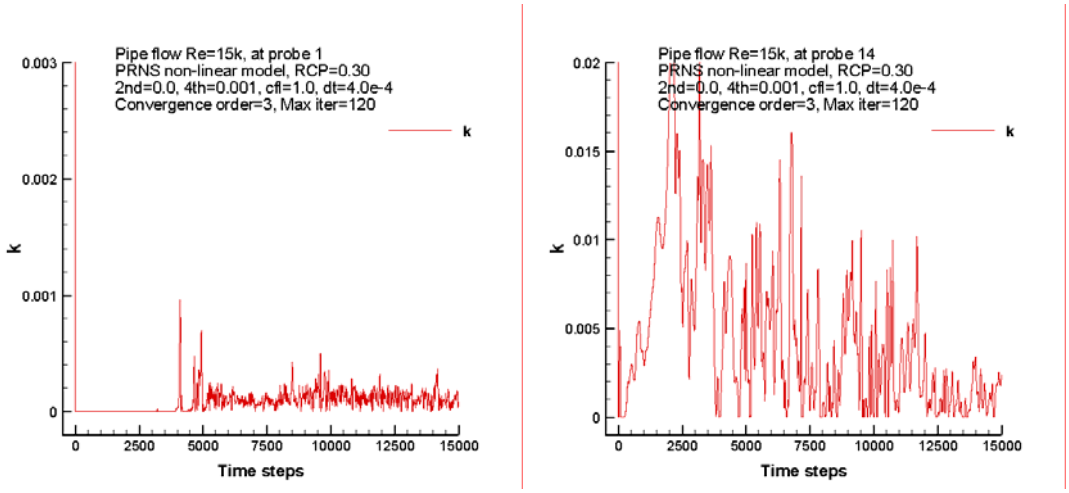

Contours of w, u, v, pg, k, $\mu + \mu_T$ at the time step 15,000:

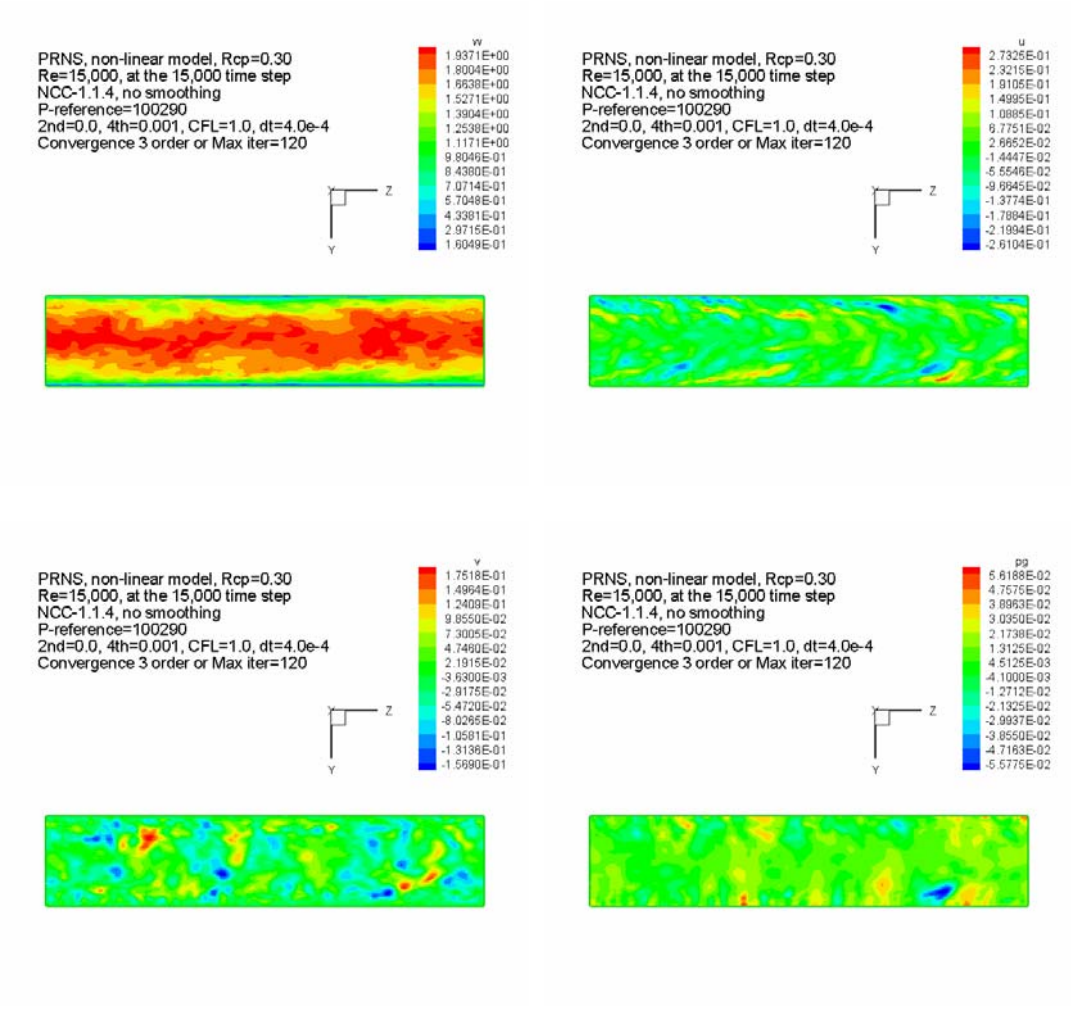

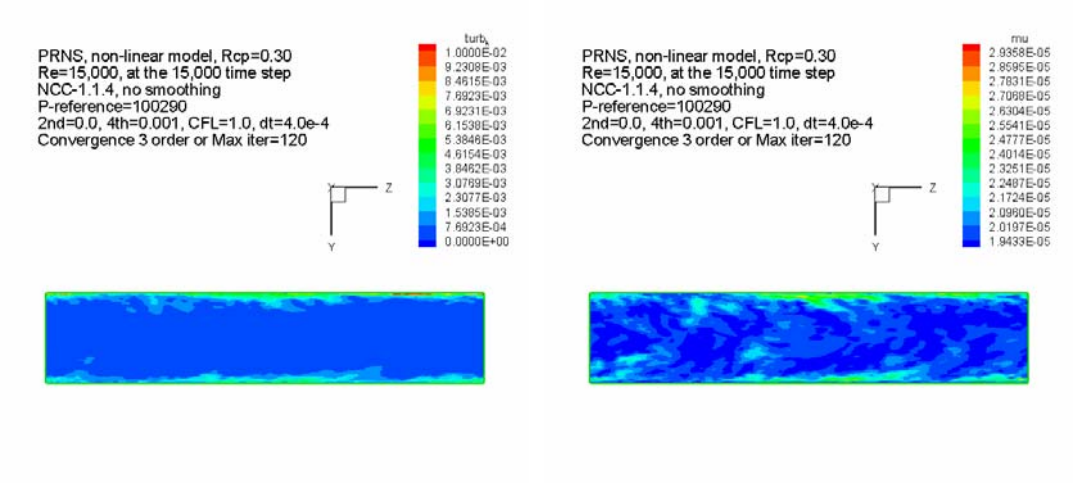

C.2 Nonlinear PRNS with RCP = 0.3 at Reynolds Number 150,000

History of velocity components at probe 1 and probe 14:

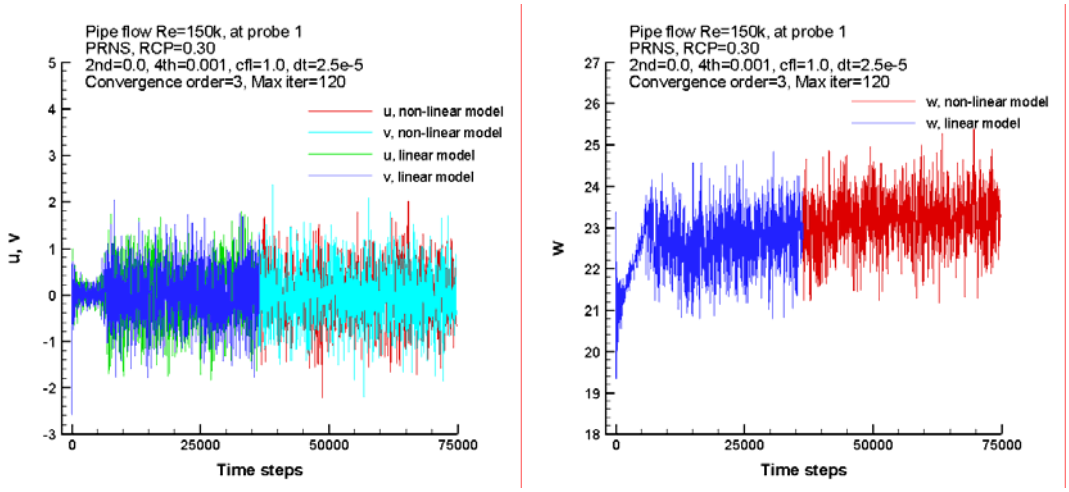

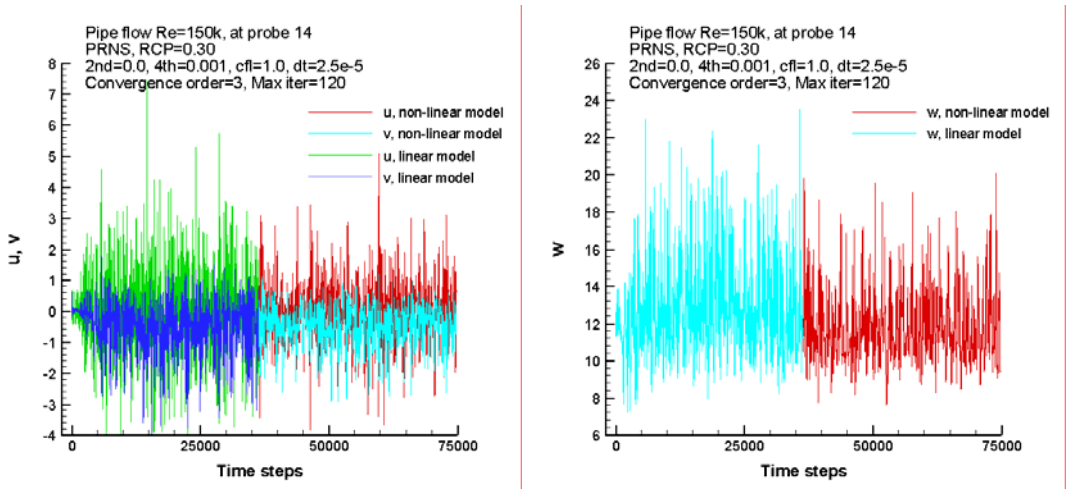

History of subscale turbulent kinetic energy at probes 1 and 14:

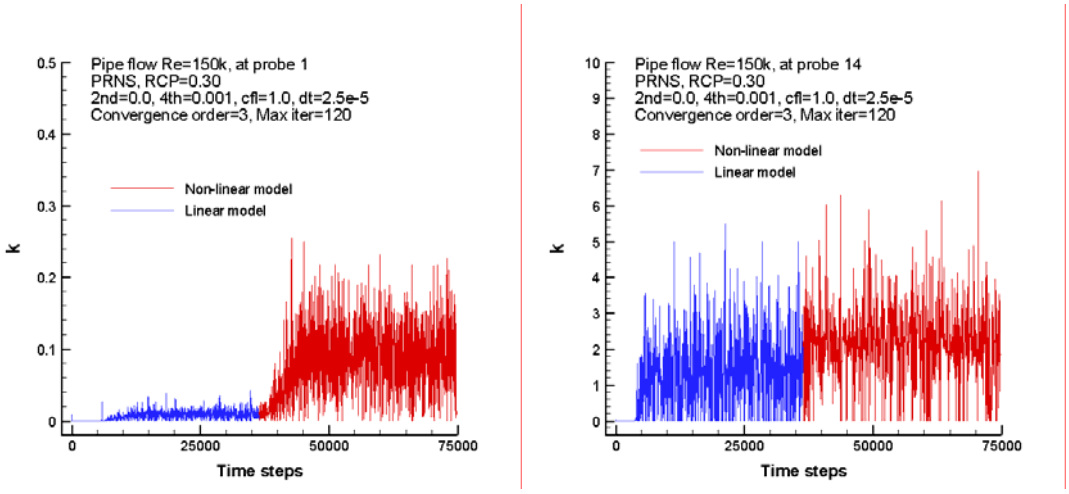

Contours of w, u, v, pg, k, $\mu + \mu_T$ at the time step 38,400:

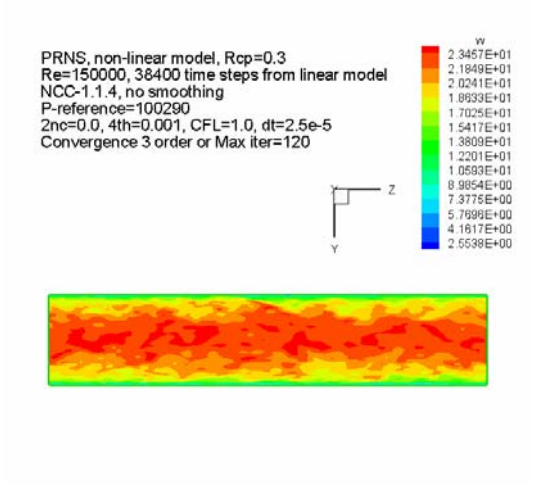

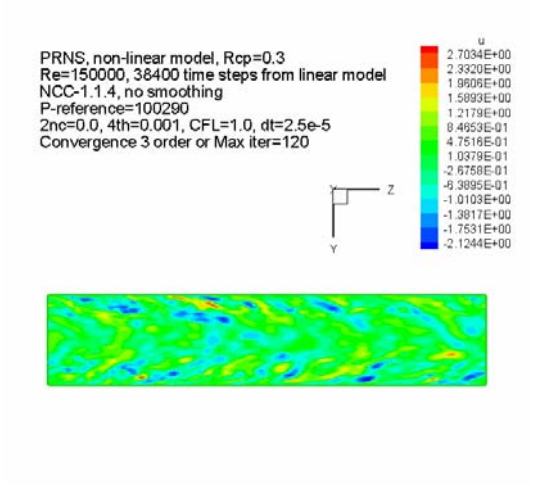

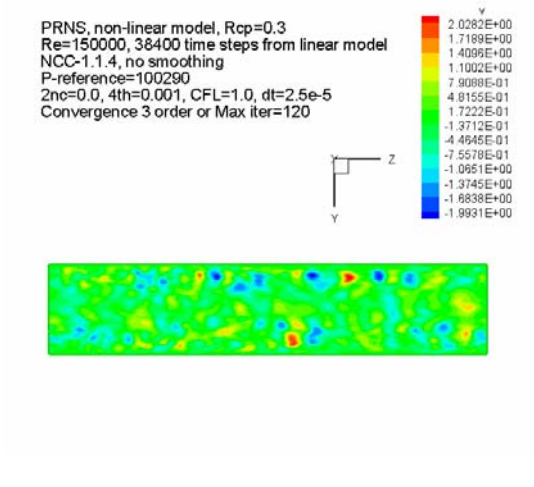

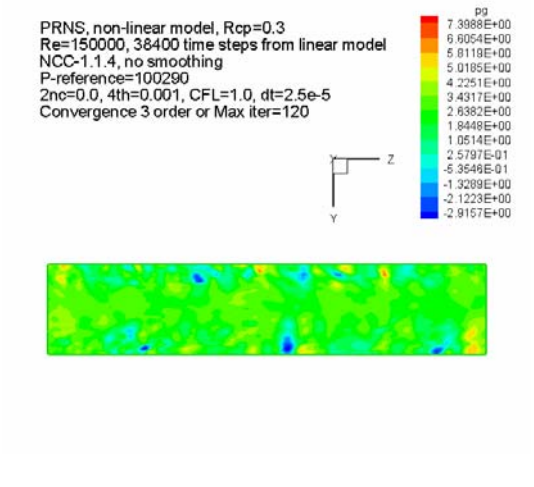

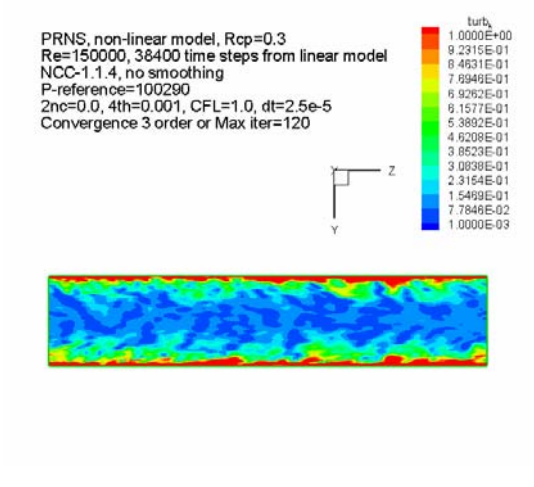

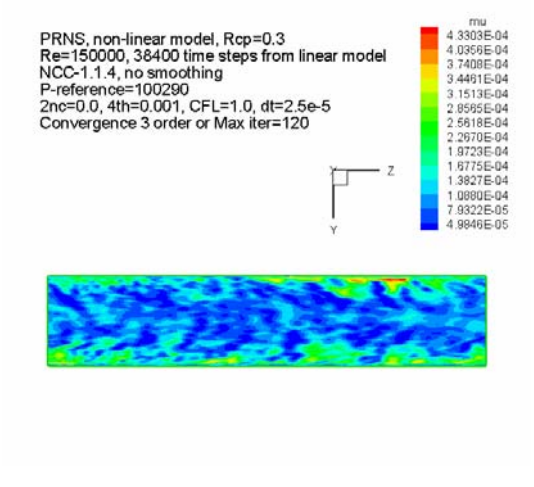

REPORT DOCUMENTATION PAGE	Form Approved OMB No. 0704-0188

1. REPORT DATE *(DD-MM-YYYY)*	2. REPORT TYPE	3. DATES COVERED *(From - To)*
01-10-2008	Technical Memorandum	

4. TITLE AND SUBTITLE
Assessment of the Partially Resolved Numerical Simulation (PRNS) Approach in the National Combustion Code (NCC) for Turbulent Nonreacting and Reacting Flows

5a. CONTRACT NUMBER

5b. GRANT NUMBER

5c. PROGRAM ELEMENT NUMBER

6. AUTHOR(S)
Shih, Tsan-Hsing; Liu, Nan-Suey

5d. PROJECT NUMBER

5e. TASK NUMBER

5f. WORK UNIT NUMBER
WBS 561581.02.08.03.16.02

7. PERFORMING ORGANIZATION NAME(S) AND ADDRESS(ES)
National Aeronautics and Space Administration
John H. Glenn Research Center at Lewis Field
Cleveland, Ohio 44135-3191

8. PERFORMING ORGANIZATION REPORT NUMBER
E-16582

9. SPONSORING/MONITORING AGENCY NAME(S) AND ADDRESS(ES)
National Aeronautics and Space Administration
Washington, DC 20546-0001

10. SPONSORING/MONITORS ACRONYM(S)
NASA

11. SPONSORING/MONITORING REPORT NUMBER
NASA/TM-2008-215418

12. DISTRIBUTION/AVAILABILITY STATEMENT
Unclassified-Unlimited
Subject Categories: 01 and 64
Available electronically at http://gltrs.grc.nasa.gov
This publication is available from the NASA Center for AeroSpace Information, 301-621-0390

13. SUPPLEMENTARY NOTES

14. ABSTRACT
This paper describes an approach which aims at bridging the gap between the traditional Reynolds-averaged Navier-Stokes (RANS) approach and the traditional large eddy simulation (LES) approach. It has the characteristics of the very large eddy simulation (VLES) and we call this approach the partially-resolved numerical simulation (PRNS). Systematic simulations using the National Combustion Code (NCC) have been carried out for fully developed turbulent pipe flows at different Reynolds numbers to evaluate the PRNS approach. Also presented are the sample results of two demonstration cases: nonreacting flow in a single injector flame tube and reacting flow in a Lean Direct Injection (LDI) hydrogen combustor.

15. SUBJECT TERMS
Turbulence model; Very large eddy simulation; Computational fluid dynamics

16. SECURITY CLASSIFICATION OF:			17. LIMITATION OF ABSTRACT	18. NUMBER OF PAGES	19a. NAME OF RESPONSIBLE PERSON
a. REPORT	b. ABSTRACT	c. THIS PAGE			STI Help Desk (email:help@sti.nasa.gov)
U	U	U	UU	86	19b. TELEPHONE NUMBER *(include area code)* 301-621-0390